Aus dem Pharmakologischen Institut

Direktor: Prof. Dr. Thomas Worzfeld

des Fachbereichs Medizin der Philipps-Universität Marburg

MRTF/SRF-dependent transcriptional regulation for bleb-associated cell invasion and entosis

Inaugural-Dissertation

Zur Erlangung des Doktorgrades der Naturwissenchaften

Doctor of Natural Sciences

Dem Fachbereich Medizin der Philipps-Universität Marburg
vorgelegt von

Laura Soto Hinojosa

aus Esplugues de Llobregat, Spanien

Marburg, 2019

Aus dem Pharmakologischen Institut

Direktor: Prof. Dr. Thomas Worzfeld

des Fachbereichs Medizin der Philipps-Universität Marburg

MRTF/SRF-dependent transcriptional regulation for bleb-associated cell invasion and entosis

Inaugural-Dissertation

Zur Erlangung des Doktorgrades der Naturwissenchaften

Doctor of Natural Sciences

Dem Fachbereich Medizin der Philipps-Universität Marburg
vorgelegt von

Laura Soto Hinojosa

aus Esplugues de Llobregat, Spanien

Marburg, 2019

Angenommen vom Fachbereich Medizin der Philipps-Universität Marburg am: 14.05.2019

Gedruckt mit Genehmigung des Fachbereichs Medizin

Dekan: Prof. Dr. Helmut Schäfer

Referent: Prof. Dr. Robert Grosse

1. Korreferent: Prof. Dr. Sven Bogdan

Dedicated to my beloved family

Table of contents

List of Figures

List of Tables

Abbreviations

AMT	Amoeboid Mesenchymal Transition
ANOVA	Analysis of variance
APS	Ammonium persulfate
BSA	Bovine Serum Albumin
cDNA	Complementary DNA
DAPI	4',6-Diamidino-2-phenylindole
DMSO	Dimethyl sulfoxide
DNA	Deoxyribonucleic acid
ECM	Extracellular Matrix
EMT	Epithelial-Mesenchymal-Transition
ERM	Ezrin-Radixin-Moesin
ERULS	Ezrin-rich-uropod-like-structure
FACS	Fluorescence-activated cell sorting
F-actin	Filamentous actin
FERM	Four-point one Ezrin-Radixin-Moesin
FCS	Fetal calf serum
G-actin	Globular monomeric actin
GFP	Green Fluorescent Protein
GPCR	G-Protein Coupled Receptor
HEMA	2-hydroxy-ethyl methacrylate
H2B	Histone 2B
Kb	Kilo-Base
KD	Kilo-Dalton

LA	Life-Act
LPA	Lysophosphatidic Acid
mDia	Mammalian Diaphanous
min	Minute
MLC	Myosin Light Chain
MMP	Matrix Metalloproteinase
MRTF-A (MAL, MKL-1)	Myocardin Related Transcription Factor, (Megakaryocytic acute leukemia)
o/n	Overnight
PBS	Phosphate Buffered Saline
PCR	Polymerase Chain Reaction
pERM	Phosphorylated-ERM
PIP_2	Phosphatidylinositol 4,5-bisphosphate
PM	Plasma Membrane
RNA	Ribonucleic acid
ROCK	Rho-associated protein kinase
RT	Room Temperature
TBP	TATA-binding protein
SD	Standard Deviation
SDS-PAGE	Sodium dodecyl sulfate-polyacrylamide gel electrophoresis
siRNA	Small interfering ribonucleic acid
SRE	Serum Response Element
SRF	Serum Response Factor
TCF	Ternary Complex Factor

Abstract

Non-apoptotic plasma membrane blebbing occurs during cell motility and tumor spread in several human malignancies. Bleb dynamics are regulated through rearrangement of the cortical actin cytoskeleton and its associated proteins. Our previous studies reported the importance of plasma membrane blebbing by the formin mDia1 in providing the driving force for entotic invasion of one cell into its neighbouring cell. Entosis is a form of homotypic cell-in-cell invasion, in which low cellular adhesion induces ROCK- and actomyosin-dependent invasion. The physiological consequences of this process are not well-understood. Entotic invasion has been suggested to induce tumor promoting effects, while other studies supported a tumor suppressor role. Although the molecular requirements and actin-binding proteins controlling bleb dynamics are well characterized, the importance of a potential transcriptional regulation underlying sustained, long-term blebbing as observed during cancer cell or entotic invasion has not been studied. Given the direct association between the Serum Response Factor (SRF) coactivator Myocardin-Related Transcription Factor (MRTF-A) and actin dynamics, we addressed the impact of the MRTF/SRF transcriptional pathway for plasma membrane blebbing and bleb-associated entotic invasion. In this study, we find that cortical contractility during plasma membrane blebbing is tightly associated to dynamic MRTF cytoplasmic-nuclear shuttling. Our findings reveal that not only the dynamics of plasma membrane blebs depend on MRTF/SRF, but also entotic invasion. Interestingly, we found that MRTF/SRF-dependent upregulation of the metastasis associated ERM protein Ezrin is fundamental for non-apoptotic blebbing and entotic invasion. Thus, our results highlight a novel mechanism, by which the actin-dependent transcription factor MRTF controls Ezrin expression to facilitate bleb-associated invasive motility. These findings may have important implications in understanding invasive motility as well as for future concepts targeting metastasis.

Zusammenfassung

Nicht-apoptotische Plasmamembranausstülpungen können während der Zellmotilität und der Dissemination von Tumoren im Rahmen vieler Erkrankungen auftreten. Dabei ist die Dynamik einer Plasmamembranausstülpung durch Umgestaltung des kortikalen Aktinzytoskelett sowie der assoziierten Proteine reguliert. Unsere vorhergehenden Arbeiten stellten über das Formin mDia1-vermittelte Plasmamembranausstülpungen als treibende Kraft der entotischen, homotyptischen Zell-in-Zell-Invasion heraus, wobei eine geringe Adhäsion diese ROCK- und aktomyosin-abhängige Form der Zell-in-Zell-Invasion förderte. Die physiologischen Konsequenzen der entotischen Zell-in-Zell-Invasion sind nicht hinreichend geklärt, da neben tumor-fördernden auch inhibierende Effekte publiziert wurden. Obwohl die generellen, molekularen Grundlagen und aktin-bindenden Proteine für Plasmamembranausstülpungen weitestgehend bekannt sind, ist eine potentielle Regulation der Genexpression bei lang-andauernden Plasmamembranausstülpungen, welche bei Krebszell- oder entotischer Zell-in-Zell-Invasion beobachtet wurden, nicht aufgeklärt. Aufgrund der direkten Interaktion zwischen dem Ko-Aktivator des Serum Response Factors (SRF), nämlich Myocardin-Related Transcription Factor (MRTF-A) und Aktindynamik haben wir die Bedeutung der MRTF/SRF-gesteuerten Genregulation für Plasmamembranausstülpungen und die assoziierte, entotische Zell-in-Zell-Invasion untersucht. Wir zeigen in dieser Arbeit, dass die kortikale Kontraktilität während der Plasmamembranausstülpungen eng mit der dynamischen, zytoplasmatisch-nukleären Translokation von MRTF korreliert. Unsere Ergebnisse veranschaulichen weiterhin, dass nicht nur die Dynamik von Plasmamembranausstülpungen, sondern auch die entotische Zell-in-Zell-Invasion von MRTF/SRF abhängig ist. Wir fanden interessanterweise eine Notwendigkeit der MRTF/SRF-abhängigen Steigerung der Genexpression des mit Metastasen-assoziierten ERM-Proteins Ezrin für nicht-apoptotische Plasmamembranausstülpungen und entotische Zell-in-Zell-Invasion. Daher erschließt sich aus unseren Ergebnissen ein neuartiger Mechanismus, bei dem der aktin-abhängige Transkriptionsfaktor MRTF die Genexpression von Ezrin kontrolliert, um invasive, mit Plasmamembranausstülpungen-assoziierte Zellmotilität zu steuern. Dies hat Auswirkungen auf das allgemeine Verständnis der invasiven Zellmotilität und liefert unter Umständen neue Konzepte für die Therapie von Metastasen.

1. Introduction

1.1. Cancer cell invasion

Tumor progression is a multistep process for cancer cells during which they acquire different characteristics, which enable them to survive, proliferate and disseminate. These characteristics are defined as hallmarks of cancer.

The fundamental hallmarks of cancer that enable tumor growth and metastatic dissemination include sustaining proliferative signaling, evading growth suppressors, avoiding immune destruction, enabling replicative immortality, tumor promoting inflammation, activation of tissue invasion and metastasis, inducing sustained angiogenesis, genome instability and mutation, resisting cell death evading apoptosis and deregulating cellular energetics (Figure 1). The tumor microenvironment and its signaling interactions within different cancer phenotypes further influence tumor cell behaviour (Hanahan and Weinberg 2011).
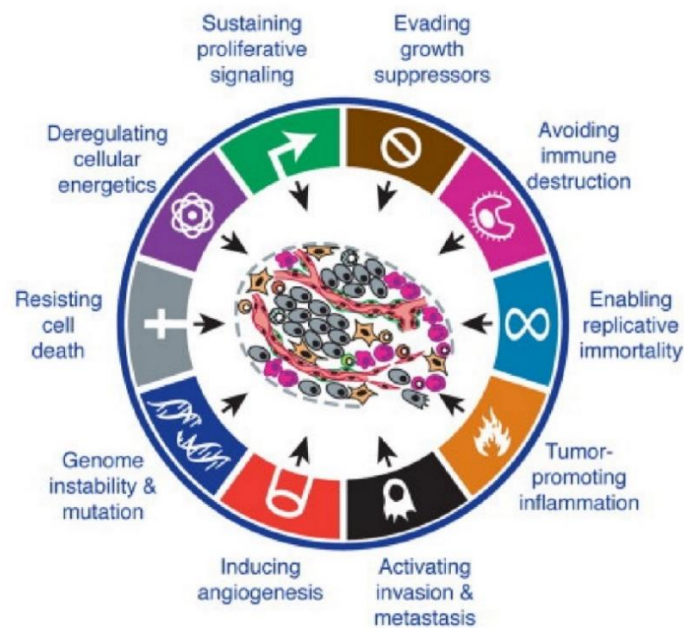
Figure 1: The hallmarks of cancer. The hallmarks of cancer define the essential alterations in cell physiology and different capabilities that cells acquire during tumor progression. This image was adapted from (Hanahan and Weinberg 2011).

The most critical feature of cancer is sustained chronic proliferation due to activation of signaling pathways by different mechanisms. An increase in cell proliferation will result in tumor growth, which in turn can trigger cell senescence and apoptosis. Accordingly, cancer cells negatively regulate the action of tumor suppressor genes to overcome senescence or apoptosis. A loss of

cell-cell contact inhibition further increases cell proliferation and impairs normal tissue homeostasis in cancer cells (Hanahan and Weinberg 2011).

It has been observed that cancer cells undergo programmed cell death by apoptosis, a process which becomes increasingly debilitated during tumor progression. In contrast to apoptosis, another form of programmed cell death is necrosis, whereby cells release proinflammatory signals into the tissue microenvironment triggering tumor-promoting factors to enhance angiogenesis, cell proliferation and invasiveness. In addition, other emerging hallmarks of cancer are the ability to reprogram cellular metabolism to support proliferation and the avoidance of immunological destruction. Interestingly, genomic instability and mutability in cancer cell, as well as tumor promoting inflammation by innate immune cells, are two features that drive tumor progression and facilitate acquisition of other hallmarks (Hanahan and Weinberg 2011).

Cancer cells can acquire multiple features leading to invasion and metastasis, in which one of the crucial steps is the regulation of signaling pathways allowing alteration of gene expression to mediate actin cytoskeleton dynamics (M. F. Olson and Sahai 2009). Furthermore, activation of signaling pathways promotes malignancy inducing cellular programs, such as epithelial-to-mesenchymal transition (EMT), which activates tissue invasion and metastasis (Hanahan and Weinberg 2011).

1.1.1. Modes of cancer cell invasion

Neoplastic diseases are characterized by high levels of metastatic dissemination, in which cancer cell migration is important to understand the invasiveness and metastasis of tumor cells (Hanahan and Weinberg 2011). Metastasis is the spread of cancer cells from the primary tumor site into other organs, known as the metastatic cascade. This multistep process defined by physiological changes in cells begins with cell motility and invasion into the surrounding tissue, followed by intravasation into the blood or lymphatic vessels, a transit through the vessels, and ultimately extravasation from the vessels into other tissues generating micro-metastasis or new site colonizations (Figure 2) (Sahai 2007; Sanz-Moreno and Marshall 2010).
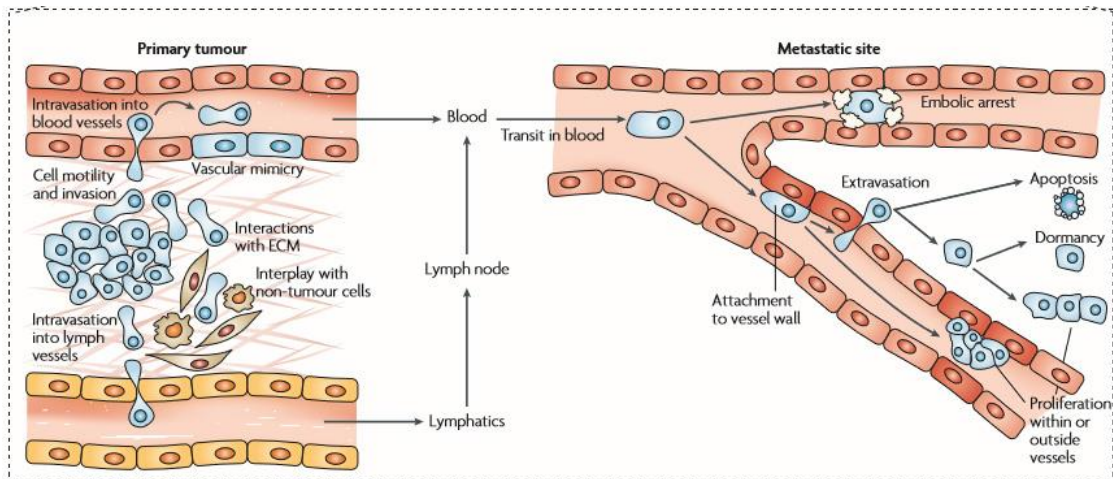
Figure 2: The metastatic process. Primary tumor cells invade into the tissue environment, then undergo dissemination and intravasation into blood or lymphatic vessels. These tumor cells transit via the blood stream and subsequently get either arrested as emboli in narrow vessels or attached to the vessel wall. The latter is followed by cancer cell extravasation, which results either in apoptosis, dormancy or can lead to tumor cell proliferation and the formation of metastasis. The image was adapted from (Sahai 2007).

Cell migration and invasion are essential for the metastatic dissemination of cancer cells. Here, metastatic cancer cells undergo molecular and cellular changes involving remodelling of the extracellular matrix (ECM) and the actin cytoskeleton. This process can be studied either in isolated cells moving across the ECM on two dimensional (2D) surfaces or under physiological conditions using mammalian cells migrating in three dimensional (3D) tissues. Accordingly, their cell motility and actin-mediated protrusions within the ECM can diverge depending on whether migration occurs in 2D or 3D. Although actomyosin-mediated protrusions and cell contractility are important for all migration types, the distinct biophysical traits are dependent on the migration mode. Moreover, some cell migration modes require pericellular proteolysis, which triggers ECM degradation and realignment during cell movement. Cell migration in 3D ECM is described by five different steps, initiated by the action of an external stimulus which results in I) the protrusion of an actin-driven leading pseudopod, followed by II) adhesion of the leading edge to the ECM and consequently force generation towards the ECM to get realigned, then III) recruitment of proteases (MMPs) to allow proteolysis at the leading edge and ECM remodelling, which results in IV) actomyosin cell contraction promoting V) rear-end retraction and forward movement. Thus, proteolytic cell migration is a mechanism dependent on the ECM and the cell type (Figure 3) (Friedl and Wolf 2009; A. J. Ridley 2003; Wolf et al. 2007).
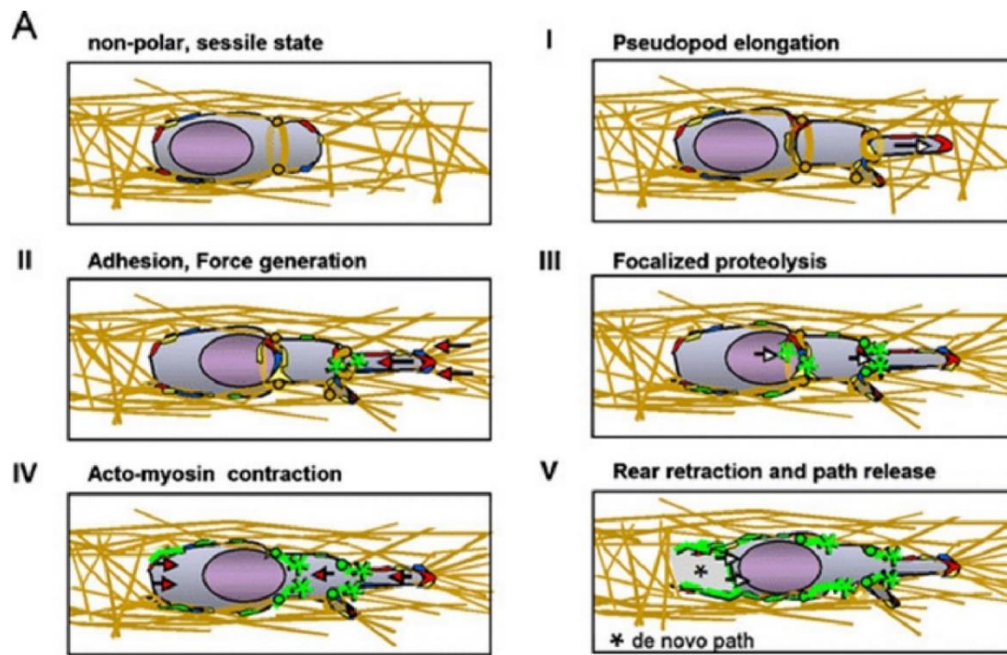
Figure 3: The five steps of cell migration. Cell migration requires the coordination of several cellular processes which can be divided into five steps: 1) actin-driven leading-edge protrusion; 2) adhesion and force generation phase by formation of integrin-mediated interactions to the substrate; 3) matrix disruption; 4) actomyosin cell contraction that leads to 5) rear-end retraction and forward sliding of the cell. This image was modified from (Friedl and Wolf 2009)**.**

Cancer cells have the ability to adapt to different environmental conditions by switching their migration strategies (Sahai 2005). Tumor cells can migrate by undergoing either individual or collective modes of cancer cell invasion (Figure 5) in response to the tissue environment and the extracellular matrix through changes in the dynamic organization of the cytoskeleton (Friedl and Wolf 2010). Cancer cells migrate individually using different mechanisms such as the spike-mediated, the elongated-mesenchymal or the bleb-dependent rounded amoeboid mode of migration. Cells undergoing collective migration move as multicellular streams, small clusters via tumor buds or as large clusters dependent on cell-cell junctions (Friedl and Alexander 2011; Pandya, Orgaz, and Sanz-Moreno 2017). This thesis is focused on the bleb-associated mode of invasion, thereby it is crucial to understand invasion of individual cancer cells.

1.1.2. The amoeboid and the mesenchymal motility modes

Individual migrating cells, such as the melanoma cell line A375-M2, are able to undergo two different modes of tumor cell invasion: amoeboid, rounded bleb-associated motility and elongated-mesenchymal cell motility (Figure 4). Several studies have reported that the GTPase RhoA promotes rounded bleb-dependent cell motility, while the elongated mode of cell motility is associated with the GTPase Rac-1 (Sahai and Marshall 2003).

The main phenotypic characteristics of the mesenchymal and amoeboid modes of invasiveness are shown in (Figure 4). The protease-dependent mesenchymal type of invasion is defined by elongated cell morphology, low cell motility speed, the formation of actin-rich protrusions such as filopodia or lamellipodia, and high catalytic activity as a result of Matrix Metalloproteinases (MMPs) recruited to the integrin-ECM binding site. Unlike mesenchymal cells, the protease-independent amoeboid invasion mode is determined by rounded cell morphology, the formation of actin-driven bleb protrusions and high cell motility speed due to a lack of tight cell-ECM adhesion (Sahai and Marshall 2003; Paňková et al. 2010; Sahai 2005). Interestingly, the blebby mode of motility requires the ERM protein Ezrin at the cell rear to drive polarized invasion (Lorentzen et al. 2011). Importantly, amoeboid invasion is driven by Rho-ROCK signaling, which enhances actomyosin contractility by increasing phosphorylation of MLC2 (Friedl and Wolf 2010).
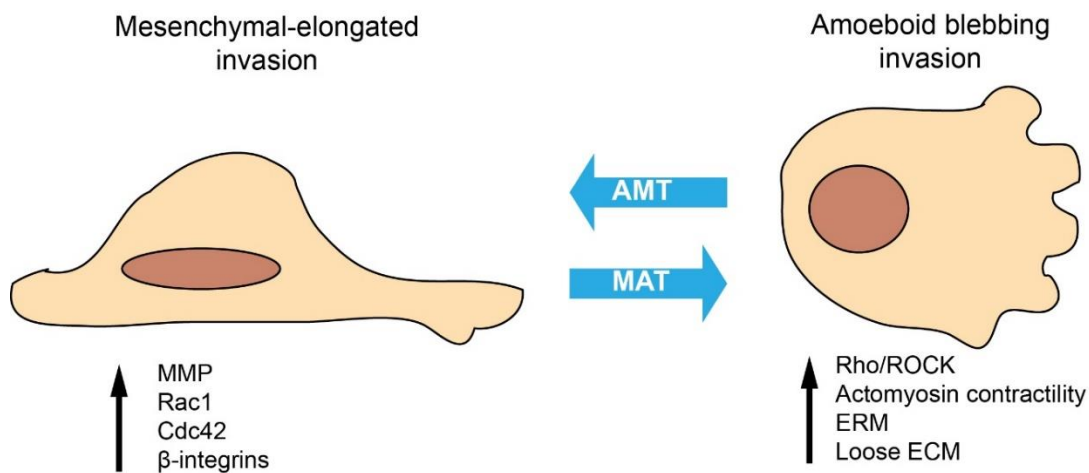
Figure 4: Cell plasticity during Amoeboid-Mesenchymal Transition. Cell motility of individual cells can be either mesenchymal-elongated or the amoeboid blebbing type. Amoeboid motility is defined by a round morphology, dependent on actomyosin contractility and does not involve ECM adhesion or degradation. In addition, these migrating cells produce plasma membrane blebs during motility. In contrast, mesenchymal motility is Rac-dependent, whereas cells show an elongated morphology and present MMP-mediated ECM degradation (Gandalovičová et al. 2016).

Matrix Metalloproteinases (MMPs) are enzymes with high proteolytic activity which degrade components of the ECM and are known to play an important role in matrix degradation in cancer cell motility (Wolf et al. 2003). Consistent with this, specific MMPs have been identified to be upregulated in different tumors (Lubbe et al. 2006; Poola et al. 2005). Recent studies have revealed that MMP9 can control cancer amoeboid migration in a catalytic-independent manner

by enhancing actomyosin contractility and increasing MLC2 phosphorylation to produce sustained blebbing for amoeboid invasion (Orgaz et al. 2014).

Plasticity or interconversion between these two cell motility modes has been described. For instance, silencing of DOCK10, a GEF specific for Cdc42, in melanoma cells was shown to promote elongated mesenchymal migration via the amoeboid to mesenchymal transition (AMT). This was associated with a decrease in actomyosin contractility as a result of reduced Rho activation and with reduced MLC2 phosphorylation (Gadea et al. 2008). Consistently, melanoma A375-M2 cells undergo an amoeboid to mesenchymal transition in a similar manner upon treatment with the ROCK inhibitor Y-27632 (Gadea et al. 2008). Alternatively, other studies have also demonstrated that mechanisms such as Rac inactivation induce a transition from mesenchymal mode to amoeboid motility (MAT) (Sanz-Moreno et al. 2008).

1.1.3. The role of tumor cell plasticity

Certain cell types are able to use different modes of motility and undergo transitions between them, a process also known as tumor cell plasticity (Figure 5). These transitions require phenotypical adaptation of the motile cells in response to the microenvironment. The ability of cells to switch between modes of invasion is controlled by the actin cytoskeleton and the extracellular matrix (ECM), and involves several factors such as actomyosin contractility, Rho signaling and the formation of actin-rich protrusions (Paňková et al. 2010; Friedl and Wolf 2010).

Cell plasticity allows cells to undergo mesenchymal to amoeboid transition (MAT) and amoeboid to mesenchymal transition (AMT) as an adaptive response to the environment. These modes of invasion are interconvertible (Figure 5) and for instance, mesenchymal to amoeboid transition can be induced in cancer cells by reducing the concentration of fibers in the ECM. This results in a weakness of cell-ECM adhesion enhancing activation of the Rho signaling pathway and increasing actomyosin contractility (Sahai and Marshall 2003). In addition, MAT is induced in cancer cells by blocking key invasion components such as MMPs (Wolf et al. 2003). Unlike MAT, the underlying mechanisms driving the amoeboid-mesenchymal transition (AMT) include inhibition of Rho signaling, abrogation of pericellular proteolysis and weakening of cell-ECM adhesions. Moreover, epithelial cancer cells can undergo a transition from collective invasion to motile individual cells, known as the epithelial-mesenchymal-transition (EMT) as a result of impaired cell-cell junctions caused by alterations in gene transcription (Friedl and Wolf 2003; Gandalovičová et al. 2016).

Dynamic rearrangement of the actin cytoskeleton is required for cell motility and invasion, and the molecular mechanisms and signaling involved are crucial for understanding these processes. Hence, the next chapter will focus on the actin cytoskeleton and its role in cellular functions.
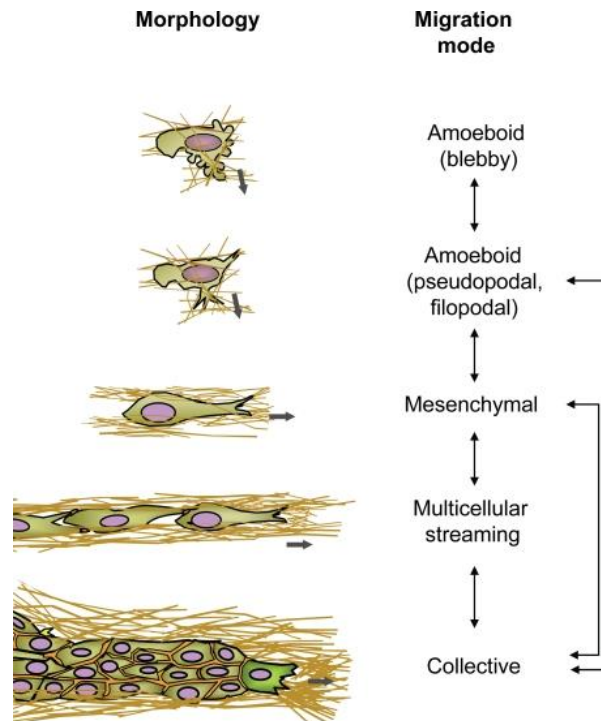
Figure 5: Mechanisms of cancer cell motility. This model shows the plasticity between the different modes of cancer cell migration. The latter can occur individually or collectively. Migratory plasticity allows interconversion between the different invasion modes, which are characterized by the cell morphology and regulated by different molecular mechanisms. When cell-cell junctions remain, cells undergo the collective invasion moving as multicellular streams, budding or large clusters. Alternatively, cells using the individual mode of invasion can use different protrusion-based mechanisms such as the elongated-mesenchymal or the bleb-dependent rounded amoeboid mode. Alteration of different parameters can lead to plasticity and conversion from one migration mode to another. This image was taken from (Friedl and Wolf 2010).

1.2.   The role of the actin cytoskeleton

The actin cytoskeleton is an important network of filaments and regulatory proteins that is crucial for cell shape, migration, cytokinesis and intracellular transport (Fletcher and Mullins 2010).

Eukaryotic cells have three different types of filaments: actin filaments, microtubules and intermediate filaments. Actin filaments are the thinnest filaments of the cytoskeleton with a diameter of 6-8 nm (Heath and Dunn 1978), and its network is modulated by dynamic actin polymerization and depolymerization (Bugyi and Carlier 2010).

1.2.1. Introduction to actin

Actin is found in two different forms, globular monomeric actin (G-actin) and filamentous actin (F-actin). Actin is a 42 kDa protein and its filaments are organized in double helical structures. Actin filaments can cooperate with bundling proteins to generate mechanical functions, including cell motility, cell shape, cell adhesion and transcription (Tseng et al. 2005), which are regulated through changes between monomeric and filamentous actin (Pollard and Cooper 2009). Actin polymerization occurs when G-actin assembles into actin filaments (Holmes et al. 1990), and the constant process of actin polymerization at the plus end (or also called barbed end) and simultaneous depolymerization at the minus end (or also called pointed end) is known as actin treadmilling (Figure 6) (Pollard and Borisy 2003).

Actin treadmilling which is also called "head to tail polymerization" is controlled through ATP hydrolysis (Wegner 1976), and plays an important role in driving cell motility (Small 1995; Bugyi and Carlier 2010). The regulation of ATP hydrolysis and ADP to ATP exchange are crucial for the speed of the actin treadmill (Pollard and Borisy 2003). ATP-bound G-actin is incorporated at the plus end of the filament and the bound ATP gets hydrolysed to ADP after polymerization. Then, ADP-bound G-actin located at the minus end of the filament readily disassembles (Figure 6) (Le and Carlier 2008; Dominguez and Holmes 2011).

Actin filament formation and its dynamics are highly regulated processes, not only by the regulation of ATP hydrolysis, but also by the action of several actin binding proteins (ABPs) (Figure 6). These include the capping proteins that control filament assembly and disassembly. Gelsolin binds at the plus end of F-actin to prevent polymerization (Kim, Cooper, and Sept 2010), tropomodulin binds at the plus end to block actin association (Yamashiro et al. 2012) and profilin binds to ATP bound G-actin, thereby promoting actin polymerization (Pring, Weber, and Bubb 1992). Additionally, actin treadmilling is also modulated in response to extracellular and intracellular signals in conjunction with Rho-GTPases.
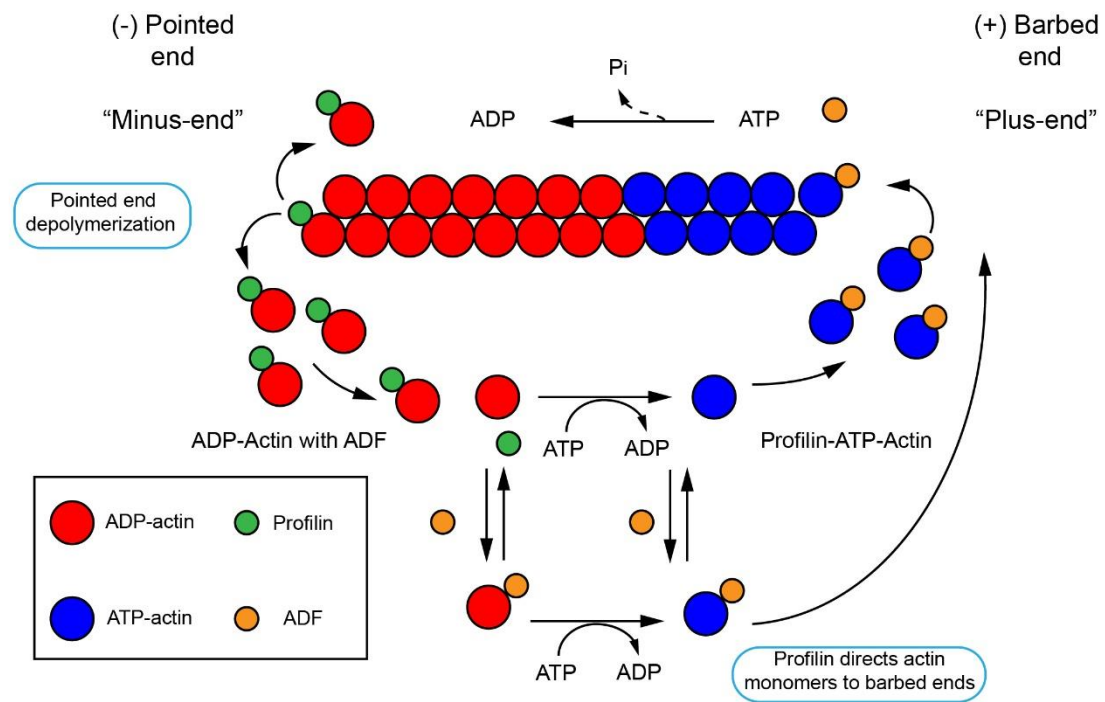
Figure 6: Regulation of actin treadmilling. Actin monomers polymerize into double-helical filaments. Profilin forms a complex with ATP-bound G-actin, which is preferentially added to the barbed end of the filament. Upon hydrolysis of the ATP to ADP, the filament is destabilized while the pointed end associates with actin-depolymerizing factors (ADFs). This leads to depolymerization of F-actin at the pointed end to free ADP-bound G-actin. As a result, nucleotide exchange recycles ADP-G-actin to ATP-G-actin, which can again be bound to profilin to restart the actin treadmill (Le and Carlier 2008).

Given that spontaneous polymerization of actin dimers or trimers is energetically unfavourable and to maintain an equilibrium between assembly and disassembly of actin filaments at steady state, additional factors called nucleation promoting factors (NPFs) are required for *de novo* actin filament formation (Pollard and Cooper 2009). Actin nucleating factors can be divided into three classes: 1) the Arp2/3 (actin-related protein 2/3) complex, 2) the tandem monomer-binding nucleators like Spire and 3) the formins. This latter family is defined by a conserved formin homology 2 domain and, in particular, the diaphanous subfamiliy (mDia) will be addressed in this study. These are fundamental regulators of the formation of actin structures such as lamellipodia, filopodia and bleb protrusions, which are essential for biological functions such as cell migration, cytokinesis, cell adhesion and morphogenesis (Bugyi and Carlier 2010; Chesarone, DuPage, and Goode 2010).

1.2.2. Organization of the actin cytoskeleton during cell processes

The dynamic actin cytoskeleton plays an important role for many physiological and pathological functions. Actin is responsible not only for the formation of membrane protrusions at the leading edge, including cellular extensions like lamellipodia, filopodia, microvilli, ruffles (Chhabra and Higgs 2007), but also other membranes protrusions, such as podosomes (Gimona et al. 2008) and membrane blebs (Fackler and Grosse 2008). These actin-driven structures are important controlling directionality in cells cultured in 2D and 3D environments (Nürnberg, Kitzing, and Grosse 2011). Furthermore, organization of actin filaments defines the cellular phenotype modulated through Rho-GTPases. For instance, filopodia protrusions are mainly regulated by Cdc42, lamellipodia protrusions are Rac-dependent, while bleb protrusions are Rho-dependent (Lehtimaki, Hakala, and Lappalainen 2017).

Actin structures are relevant for a wide variety of cellular processes including, among others, cytokinesis (Glotzer 2001), cell adhesion (Adams 2004), endocytosis (Kaksonen, Toret, and Drubin 2006), cell shape (Pollard and Cooper 2009), cell migration (M. F. Olson and Sahai 2009) and cell polarity (Dominguez and Holmes 2011).

The dynamic organization of the actin cytoskeleton is critical for cell migration in development and disease. For example, cell migration is necessary for gastrulation in zebrafish germ cells, while neoplastic diseases are characterized by high levels of metastatic cell migration. Thus, cell migration and motility of cells are fundamental to understand invasiveness and metastasis of tumor cells. Actin polymerization takes place at the cell front leading to the formation of actin structures, whereas Rho-ROCK-mediated actomyosin contractility occurs at the rear edge of the cell providing actin-dependent force generation to drive cell motility (Anne J. Ridley 2011; Lehtimaki, Hakala, and Lappalainen 2017).

Invasive cell migration requires actin assembly, which is the essential driving force to generate protrusive membrane structures such as plasma membrane blebs, invadopodia or pseudopodia (Figure 7). Besides the rearrangement of the actin cytoskeleton is critical for structures like invadopodia and lamellipodia, some evidence has shown that bleb-dependent invasion is the most efficient way of migration and requires less energy than the lamellipodium or filopodia-mediated motility (G. Charras and Paluch 2008). Consistent with this, the work presented in this thesis is focused on bleb structures, which are known to regulate migration and invasion in invasive cancer cell phenotypes. Additionally, plasma membrane blebs are regulated through the actomyosin cortex, which will be addressed in the following chapters.
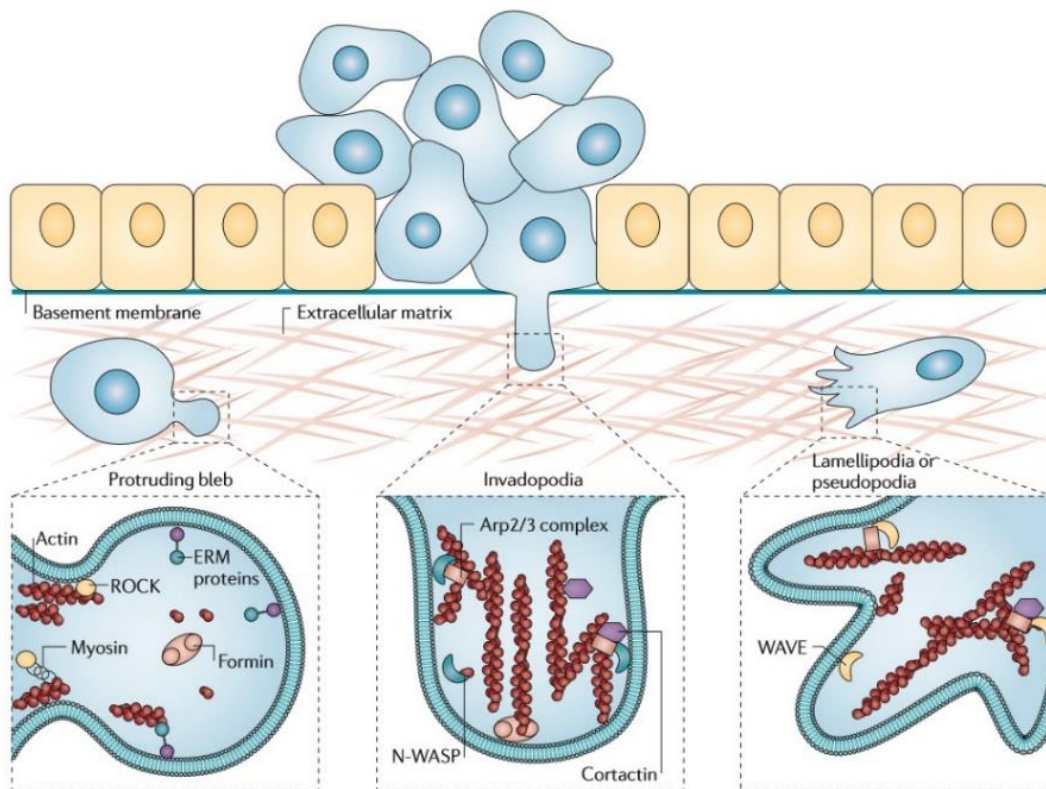
Figure 7: Protrusive actin-driven structures in cancer cell invasion. Cancer cell invasion phenotypes require the rearrangement of the actin cytoskeleton, which in turn involves the formation of different actin-driven protrusions, such as plasma membrane blebs, invadopodia or pseudopodia. The image was taken from (Nürnberg, Kitzing, and Grosse 2011).

1.3. Plasma membrane blebbing

Plasma membrane (PM) blebbing is required for cell motility during tumor cell invasion and metastasis (Sahai and Marshall 2003; Madsen et al. 2015). Cancer cells can move generating different actin-rich plasma membrane protrusions, such as lamellipodia and filopodia when cultured on rigid matrix or generating membrane blebs in 3D extracellular matrix (M. Bergert et al. 2012).

1.3.1. Plasma membrane bleb structures

Cellular blebs, first described as bubbles (Holtfreter 1943), are spherical membrane protrusions generated by changes in hydrostatic pressure at the contractile cell cortex (Cunningham et al. 1992). These structures are highly dynamic actin-regulated cell protrusions as a result of membrane detachment from the actin cell cortex (Guillaume T Charras et al. 2006) involved in common physiological features from different cellular processes, including cell motility, apoptosis, cell spreading, cell migration and cytokinesis (Fackler and Grosse 2008). In addition, blebs are actin-driven structures observed in different cell types such as zebrafish germ cells, ameba, parasites, bacteria, fibroblasts, endothelial cells, mesenchymal cells, immune cells and tumor cells (Sanz-Moreno et al. 2008; Blaser et al. 2006; Norman, Sengupta, and Aranda-Espinoza 2011; Laster and Mackenzie 1996; Loitto et al. 2002; Ruprecht et al. 2015; Tournaviti et al. 2007; Angus et al. 2008).

These protrusions of the PM can be either reversible (non-apoptotic blebs) or irreversible (apoptotic blebs). Apoptotic blebbing during cell death is uniform and leads to cell lysis, whereas non-apoptotic prominent blebbing has a polarized distribution allowing cell motility during cell migration (G. Charras and Paluch 2008). Both types of blebbing are induced in response to different mechanical or chemical stimuli resulting in contraction of the actin cortex and thereby, initiating signaling transduction pathways that are regulated by the rearrangements of the actin cytoskeleton (Guillaume T Charras et al. 2006). Non-apoptotic blebbing is typically defined by the dynamic bleb cycle.

In general, the bleb cycle is divided in three phases: rapid bleb expansion, a short static phase and slower bleb retraction. Disruption of the plasma membrane from the actin cortex is caused by an increase of intracellular hydrostatic pressure generating bleb growth. Bleb expansion, which usually lasts about 5-30 seconds, is characterized by the protrusion of the plasma membrane and the recruitment of the actin-membrane linkers such as ERM proteins and the epidermal growth factor Eps8 to the protruding bleb membrane. Blebs can expand up to 2 µm from the plasma membrane, until actin reassembly occurs at the bleb cell cortex. As a result,

forces derived from actomyosin contractility mediate bleb retraction, which occurs in about 60-120 seconds (Figure 8) (Guillaume T Charras et al. 2005, 2006, 2008; Aoki et al. 2016).
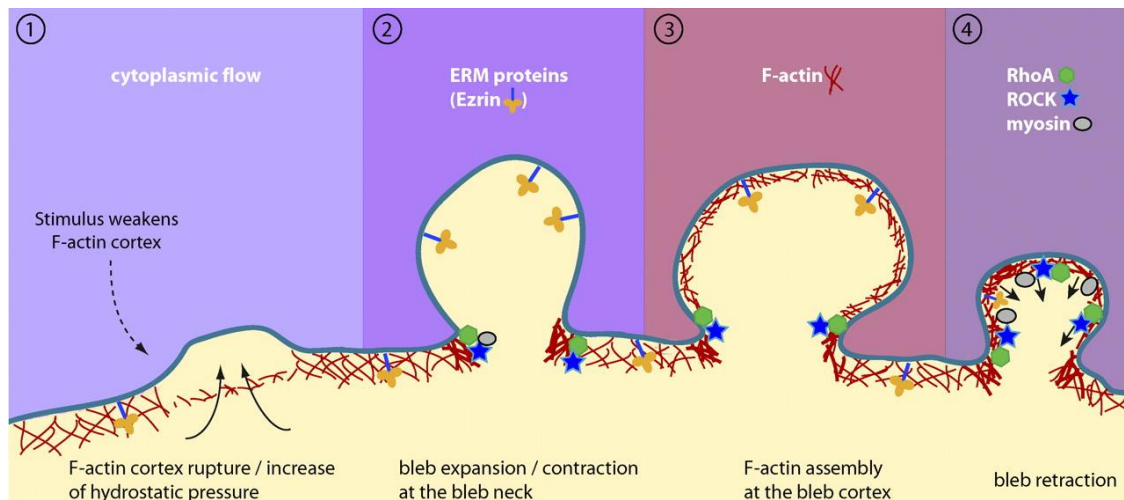
Figure 8: The life cycle of a plasma membrane bleb. The bleb cycle is initiated by extracellular triggers, which results in disruption of the PM-actin cortex leading to an increase of hydrostatic pressure generating bleb expansion (1). The protrusion of the plasma membrane is characterized by the recruitment of actin-membrane crosslinkers of the ERM family such as Ezrin (2). Then, cortical actin assembly takes place during a static phase (3), followed by actomyosin contractility to retract the bleb (4). This image was taken from (Fackler and Grosse 2008).

1.3.2. Actin regulation during PM blebbing

Plasma membrane blebbing is dependent on the actin cytoskeleton and regulated by different factors including actin polymerization, actomyosin contractility, substrate rigidity and the ECM. Several studies have reported that Rho-ROCK signaling drives PM blebbing through activation of the ERM proteins (G. T. Charras 2008). RhoA activates the actin nucleator mDia1, which is essential for membrane blebbing (Thomas M Kitzing et al. 2007; Purvanov et al. 2014). Other formins, such as FHOD1 and DIAPH3, have been shown to be recruited to membrane blebs (Stastna et al. 2012; Hannemann et al. 2008). Recent studies identified the epidermal growth factor receptor kinase substrate 8 (Eps8) together with the Rho family protein Rnd3 as key regulators for the formation of bleb structures mediated by Rho-ROCK signaling. When Rnd3 is recruited to blebs, RhoA is activated inducing ROCK-dependent phosphorylation of Ezrin. In addition, enhancing recruitment of Eps8 to the bleb cortex will lead to bleb retraction through myosin activation downstream of RhoA (Aoki et al. 2016).

1.4. The actomyosin cell cortex

The cellular cortex is a thin actomyosin network tightly bound to the plasma membrane which controls cell shape changes by the action of cellular mechanics. This actomyosin cortex is composed of cortical actin filaments crosslinked with actin-binding proteins (ABP), and generates cortical tension to modulate changes in cell shape, which contributes to cell migration, morphogenesis, cell division, cell polarization and cell-cell contact formation (Stewart et al. 2011; Sedzinski et al. 2011; Levayer and Lecuit 2012; Chugh and Paluch 2018).

1.4.1. The cell cortex composition

The cellular actin cortex composition was first evaluated in isolated individual cellular blebs from human melanoma M2 cells using mass spectrometry. This study identified several actin-binding proteins (ABP) including, among others, actin crosslinkers, nucleators, capping proteins, actin-membrane linkers, myosin motors, scaffold proteins and contractility regulators (Biro et al. 2013).

Actin filament nucleators like formins are found at the cortex where they nucleate and elongate actin filaments (Bovellan et al. 2014). Other regulators of actin assembly and disassembly are the capping proteins, profilin and cofilin, which act by binding to actin monomers to enhance actin polymerization to control cellular processes like cell division. In addition, the actin crosslinkers α-actinin, filamin and fascin play a role in organizing actin filaments into networks in the cell cortex to regulate actomyosin contractility (Ennomani et al. 2016). Moreover, myosin motors are key components providing contractile cortical tension, and together with actin crosslinkers and the actin-membrane linkers they control actomyosin contractility within the cell cortex (Biro et al. 2013). Importantly, actin-membrane linkers such as myosin and ERM (Ezrin, Radixin, Moesin) proteins were shown to be required for the association of the plasma membrane (PM) with the underlying cortical actin cytoskeleton and to contribute to PM tension (Anthony Bretscher, Edwards, and Fehon 2002; Biro et al. 2013; Diz-Muñoz et al. 2010).

1.4.2. The ERM proteins

The Ezrin, Radixin and Moesin (ERM) proteins are an evolutionary conserved group of proteins of the FERM superfamily (Sato et al. 1992). The first protein identified was Ezrin (80 kDa) which was originally detected at the microvillus cytoskeleton from chicken intestinal epithelial cells (A Bretscher 1983). A few years later, Radixin (82 kDa) was purified from cell-cell adherent junctions isolated from rat liver (Tsukita, Hieda, and Tsukita 1989). Moesin (78 kDa) was first found as a heparin-binding protein isolated from smooth muscle cells in bovine uterus (Lankes et al. 1988).

This family of actin-membrane linkers are defined by their common N-terminal region, the FERM (Four-point-one ERM) domain (Gary and Bretscher 1995). They are essential for many cellular processes including signal transduction pathways, cell division (Kunda et al. 2008; McClatchey 2014), morphogenesis (Crepaldi et al. 1997; Gautreau, Louvard, and Arpin 2000), cell adhesion (Takeuchi et al. 1994; Pujuguet et al. 2003), cell migration (Crepaldi et al. 1997; Valderrama, Thevapala, and Ridley 2012), and pathological conditions such as cancer cell invasion and metastasis (Martin et al. 2003; Mak et al. 2012; Clucas and Valderrama 2015).

Structurally, these fundamental cell cortex integrators are organized with a N-terminal FERM domain containing the F1, F2 and F3 subdomains. The FERM domain is followed by an α-helical domain, a linker region and the carboxy-terminal domain known as C-terminal ERM-association domain (C-ERMAD), which is able to bind the FERM domain or F-actin depending on the protein conformation (Figure 9) (Arpin et al. 2011; Fehon, McClatchey, and Bretscher 2010).

Originally, the F-actin binding site was identified at the C-terminus of Ezrin in its active state (Turunen, Wahlström, and Vaheri 1994). The C-ERMAD domain is bound to the FERM domain in the autoinhibited state of Ezrin (Gary and Bretscher 1995).
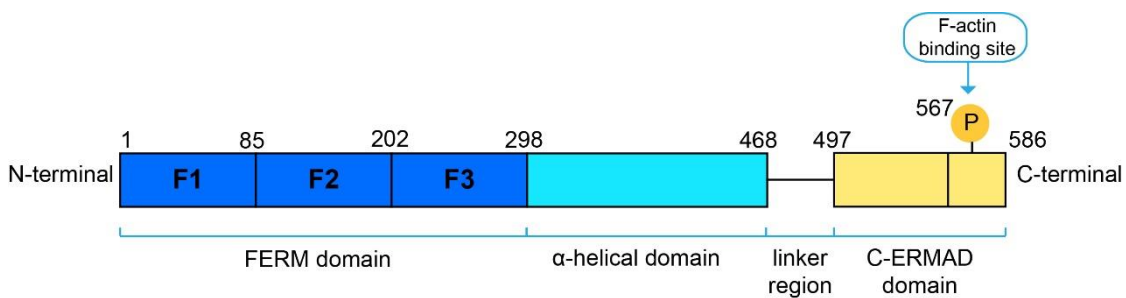
Figure 9: Domain structure of ERM proteins. ERMs are composed of an N-terminal FERM domain (dark blue), which consists of three subdomains: F1, F2 and F3. The FERM domain is followed by an α-helical domain (light blue), a linker region and the C-terminal domain called C-ERMAD (yellow), where F-actin binding and phosphorylation take place (Arpin et al. 2011; Fehon, McClatchey, and Bretscher 2010).

1.4.2.1. Regulation and function of ERM proteins

The function of the ERM proteins is regulated by an open (active) and a closed (inactive) conformation. Both structures are controlled via conformational changes resulting from the action of phospholipids and kinases (Canals et al. 2010).

First studies reported that the regulation of ERM proteins is dependent on conformational changes, in which the intramolecular association between FERM and C-ERMAD leads to the dormant form of the Ezrin protein (Gary and Bretscher 1995). Subsequent studies showed that ERM activation is a two-step process with sequential events involving FERM domain recruitment to plasma membrane regions rich in Phosphatidylinositol 4,5-bisphosphate (PIP_2) (Niggli et al.

1995; Hirao et al. 1996), which then triggers phosphorylation of threonine residues at the F-actin binding site (Yonemura S, Matsui T 2002). Thus, activated ERMs are associated with the plasma membrane bound to membrane proteins through their N-terminal FERM domain and to F-actin through the C-terminal C-ERMAD domain (Figure 10). In contrast, inactive ERMs remain in a resting state through self-association until the FERM domain initiates its activation by binding PIP$_2$ (Fehon, McClatchey, and Bretscher 2010; Anthony Bretscher, Edwards, and Fehon 2002) (Figure 10).
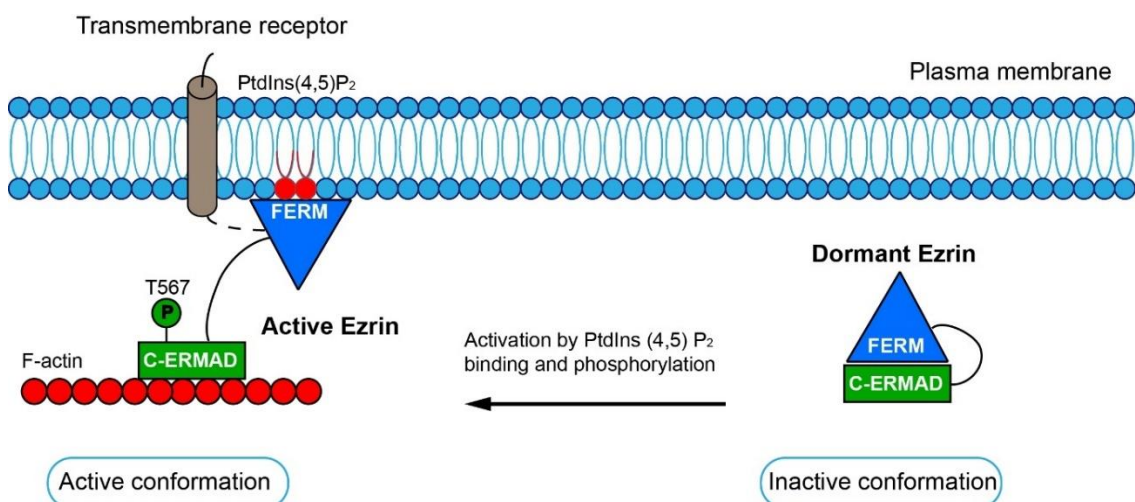
Figure 10: ERM activation by phosphorylation. ERM proteins are found in two different states, an active "open" conformation and a dormant, inactive "closed" conformation. Dormant Ezrin is defined by a direct inhibitory association of the FERM and C-ERMAD domain. ERM proteins are activated through PIP$_2$ binding. Thereby, ERMs are recruited to the plasma membrane leading to subsequent phosphorylation at T567 by Rho-kinase or PKC, which reduces the affinity of the FERM for the C-ERMAD domain. This allows them to bind transmembrane receptors linking the actin cortex to the plasma membrane and initiating different signaling transduction pathways (Fehon, McClatchey, and Bretscher 2010; Anthony Bretscher, Edwards, and Fehon 2002).

Hence, ERM phosphorylation is a key process controlling the regulation and activation of these actin-membrane linkers proteins. The first identification of the phosphorylation sites regulating ERMs was at the threonine 558 (T558) in Moesin upon platelet activation (Nakamura, Amieva, and Furthmayr 1995). Later on, studies revealed that phosphorylation of the corresponding threonine in Ezrin and Radixin reduces the affinity of the C-ERMAD for the FERM domain (Matsui et al. 1998). Accordingly, expression of the phosphomimetic threonine residue T567D (constitutively active form) shows a remarkably reduction in the oligomerization of Ezrin at the plasma membrane (Fievet et al. 2004). Alternatively, expression of the non-phosphorylatable

T567A Ezrin (inactive form) is found to be poorly associated with the actin cytoskeleton (Gautreau, Louvard, and Arpin 2000).

Several kinases have been reported to phosphorylate the conserved threonine residues: Rho-associated kinase (ROCK) (Matsui et al. 1998), protein kinase Cα (PKCα) (Ng et al. 2001), PKCθ (Pietromonaco et al. 1998), G-protein coupled receptor kinase 2 (Cant and Pitcher 2005), Nck-interacting kinase (Baumgartner et al. 2006), Lymphocyte-oriented kinase (LOK) (Belkina et al. 2009) and MST4 (ten Klooster et al. 2009). Activated ERM proteins bind several transmembrane receptors through their FERM domain via direct association with cytoplasmic tails of receptor tyrosine kinases (RTKs) and growth factor receptors (Crepaldi et al. 1997; Reczek, Berryman, and Bretscher 1997). ERM proteins also associate with co-receptors like CD44 for directional cell motility (Legg et al. 2002) or with the Intercellular Adhesion Molecule-2 (ICAM-2) for recruitment by natural killer cells (Helander et al. 1996).

Even though these proteins are known to interact with transmembrane receptors upon ERM activation, they are consequently involved in signal-transduction pathways by association with signaling molecules, for instance the RhoA signaling pathway. RhoA, a GTPase, is a key regulator of the cortical actin cytoskeleton and previous work has shown the importance of ERMs as RhoA downstream effectors mediating cytoskeletal rearrangements (Hirao et al. 1996; Mackay et al. 1997). Interestingly, ERM proteins have also been reported to play a crucial role upstream of the RhoA pathway (Hatzoglou et al. 2007). Therefore, ERM proteins regulate Rho-signal transduction pathways.

ERM proteins are involved in regulating diverse cell functions through reorganization of the cytoskeleton during development and differentiation. These include stable maintenance of oocyte polarity, allowing mitotic rounding and spindle orientation during cell division, driving epithelial morphogenesis and apical surface formation, controlling cell-cell junction assembly and playing a role during podocyte formation (Fehon, McClatchey, and Bretscher 2010; Arpin et al. 2011; McClatchey 2014). Besides the broad functions of ERMs during development, further studies have also shown their pivotal role in physiology and disease. For instance, these proteins participate in cancer progression, metastasis, melanoma cell migration, leukocyte adhesion, B cell activation and the formation of the immunological synapse (Pore and Gupta 2015; Clucas and Valderrama 2015; Lorentzen et al. 2011).

Activation of Moesin (the only ERM in Drosophila) in Drosophila S2 cells is crucial for cortical stability, microtubule organization and spindle morphogenesis during mitosis (Kunda et al. 2008; Carreno et al. 2008), whereas in mammalian cells activation of ERM proteins is essential for a functional spindle orientation during mitosis (Machicoane et al. 2014).

Several studies provided evidence for the crucial role of ERMs in plasma membrane protrusions. Moesin and Ezrin are required for efficient bleb retraction (Guillaume T Charras et al. 2006). Consistent with this, ERM proteins are known to be essential at the actin cortex for plasma membrane attachment and bleb-based cell migration (Paluch and Raz 2013). However, interfering with ERM activity decreases membrane to cortex attachment, which in turn increases the proportion of cellular blebs and triggers a reduction in the directionality of migrating cells in zebrafish during gastrulation (Diz-Muñoz et al. 2010). Alternatively, increased overall ERM activity is associated with reduced cell blebbing in melanoma cells, mast cells and zebrafish germ cells (Lorentzen et al. 2011; Paluch and Raz 2013).

1.4.3. Ezrin and its role in cell invasion

Although ERM proteins have been reported to be involved in several cellular processes, alteration of their physiological expression level might lead to aberrant gene expression enhancing cancer progression through the metastatic cascade. Consistently, Ezrin has been identified as a metastasis-associated protein and therefore plays a crucial role during cancer progression (Clucas and Valderrama 2015). However, the mechanisms by which Ezrin contributes to a metastatic phenotype still remain unclear. Since then, understanding the role of Ezrin in cancer cell invasion has been an emerging topic.

Overexpression of Ezrin has been related to an increase in metastatic potential in different tumor entities, such as osteosarcoma (Ren et al. 2009), breast cancer (Elliott et al. 2005), lung cancer (Deng et al. 2007), pancreatic cancer (Meng et al. 2010), hepatocellular cancer (Kang et al. 2010), colorectal adenocarcinoma (Patara et al. 2011), prostate cancer (Y-C Chuan et al. 2010) and melanoma (Federici et al. 2009). In addition, a tissue microarray immunohistochemistry study supported a role for Ezrin expression in a wide number of human cancers (Bruce et al. 2007).

Interestingly, several studies revealed that Ezrin is implicated in tumor metastasis. For instance, mutation of the tyrosine Y477 leads to reduced cell migration and tumor invasion in breast carcinoma cells (Debnath and Brugge 2005; Mak et al. 2012). This suggests an important role for Y477, which is phosphorylated by Src in the regulation of tumor invasion and metastasis. Therefore indicates that the Src-Ezrin pathway may be a potential prognostic marker for human

breast cancer (Srivastava et al. 2005; Mak et al. 2012). In breast cancer cell lines, silencing of Ezrin resulted in decreased cell invasion in non-invasive MCF10A and metastatic MDA-MB-231 cells (Konstantinovsky, Davidson, and Reich 2012). Ezrin expression levels increase from benign to malignant breast cancers (Gschwantler-Kaulich et al. 2013). Furthermore, the well-known tumor suppressor gene BRCA1 is associated with ERMs at the plasma membrane and controls cell spreading and motility of breast cancer cells via ubiquitin ligase activity (Figure 11) (Coene et al. 2011). Other features like abnormal Ezrin distribution are also associated with invasive breast carcinomas (Sarrió et al. 2006). In addition, Ezrin localization switches from the apical membrane to the cytoplasm in lung cancer cells, and Ezrin expression was notably increased in highly metastatic lung cancer cell lines (Li et al. 2012). These findings suggest that Ezrin localization is fundamental for its activation leading to signal transduction pathways regulating cancer progression (Figure 11).
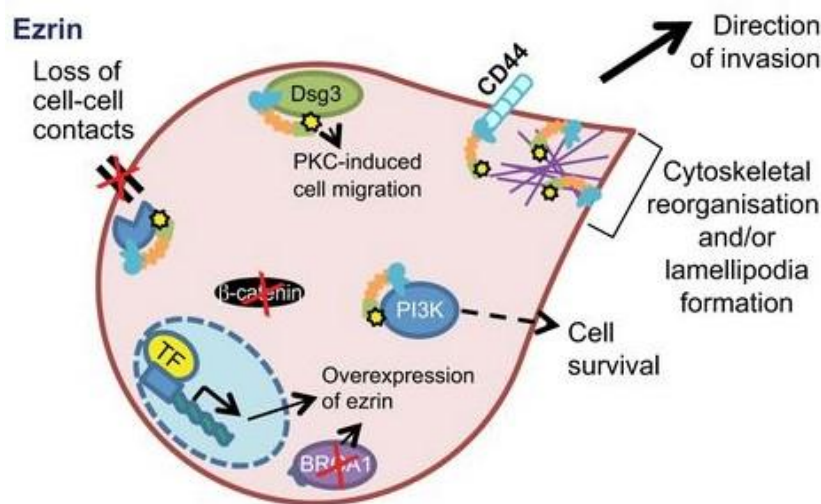
Figure 11: Ezrin in cancer progression. This cartoon illustrates the oncogenic potential of Ezrin in epithelial cells. Ezrin overexpression increases survival of cancer cells, thereby allowing invasion into other tissues, and interferes with cell-cell contacts. Additionally, Ezrin is upregulated in a Myc-dependent manner and downregulated by the tumor suppressor BRCA1. This image was adapted from (Clucas and Valderrama 2015).

A recent study has identified a mechanism by which Dsg3 regulates the transcriptional factor AP-1 and PKC through Ezrin phosphorylation in cancer cell invasion (Figure 11) (Brown et al. 2014). A role for Ezrin in cell adhesion has been determined where it controls E-cadherin-dependent adherens junctions through Rac-1 activation (Pujuguet et al. 2003). Moreover, loss

of E-cadherin function enhances tumor progression (Canel et al. 2013), which it is regulated by Ezrin (Figure 11).

Ezrin also plays a role in prostate cancer. Depletion of Ezrin or overexpression of the T567A dominant-negative mutant resulted in reduced androgen-mediated prostate cancer invasion (Yin-Choy Chuan et al. 2006), indicating the importance of Ezrin phosphorylation and its correlation with tumor invasiveness. Importantly, early studies already highlighted that Ezrin activation is essential for transformation, in particular overexpression of the mutant T567A inhibited cell transformation by the DbI and Net oncogenes (Tran Quang et al. 2000). Consistent with this, an increase of Ezrin expression in prostate cancer is associated with higher expression of the Myc oncogene. Further studies showed that Ezrin regulates Myc through the PI3K/Akt pathway, which in turn is essential for cancer cell invasion (Y-C Chuan et al. 2010). These data supported the notion that Myc-dependent effects leading to Ezrin overexpression are mediated by the PI3K/Akt pathway (Figure 11). Together, Ezrin has multiple effects on tumor metastasis, including adhesion, tumor extravasation and invasiveness. Thus, Ezrin has emerged as a potential therapeutic target for cancer therapy.

1.5. Entosis

Entosis is a cell-in-cell phenomenon that has been observed in several human malignancies, for instance in pleural exudates from metastatic breast cancer. Entosis is defined by homotypic cell-in-cell invasion, in which one cell actively invades into a neighbouring cell where it undergoes non-apoptotic cell death (Overholtzer et al. 2007). A recent study reported that non-apoptotic plasma membrane blebbing together with polarized actin dynamics are the driving force for entotic invasion in MCF10A cells (Figure 12) (Purvanov et al. 2014).

Cell-in-cell structures are found in many human tumors including breast carcinoma, melanoma, pancreatic carcinoma, cervical carcinoma, liver carcinoma, urothelial carcinoma, stomach carcinoma or colon carcinoma, but also among non-invasive epithelial cells (Overholtzer and Brugge 2008). Thus, entosis is prevalent in cancer and like matrix detachment, anchorage independence, aberrant proliferation or metabolic stress represents a hallmark feature of cancer cells (Hanahan and Weinberg 2011).
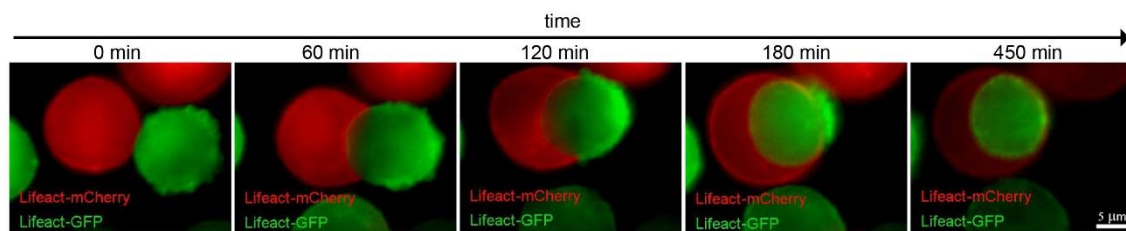
Figure 12: PM-blebbing provides the driving force for entotic invasion. This time series shows MCF10A cells in suspension undergoing entosis. A blebby cell stably expressing LifeAct-GFP to label the actin cytoskeleton invades into another non-blebbing cell expressing LifeAct-mCherry. Actin is enriched at the uropod-like structure at the rear end of the invading cell, which provides the driving force for invasion. This image was adapted from (Purvanov et al. 2014).

Entosis was described as an integrin-independent process that can be triggered by extracellular matrix detachment under conditions of low adhesion (Overholtzer et al. 2007). However, recent studies revealed additional triggers for entotic cell-in-cell invasion in adherent epithelial cells. For example, nutrient starvation can induce entosis in adherent cells. In particular, long term glucose starvation enhances entosis via AMP-activated protein kinase (AMPK) activity dependent on changes in cell stiffness (Hamann et al. 2017). Interestingly, mitosis has been identified as a trigger for entotic invasion in dividing epithelial adherent cells through mitotic rounding mediated by inhibition of Cdc42 in a RhoA-dependent manner (Joanne Durgan et al. 2017).

Entotic invasion requires expression of the tumor suppressor E-cadherin as well as P-cadherin-associated epithelial adherens junctions between the entotic cells (Sun, Cibas, et al. 2014). As a result of epithelial cell-cell contacts, polarized actomyosin contractility is necessary in the invading cell to provide the mechanical force allowing cell engulfment, which is regulated by Rho-actin signaling and changes in mechanical deformability between the inner and outer cell (Overholtzer et al. 2007; Sun, Luo, et al. 2014). Consistent with this, recent studies identified the G-protein-coupled LPA receptor 2 (LPAR2) as a promotor of entosis, thus providing evidence that extracellular cues can trigger cell-in-cell invasion (Purvanov et al. 2014).

After cell-in-cell invasion, the most common fate for the invading cell is non-apoptotic cell death where the host cell kills and digests the internalized cell through cell cannibalism. This is mediated by non-canonical autophagy, lysosomal degradation and nutrient recovery (Figure 13). In contrast to phagocytosis, the internalized target cells are viable inside the entotic vacuole for an extended period of time. In addition, other cell fates after internalization have been observed in which cells occasionally are able to escape from their host cells or divide inside them (Figure 13) (Overholtzer et al. 2007; Florey et al. 2011). Although the consequences of entosis are not well known, some evidence indicates that entosis triggers cancer cell aneuploidy enhancing tumor progression. Indeed, after internalization, the host cell sometimes divides, but often fails due to aberrant cell division leading to multinucleation, which in turn enhances aneuploidy and genomic instability (Figure 13) (Matej Krajcovic et al. 2011; Matej Krajcovic and Overholtzer 2012; Sun, Luo, et al. 2014). Consistently, the outer cell has been shown to recover nutrients from the digested inner cell, promoting cell survival and proliferation (M. Krajcovic et al. 2013). A recent study reported that expression of the tumor suppressor CDKN2A inhibits formation of cell-in-cell structures (Liang et al. 2018). In contrast, other studies reveal that entosis could act as a tumor-suppressive mechanism to clear dysfunctional cells by cell death of the inner cell, for instance eliminating aberrant invading cancer cells after internalization (Figure 13) (Sun, Cibas, et al. 2014; Florey et al. 2011).

In conclusion, entosis is a form of non-apoptotic cell death, which can be induced by multiple triggers and it is regulated by Rho-actin-signaling and actomyosin contractile forces. However, the detailed mechanisms mediating entosis and the impact of transcriptional activity were unclear and will be elucidated on this thesis.
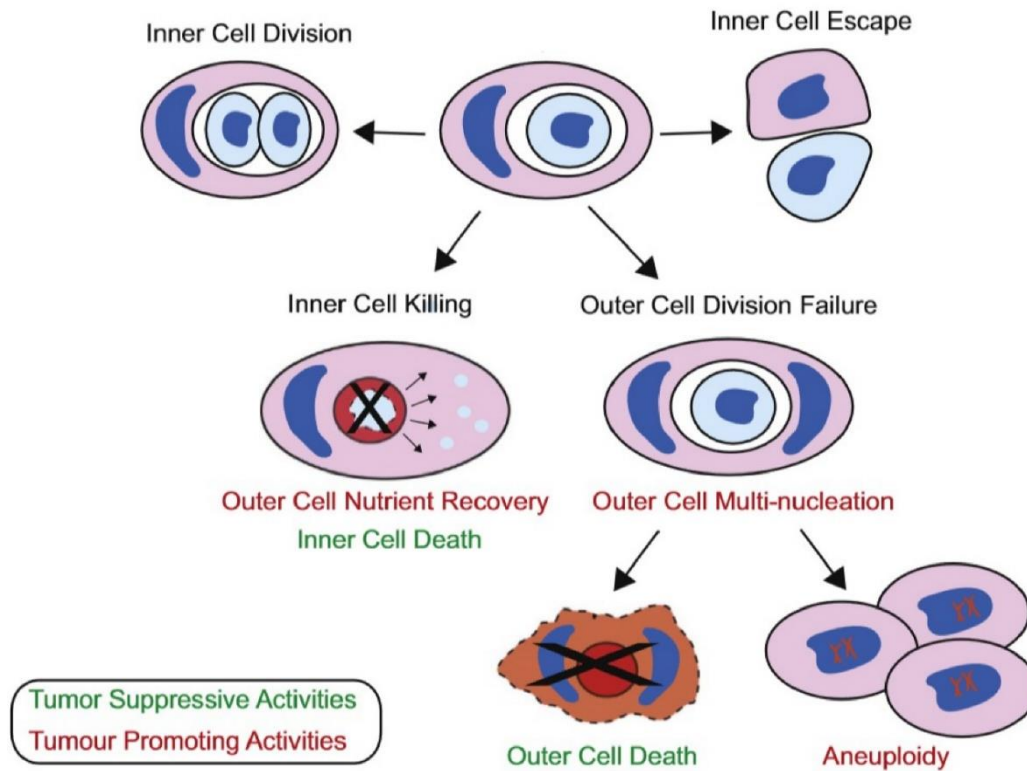
Figure 13: Consequences of entosis. Cell-in-cell structures most likely end in entotic cell death, whereby inner cell death occurs while the outer cell recovers nutrients from the digested internalized cell. Alternatively, some entotic cells undergo cell division inside their hosts or escape from the host cells. This process has been shown to present anti-tumorigenic effects as a result of killing the internalized tumor cell, whereas some evidence supports an oncogenic role, for instance cytokinetic failure in outer cells can promote aneuploidy. This image was adapted from (J. Durgan and Florey 2018).

1.6. Regulation of the MRTF/SRF transcriptional pathway

1.6.1. The SRF transcriptional network

SRF was discovered through the c-fos gene, a homolog oncogene of the FBJ murine osteosarcoma gene v-fos (Curran et al. 1982). Early studies with c-fos showed fast RNA synthesis upon exposure to growth or differentiation factors (Greenberg and Ziff 1984; Greenberg, Greene, and Ziff 1985). A study of the human c-fos gene revealed a cis-element called the Serum Response Element (SRE), which was identified to be required for c-fos serum stimulation (Treisman 1985) and led to the identification of the Serum Response Factor (SRF) (Treisman 1986). Analysis of the SRF-DNA interactions showed that SRF binds to its consensus sequence CArG-box, a palindromic $CC(A/T)_6GG$ sequence (Treisman 1986; Pellegrini, Tan, and Richmond 1995). This was also demonstrated later by genome-wide analysis (Sullivan et al. 2011; Esnault et al. 2014).

SRF requires the recruitment of co-activators: the Myocardin-related transcriptions factors (MRTFs) or the Ternary Complex Factors (TCFs). These two transcriptional cofactors are activated by different signaling pathways and control the expression of multiple target genes (Figure 14).

The TCF family is phosphorylated via Erk and activated by MAPK (Mitogen-Activated Protein Kinase) (Figure 14) (Gille, Sharrocks, and Shaw 1992; Janknecht et al. 1993). The MAPK signaling pathway activates TCFs in the nucleus and forms a complex with SRF at the TCF motif (Buchwalter, Gross, and Wasylyk 2004). The discovery of TCFs explained how activation of MAPK signaling via mitogens controls SRF regulated genes. Other evidence suggested the involvement of another signaling pathway, in which activation of SRF target genes was TCF-independent (C S Hill and Treisman 1995) by Rho-mediated signaling (Caroline S Hill, Wynne, and Treisman 1995). The discovery of Myocardin, which is involved in cardiac gene expression (D. Wang et al. 2001), led to the identification of Myocardin homologues termed Myocardin-related transcription factors MRTF-A and MRTF-B (D.-Z. Wang et al. 2002). Myocardin-related transcription factors are SRF transcriptional coactivators regulated via the Rho-actin pathway (Figure 14) (Miralles et al. 2003). TCFs and MRTFs are independently controlled, although both cofactors allow SRF to activate target gene transcription controlling the balance between cell proliferation and contractility (Figure 14) (Gualdrini et al. 2016).
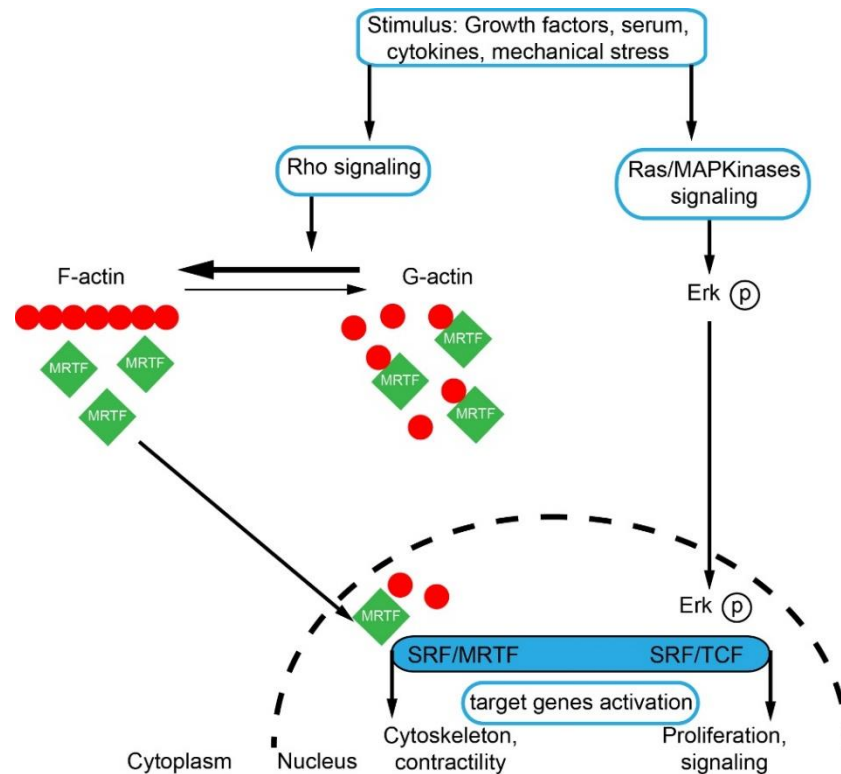
Figure 14: The SRF transcriptional network: TCF and MRTF. Serum Response Factor (SRF) is activated by two different families of transcription factors, the Ternary Complex Factors (TCFs) and the Myocardin-Related Transcription Factors (MRTFs). The TCF pathway links SRF activity to Ras-Erk signaling, while the MRTF pathway associates SRF activity to Rho-actin signaling. Both transcriptional co-activators compete for SRF binding and regulate gene expression. TCF-dependent transcription enhances the expression of genes involved in cell proliferation, whereas association with MRTFs controls cell contractility and pro-invasive behaviour (Esnault et al. 2014; Gualdrini et al. 2016).

1.6.2. The MRTF family of SRF coactivators

MRTF, also known as megakaryocytic acute leukemia (MAL) and myocardin like protein (MKL-1), has been shown to be involved in muscle differentiation and cell proliferation (Creemers et al. 2006; Wu et al. 2010).

MRTFs consist of a conserved N-terminal region containing the RPEL motif defined by the amino acid sequence Arg-Pro-X-X-X-Glu-Leu, which is essential for G-actin binding (Miralles et al. 2003; Guettler et al. 2008). The three RPEL sequences each interact with actin molecules. The linker sequences between RPEL1-2 and RPEL2-3 also bind two additional actin molecules with low affinity thereby creating a pentavalent G-actin-MRTF complex (Mouilleron et al. 2011). Moreover, the MRTF RPEL domain contains two elements called B2 and B3 (Figure 15), which are required for nuclear MRTF import allowing the NLS sequence to interact with importin α and β (Pawłowski et al. 2010).

MRTF further contains a B1 box necessary for ternary complex formation (TCF) and for the association of SRF with its target DNA. A hydrophobic region known as Q-box, rich in Q amino acids, affects MRTF nuclear localization and is responsible for its interactions with SRF. The MRTF C-terminal region contains the conserved SAP domain (SAF-A/B Acinus Pias) providing promoter specificity, followed by a leucine-zipper (LZ), which mediates homo- and hetero-dimerization, while the transactivation domain (TAD) is essential for SRF activation (Figure 15) (Miralles et al. 2003; Z. Wang et al. 2003; Zaromytidou, Miralles, and Treisman 2006; E. N. Olson and Nordheim 2010).
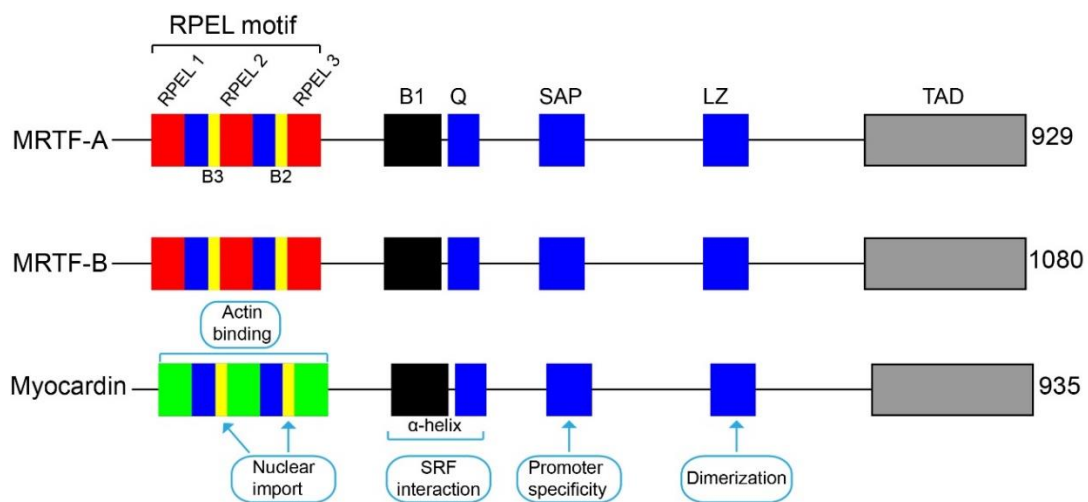
Figure 15: Structure of myocardin-related transcription factors (MRTFs). This figure shows the domain organization of the MRTF family, which consists of the myocardin-related transcription factors (MRTF-A and MRTF-B) and myocardin (MC). Numbers of amino acids are indicated for each myocardin family protein on the right. The RPEL motif contains actin binding sites and the regions B3 and B2, which are important for nuclear import, followed by the region B1 involved in ternary complex formation and the Glu-rich region Q. An α-helical region between the B1 and Q regions mediates association with SRF. All members of the MRTF family present a homologous SAP domain (also called as SAF-A/B, acinus, PIAS) required for promoter specificity and the LZ region (leucine zipper) enables MRTF homo- and heterodimerization. Finally, the TAD is the transactivation domain which is phosphorylated when MRTF is in the nucleus and bound to SRF (Miralles et al. 2003; E. N. Olson and Nordheim 2010).

1.6.3. Actin-mediated regulation of MRTF

MRTFs are well characterized actin-binding proteins involved in the regulation of SRF target genes (Gineitis and Treisman 2001). MRTF-mediated transcription is dependent on the rearrangement of the actin cytoskeleton (Miralles et al. 2003). The subcellular localization of MRTF in cells is determined by changes in actin dynamics (Posern, Sotiropoulos, and Treisman 2002). Stimulation of F-actin polymerization appears to sequester actin from MRTF (Miralles et al. 2003; Vartiainen et al. 2007). Thus, G-actin is dissociated from MRTF, thereby exposing the

nuclear localization sequence (NLS) at the RPEL domain for subsequent nuclear MRTF import (Pawłowski et al. 2010; Miralles et al. 2003). Alternatively, MRTF nuclear export is enhanced with the depolymerizing drug Latrunculin B (Lat B), which increases the monomeric G-actin concentrations (Vartiainen et al. 2007). Generally, nuclear import of MRTF leads to enhanced SRF transcriptional activity (Z. Wang et al. 2004) (Figure 16).

The MRTF-SRF signaling pathway is regulated by the Rho GTPase-dependent reorganization of the actin cytoskeleton. In particular, serum stimulation activates Rho GTPases for formin-mediated actin polymerization (Copeland and Treisman 2002). As a result, the G-actin concentration is reduced in response to Rho signaling, leading to MRTF nuclear accumulation, where MRTF binds to SRF and enhances SRF-dependent gene expression (Miralles et al. 2003). Previous studies from our group reported the importance of formins in nuclear actin polymerization (Baarlink, Wang, and Grosse 2013; Plessner et al. 2015). Importantly, MRTF is also regulated by phosphorylation, which in turn contributes to SRF transcriptional activation (Panayiotou et al. 2016). In conclusion, regulation of actin-MRTF/SRF transcription is controlled by phosphorylation, Rho activation and changes in F-actin/G-actin concentration (Figure 16).
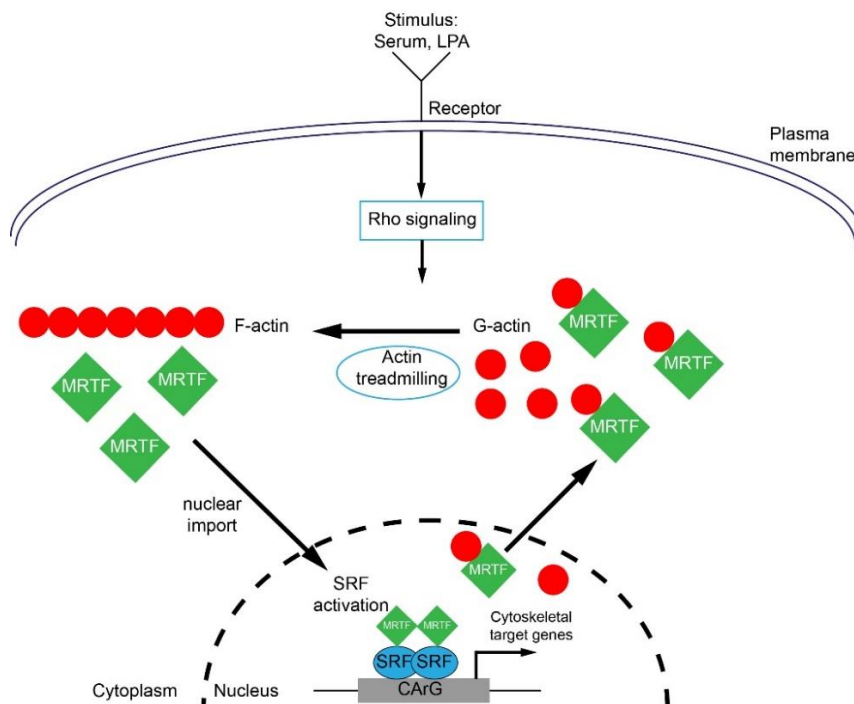
Figure 16: The actin-MRTF/SRF transcriptional feedback. Schematic representation of Rho-actin signaling to MRTF/SRF. A pool of cytoplasmic monomeric G-actin binds MRTF preventing MRTF nuclear translocation. Upon a stimulus such as serum or LPA, Rho signaling is activated and the total G-actin pool is depleted through increased actin polymerization. The change in the G/F-actin ratio releases MRTF, which accumulates in the nuclear compartment leading to SRF-dependent transcription of cytoskeletal target genes representing a feed-forward loop.

42

1.6.4. MRTF functions

Previous work has identified 960 serum-inducible SRF target genes, which are mostly controlled by MRTF (Esnault et al. 2014). MRTF/SRF-dependent target genes are involved during rearrangements of the actin cytoskeleton, thereby controlling cell motility, cell proliferation, cell contractility, cell adhesion, extracellular matrix synthesis, muscle differentiation and cell growth (Gualdrini et al. 2016; Esnault et al. 2014). Interestingly, a recent study showed that MRTF/SRF target genes are also dependent on the Hippo-YAP/TAZ signaling pathway and their crosstalk regulates cytoskeletal dynamics (Foster, Gualdrini, and Treisman 2018).

The SRF transcription factor is a key regulator of cytoskeletal gene expression in many cell types and, thus, it is crucial for a variety of physiological and developmental processes such as gastrulation, muscle cell function, neuronal development, the immune system and liver development and regeneration (E. N. Olson and Nordheim 2010). For instance, SRF is a key factor for focal adhesion assembly in mouse embryonic stem cells and deletion of the SRF gene affects cell spreading and migration in mouse fibroblasts (Schratt et al. 2002).

MRTF/SRF and their target genes also play an important role in cell proliferation, invasiveness and motility implicated in cancer (E. N. Olson and Nordheim 2010). Studies revealed that MRTF-A/B are important for motility, adhesion, proliferation, invasiveness and colonization of metastatic tumors in melanoma and breast cancer cells (Medjkane et al. 2009). Similarly, deletion of MRTF-A affected cell proliferation and the cell cycle in fibroblasts (Shaposhnikov et al. 2013). The importance of MRTF for invasive migration was further supported by the transcriptional repressor SCAI blocking MRTF in cancer cell invasion (Brandt et al. 2009). Moreover, high levels of αV and β1 integrins activate MRTF/SRF activity triggering upregulation of ISG15, which enhances breast cancer cell motility (Hermann et al. 2016). Recently, the relevance of MRTF for cancer cell metastasis was further demonstrated, as MRTF and YAP are activated through L1CAM in disseminated cancer cells for metastatic colonization (Er et al. 2018). Consistent with this, MRTF-A and YAP are shown to regulate glioblastoma tumorigenicity (O. M. Yu et al. 2018). In summary, these findings suggest that MRTF/SRF signaling is fundamental for cancer cell invasion controlling a transcriptional-actin cytoskeleton regulatory circuit.

2.   Aim of this study

Non-apoptotic plasma membrane blebbing is critical for cancer cell motility and subsequent tumor dissemination regulated by actin cytoskeleton dynamics (Nürnberg, Kitzing, and Grosse 2011). A form of bleb-associated invasion characterized by cell-in-cell invasion also termed as entosis occurs in human malignancies and can promote tumor progression (Matej Krajcovic et al. 2011).

Previous work reported the importance of polarized actin dynamics mediated by plasma membrane blebbing at the invading cell in providing the driving force for entotic invasion (Purvanov et al. 2014). Although some of the actin cytoskeleton molecular regulators involved during non-apoptotic blebbing are well characterized (Fackler and Grosse 2008), the underlying signal transduction pathways for sustained long-term blebbing and consecutive bleb-associated cell invasion are not well understood. This invasive phenomenon is a long-term actin-controlled process described as a bleb-associated mode of invasive motility. However, whether this actin-driven blebbing requires transcriptional regulation has not been investigated before.

One of the prototypic transcriptional pathways known to regulate actin cytoskeleton dynamics and enhance the expression of cytoskeletal genes is the MRTF/SRF signaling pathway. MRTF/SRF is known to be involved in cell motility and cancer cell invasion. The aim of this thesis was to elucidate the potential role of MRTF/SRF transcriptional activity in non-apoptotic plasma membrane blebbing for invasive motility during entotic invasion (Figure 17). For that, our first objective was to investigate the underlying transcriptional feedback driving long-term plasma membrane blebbing. As plasma membrane blebbing occurs during entotic or amoeboid invasion, this study will provide insights into the relevance of long-term blebbing for these processes. We based our hypothesis on the actin-MRTF/SRF transcriptional pathway and assumed a critical function due to high actin remodelling during non-apoptotic blebbing and bleb-associated invasion (Figure 17). This study will therefore elucidate the molecular mechanisms regulating bleb-associated invasion and provide insights for its physiological relevance.
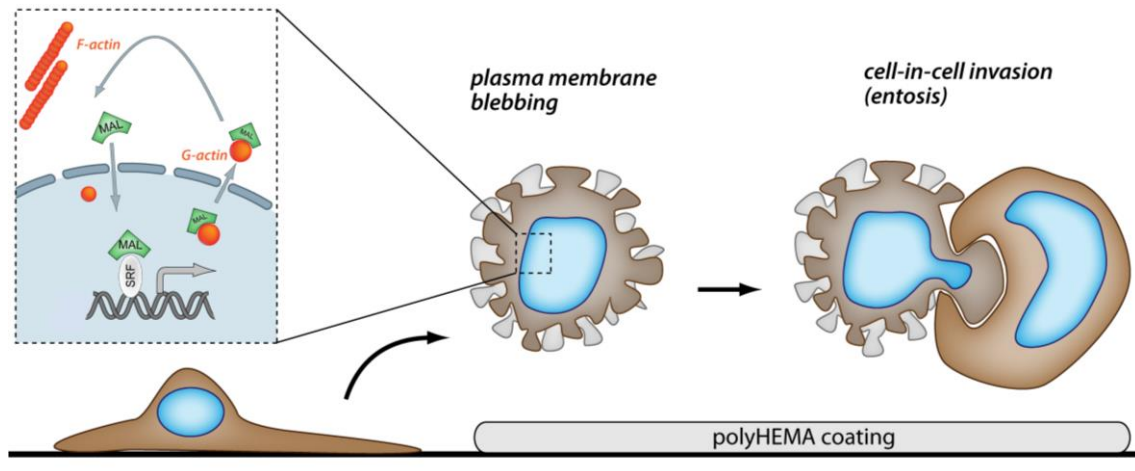
Figure 17: Investigating the role of the MRTF/SRF pathway in a bleb-dependent mode of invasion. This illustration represents an experimental model to study induced plasma membrane blebbing and subsequent entotic invasions. Cells in suspension are seeded on poly-HEMA coated dishes to prevent cellular attachment and matrix adhesion. The image was adapted from (Soto Hinojosa et al. 2017).

3. Materials and Methods

3.1. Materials

Table 1: Reagents used in this work

Reagent	Provider
Acetic acid	Roth
Acrylamide (30%)- Bisacrylamide (0,8%) (Rotiphorese Gel 30)	Roth
Actinomycin D	Santa Cruz Biotechnology
Agar	Roth
Agarose NEEO	Roth
Ammonium persulfate (APS)	Merck
Ampicillin	Roth
ATP	Sigma-Aldrich
BES	Sigma-Aldrich
Blebbistatin	Sigma-Aldrich
(S)-nitro-blebbistatin	Cayman Chemical
Bovine Serum Albumin, Fraction V (BSA)	Roth
Bromophenol Blue	Roth
Buffer Reverse Transcriptase	Thermo Scientific
Calcium Chloride (CaCl$_2$)	Roth
Chloroform	Roth
Cholera toxin	Sigma-Aldrich
Coenzyme A	NanoLight Technology
Collagen	Advanced Biomatrix
Cycloheximide	Sigma-Aldrich
DAPI	Sigma-Aldrich
Dimethyl Sulfoxide (DMSO)	Roth
DMEM (Dulbecco´s Modified Eagle´s Medium) high glucose	Capricorn
DMEM/F12	Gibco Life Technologies
DNA ladder 1kb	Thermo Scientific
DNA loading dye 6x	Thermo Scientific
dNTPs	Promega
Doxycycline	Sigma-Aldrich
DTT (1,4- dithiothreitol)	Roth
EDTA (Ethylenediaminetetraacetic acid)	Roth
EDTA-Disodium salt dihydrate	Roth
EGTA (ethylene glycol-bis(β-aminoethyl ether)-N,N,N',N'-tetraacetic acid)	Roth
Epidermal growth factor	Promo-kinase
Ethanol	Roth
Ethidium bromide	Roth
Fetal Calf Serum (FCS)	Invitrogen
Fluorescence mounting media	DAKO
Formaldehyde (37%)	Roth
Fugene HD	Promega
Glutamine	Capricorn
Glycerol	Roth
Glycine	Roth
H$_2$O$_2$	Sigma-Aldrich

HEPES (Hydroxyethyl piperazine ethanesulfonic acid)	Roth
Horse Serum	Invitrogen
Hydrochlorothiazide (h-CTZ)	NanoLight Technology
Hydrocortisone	Sigma-Aldrich
Insulin	Gibco
Isopropanol	Roth
Kanamycin	Roth
Lipofectamine LTX	Life Technologies
Lipofectamine RNAiMax	Life Technologies
Luciferin	Cayman Chemical
Magnesium Chloride (MgCl$_2$)	Roth
Matrigel	Corning
MEM Powder	GE Healthcare
2-Mercaptoethanol	Merck
Methanol	Roth
Milk powder (fat free)	Roth
Nocodazol	Cell Signaling
OptiMEM	Invitrogen
PageRuler Prestained Protein Ladder	Thermo Scientific
Penicillin	Capricorn
Phosphate Buffered-Saline (PBS)	Capricorn
Phusion HF buffer	Thermo Scientific
Phusion Hot Start II DNA Polymerase	Thermo Scientific
Plasmocyn	Invitrogen
Poly-HEMA (poly 2-hydroxyethyl methacrylate)	Polysciences
Ponceau S solution	Sigma-Aldrich
Potassium chloride	Roth
Primers	Sigma-Aldrich
Protease Inhibitor cocktail	Roche
PTC 124	Selleck Chemicals
Puromycin	Sigma-Aldrich
Random Hexamer Primer	Thermo Scientific
Restriction enzymes for cloning	Thermo Scientific/ New England BioLabs (NEB)
RevertAid Reverse Transcriptase	Thermo Scientific
RiboLock Ribonuclease Inhibitor	Thermo Scientific
RNAase-free water	Promega
si RNA Oligonucleotides	QIAGEN
Sodium chloride (NaCl)	Roth
Sodium dodecyl sulfate (SDS)	Roth
Sodium hydrogen phosphate (Na$_2$HPO$_4$)	Roth
Sodium pyrophosphate (Na$_4$P$_2$O$_7$)	Roth
Streptomycin	Capricorn
SYBR-Green	Bio-Rad
T4 DNA Ligase	Thermo Scientific
TEMED (N, N, N', N'-Tetramethylethane-1,2-diamine)	Roth
Tris (Tris (hydroxymethyl) aminomethane)	Roth
Triton X-100	Merck
Trizol	Peqlab
Trypsin-EDTA 0,05%	Capricorn

Tryptone	Roth
Tween-20	Roth
Y-27632	Sigma-Aldrich
Yeast extract	Roth

Table 2: Antibodies list

Antibody	Provider
Alexa Fluor 488 donkey anti-goat IgG Catalog No A11055	Life Technologies
Alexa Fluor 488 goat anti-mouse IgG Catalog No A11029	Life Technologies
Alexa Fluor 488 phalloidin Catalog No A12379	Life Technologies
Alexa Fluor 555 donkey anti-rabbit IgG Catalog No A31572	Life Technologies
Alexa Fluor 555 phalloidin Catalog No A22287	Life Technologies
Alexa Fluor 647 phalloidin Catalog No A34055	Life Technologies
Donkey anti–goat IgG HRP Catalog No.705-035	Jackson Immuno Research
Donkey anti–rabbit IgG Alexa Fluor 488 #R37118	Life Technologies
Goat anti–mouse IgG Alexa Fluor 555 #A28180	Life Technologies
Goat anti–MRTF-A C-19 sc-21558	Santa Cruz Biotechnology
Goat anti–rabbit IgG HRP Catalog No. 170-6515	Bio-Rad
Mouse anti-Ezrin Catalog No. 610602	BD Biosciences
Mouse anti–GFP B-2 sc-9996	Santa Cruz Biotechnology
Mouse anti-Integrin β1	BD Biosciences
Mouse anti-mDia1 610849 Catalog No. 610848	BD Biosciences
Mouse anti–MRTF-A G-8 sc-390324	Santa Cruz Biotechnology
Rabbit anti–MRTF-B #14613	Cell Signaling Technology
Rabbit anti-phospho-Ezrin(Thr567)/Radixin(Thr564)/Moesin (Thr558) 48G2 #3726	Cell Signaling Technology
Rabbit anti-phospho-myosin light chain 2 (Thr18/Ser19) #3674	Cell Signaling Technology
Rabbit anti-Rac-1/2/3 #2465	Cell Signaling Technology
Rabbit anti–SRF G-20 sc-335	Santa Cruz Biotechnology
Rabbit anti-tubulin 11H10 #2125	Cell Signaling Technology
Sheep anti–mouse IgG HRP Catalog No. NA9310	GE Healthcare

Table 3: Biochemical kits used in this work

Kit	Provider
CellTiter-Fluor Cell Viability Assay	Promega
GenElute Mammalian Total RNA Miniprep kit	Sigma-Aldrich
Lipofectamine LTX	Life Technologies

Lipofectamine RNAiMax	Life Technologies
Nextera XT DNA Sample Preparation kit	Ilumina
NucleoBond Xtra Midi Plus	Macherey-Nagel
NucleoSpin gel and PCR clean-up	Macherey-Nagel
NucleoSpin Plasmid	Macherey-Nagel
PureLink HiPure Plasmid Filter Maxiprep kit	Thermo Scientific
SMART-Seq v4 Ultra Low Input RNA kit	ClonTech
SuperSignal West Femto Maximum Sensitivity ECL Western Blotting Substrate	Thermo Scientific

Table 4: Buffers and solutions list used in this work

Solutions	Composition	
2x BBS transfection buffer	BES NaCl Na_2HPO_4	50 mM 280 mM 1.5 mM pH 6.92
8% Formaldehyde	Formaldehyde in PBS	8% (v/v)
4% Formaldehyde	Formaldehyde in PBS	4% (v/v)
ECL solution 2 (Enhanced Chemiluminescence)	Tris-HCl H_2O_2	0.1 M 1.8% pH 8.5
ECL solution 1 (Enhanced Chemiluminescence)	Tris-HCl Luminol p-Coumaric acid	0.1 M 2.5 mM 0.4 mM pH 8.5
Firefly assay buffer 3X	DTT Coenzyme A ATP Luciferin In Triton-lysis-buffer without Triton	15 mM 0.06 mM 0.45 mM 4.2 mg/ml
Laemmli buffer 4X	Tris-HCl EDTA Glycerol SDS Bromophenol blue 2-Mercaptoethanol	286 mM 10 mM 28 % (v/v) 5.7 % (w/v) 3.5 mg/ml 4.7 mg/ml pH 6.8
LB agar	NaCl Yeast extract Tryptone Agar	1% (w/v) 0.5 % (w/v) 1 % (w/v) 1.5 % (w/v)
LB medium	NaCl Yeast extract Tryptone	1 % (w/v) 0.5 % (w/v) 1% (w/v)
Loading buffer for PCR 6X	Glycerol Bromophenol blue Orange G	40 % (v/v) 0.04 % (w/v) 0.2 %
PBS	Na_2HPO_4	8 mM pH 7.4

	KH$_2$PO$_4$	1.5 mM
	NaCl	140 mM
	KCl	2.7 mM
PBS-T	PBS	1x
	Triton X-100	0.3 % (v/v)
Renilla assay buffer 3X	10 mM PTC124 in DMSO	0.06 mM
	2 mM h-CTZ in ethanol	0.01 mM
	in Renilla solution	
Renilla solution 10X	Na$_2$EDTA	45 mM
	Na Pyrophosphate	30 mM
	NaCl	1.452 M
	in H$_2$O	
SDS-PAGE running buffer 1x	Tris-HCl	25 mM
	Glycine	192 mM
	SDS	0.1 % (w/v)
		pH 8.3
SDS-PAGE stacking gel	30% Acrylamide/ 0.8% Bisacrylamide	1 ml (v/v)
	4X buffer Tris/SDS	1.25 ml pH 6.8
	Tris-HCl	0.5 M
	SDS	0.2 % (w/v)
	TEMED	10 µl
	10% APS	25 µl (w/v)
	in H$_2$O	3 ml
SDS-PAGE separating gel	30% Acrylamide/ 0.8% Bisacrylamide	6-15 % (v/v)
	4X buffer Tris/SDS	1.25 ml pH 8.8
	Tris-HCl	3 M
	SDS	0.2 % (w/v)
	TEMED	20 µl
	10% APS	100 µl (w/v)
	in H$_2$O	
TBST buffer	NaCl	500 mM
	Tris-HCl	20 mM
	Tween-20	1 % (v/v)
		pH 7.5
Tris-Acetat (TAE) buffer	Tris	40 mM pH 8.0
	EDTA	2 mM
	Acetic acid	20 mM
Triton lysis buffer 10X	Tris-HCl	0.1082 M
	Tris-Base powder	0.0419 M
	5 M NaCl	75 mM
	1 M MgCl$_2$	3 mM
	Triton-X-100	0.25 % (v/v)
	in H$_2$O	
Western blot blocking buffer	Milk powder	5% (w/v)
	in TBS-T buffer	
Western blot transfer buffer	Tris	25 mM pH 8.5
	Glycine	192 mM
	Methanol	10 % (v/v)
	SDS	0.2 % (w/v)

Table 5: Lab equipment and material list

Device	Provider
40x oil objective	Carl Zeiss
63x 1.4 NA oil objective	Carl Zeiss
Centrifuge 5415R	Eppendorf
Centrifuge Biofuge Pico	Heraeus
Centrifuge Biofuge Stratos	Heraeus
CO_2 humidified incubation chamber	Pecon
Forma Series II 3110 Water-Jacketed CO_2 Incubators	Thermo Scientific
GenAmp PCR system 9700	Applied Biosystems
INFINITY Gel Documentation	Peqlab
Laser scanning confocal microscope LSM 700	Carl Zeiss
Laser scanning confocal microscope LSM 800	Carl Zeiss
Luminoskan Ascent Microplate Luminometer	Thermo Scientific
Medical X-ray Film	Kodak Film
Mini-PROTEN Tetra Cell System	Bio-Rad
Mini-Trans Blot Electrophoretic Cell System	Bio-Rad
NanoDrop 1000	Peqlab
Nikon Eclipse microscope	Nikon
Nitrocellulose blotting membrane	GE Healthcare
PCR Thermocycler T3	Biometra
pH-meter 70	Mettler Toledo
qPCR 96-wells plate	Sarstedt
Real time Quantitative Thermal Cycler iQ5 (qPCR) 96 well	Bio-Rad
Thermomixer compact	Eppendorf
Vortex Genie 2	Scientific Industries
xCELLigence system Real-Time Cell Analyzer RTCA-MP	Roche Diagnostics
X-ray film processor	Medical Index

Table 6: Software list

Software	Provider
Ascent software	Thermo Scientific
DNA Strider	Christian Marck
Illustrator CS6	Adobe
Image J /Fiji	National Institute of Health
MS Office 2015	Microsoft
Photoshop CS6	Adobe
Prism 6	Graph Pad Software
RTCA Software 1.2	Roche Diagnostics
ZEN software	Carl Zeiss

3.2. Cell culture methods

3.2.1. General cell culture

Human MCF10A cells were cultured in DMEM/F12 (Gibco Life Technologies) supplemented with 5% horse serum, 20 ng/ml epidermal growth factor, 10 µg/ml insulin, 0.5 µg/ml hydrocortisone, 100 ng/ml cholera toxin, 100 U/ml penicillin, and 100 µg/ml streptomycin at 37 °C in a 5% CO_2 atmosphere as described by (Debnath, Muthuswamy, and Brugge 2003).

Human HEK293T, HeLa and A375-M2 were maintained in DMEM HPSTA-high glucose, stable glutamine and sodium pyruvate (Capricorn) supplemented with 10% FCS, 2 mM glutamine, 100 U/ml penicillin, and 100 µg/ml streptomycin at 37 °C in a 5% CO_2 atmosphere.

Culturing of all cell lines was performed in a cell culture laminar-flow hood under sterile conditions. All solutions were stored at +4 °C and warmed up to 37 °C in a water-bath before use. In order to split cells, the medium was completely aspirated and the cells were washed with PBS. Then, cells were incubated with Trypsin at 37 °C until cells were detached. Finally, Trypsin was inactivated by adding cell medium.

Freezing Cultured Human Cell Lines

To freeze cells for long term storage, cells were trypsinized and mixed with cell medium to harvest them. Subsequently, cells were centrifuged at 3000 rpm for 5 minutes. Afterwards, the medium was aspirated and cells were resuspended in 1 ml of cell culture freezing medium containing 5 % DMSO and 20% FCS. The resuspended cell solution was transferred to Cryo-tubes and placed at -80 °C in an isopropanol-containing cell freezing container to guarantee a slow freezing process. After 24 hours, the tube was placed at -80 °C or in liquid nitrogen for long term storage.

Thawing Human Cell Lines

The cell line aliquots were stored in 1 ml freezing medium at -80 °C or in liquid nitrogen. To grow a cell line, the frozen sample was thawed in a 37 °C water bath for 5 minutes. Afterwards, samples were transferred into a 15 ml tube and mixed with 10 ml of medium. The suspended cells were centrifuged at 3000 rpm for 5 minutes to isolate the cell pellet free of DMSO from the freezing medium. After removing the supernatant, the pellet was resuspended in 10 ml of the cell line´s medium and, finally cells were stored in a 5% CO_2 atmosphere at 37 °C.

Table 7: Cell lines

Cell line	Species	Media	Origin
MCF10A	Homo Sapiens	DMEM/F12	Epithelial mammary gland (Tait, Soule, and Russo2 1990)
HEK 293 T	Homo Sapiens	DMEM	Epithelial embryonic kidney (Graham et al. 1977)
A375-M2	Homo Sapiens	DMEM	Malignant melanoma, provided by E. Sahai (The Francis Crick Institute, London)
HeLa	Homo Sapiens	DMEM	Epithelial cervix adenocarcinoma (SCHERER, SYVERTON, and GEY 1953)

3.2.2. DNA transfection

a. Calcium Phosphate Precipitation Method

HEK293T cells were transfected using the calcium phosphate method. Cells were seeded 24 hours before transfection. For a 3.5 cm culture dish, 1μg of DNA was diluted and mixed with 112.5 μl of H_2O. Subsequently, 125 μl 2xBBS was added, followed by 12.5 μl $CaCl_2$. After vortexing, the transfection mixture was incubated for 15 minutes at room temperature before adding it to the cells. After four hours transfection, the cell medium was replaced with fresh 10% FCS DMEM medium and cells were incubated overnight (o/n) at 37 °C in a 5% CO_2 atmosphere.

b. Fugene Transfection Method

Cells were transfected using Fugene (Promega) according to the manufacturer´s instructions. The DNA was mixed in 200 μl OptiMEM (Invitrogen), followed by 4 μl of Fugene for each μg DNA. After 15 minutes of incubation at room temperature, the transfection mixture was added to the cells which were plated in a 3.5 cm culture dish the day before. Cells were incubated overnight at 37 °C with 5% CO_2.

c. Lipofectamine Transfection LTX

Cells were transfected using Lipofectamine LTX and Plus Reagent kit (Invitrogen) according to the manufacturer´s instructions. Cells were seeded the day before transfection in a 3.5 cm culture dish to be 70% confluent for transfection. To transfect the plasmids, 1μg of DNA was diluted in 200 μl of OptiMEM Medium (Invitrogen), followed by 7-10 μl Lipofectamine LTX Reagent and then 5 μl of Plus Reagent was added to the solution. Upon mixing and vortexing, the solution was incubated for 10 minutes at room temperature. Subsequently, the transfection mixture was added to the cells and they were incubated overnight at 37 °C with 5% CO_2.

3.2.3. siRNA transfection

MCF10A, HeLa and A375-M2 cells were transiently transfected with 30 nM of siRNA oligonucleotides using Lipofectamine RNAiMAX (Invitrogen) according to the manufacturer´s

instructions. For gene silencing, cells were seeded the day before transfection in a 3.5 cm culture dish to be 50-60% confluent during transfection. Then, 5 µl of Lipofectamine RNAiMAX Reagent was diluted and mixed in 125 µl OptiMEM Medium. Simultaneously, 3.1 µl siRNA of a 20 µM siRNA solution were diluted with 125 µl OptiMEM Medium. Both solutions were mixed together and incubated for 10-15 minutes at room temperature. Afterwards, the transfection mixture was added to the cells and incubated for 72h at 37 °C with 5% CO_2. After 72 hours, knockdown efficiency was quantified and confirmed by Western blot analysis or by quantitative PCR.

All siRNAs were purchased from Qiagen. The targeting sequences of siRNAs used in this work are indicated in Table 8.

Table 8: siRNA sequences

siRNA name	Gene	Target sequence (5' -> 3')
Hs_SRF_5	SRF	5'-CAAGATGGAGTTCATCGACAA-3'
Hs_VIL2_1	Ezrin	5'-ACTAAGCTCTTATTAGCGCTC-3
Hs_MKL1_7	MRTF-A	5'-ATCACGTGTGATTGACATGTA-3'
Hs_MKL1_9	MRTF-A	5'-TACCTCTATATTATATATCGA-3'
Hs_MKL2	MRTF-B	5'-AAGTAACAGTGGGAATTCAGC-3'
Hs_DIAPH1_1	mDia1	5'-AAGATATGAGAGTGCAACT-3'
All stars negative control siRNA	control siRNA	5'-AATTCTCCGAACGTGTCACGT-3'

3.2.4. Generation of stable cell lines by virus transduction

3.2.4.1. Lentiviral plasmids transfection

The advantage of stable transduction over transient transfection is the incorporation of the genetic material into the genome of the transduced cell. For that, HEK293T cells were seeded in a 6-well plate the day before transfection until reaching 70% confluence. To produce the lentivirus, HEK293T cells were co-transfected using the calcium phosphate method with the lentiviral packaging vector psPAX, the envelope vector pMDG.2 and a lentiviral vector such as the pInducer20 (pIND20), pWXPL or FUGW cloned with the targeted DNA of choice. The pInducer20 system presents doxycycline-inducible expression (Meerbrey et al. 2011) while the pWXPL and FUGW lentiviral systems show constitutive expression. In order to co-transfect cells, the total amount of DNA (2 µg pMDG.2, 2 µg psPAX and 1 µg of the targeted lentiviral vector of interest) was diluted in 112.5 µl of H_2O. Then, 125 µl 2xBBS were added to the transfection mixture, followed by 12.5 µl of $CaCl_2$. After mixing and vortexing, the transfection mixture was incubated for 15 minutes at room temperature and afterwards added to the cells. After four hours transfection, the cell medium was replaced with fresh 10% FCS DMEM medium and cells were incubated at 37 °C with 5% CO_2.

The lentiviral packaging vector psPAX, the envelope lentiviral vector pMDG.2 and the lentiviral pWPXL were provided by J. Swiercz (Max Planck Institute for Heart and Lung Research, Bad Nauheim, Germany). The lentiviral vector FUGW was kindly provided by D. Oliver (University of Marburg). Table 9 shows the lentiviral plasmids used on this study to generate stable cells lines.

Table 9: Lentiviral expression vectors used to generate stable cell lines

Donor organism	Receiver organism	Lentiviral Vector	DNA transferred
Aequorea Victoria and Homo Sapiens	MCF10A	3RPEL-2GFP-pWPXL	3RPEL-2GFP
Aequorea Victoria and S. Cerevisiae	MCF10A	LifeAct-GFP-pWPXL	LifeAct-GFP
Homo Sapiens and Aequorea Victoria	MCF10A	Ezrin-GFP-pWPXL	Ezrin-GFP
Homo Sapiens and Aequorea victoria	MCF10A	Ezrin-T567A-GFP-pWPXL	Ezrin-T567A-GFP
Discosoma sp, S. Cerevisiae and Homo sapiens	MCF10A	Ezrin-mCherry-pWPXL	Ezrin-mCherry
Aequorea Victoria	MCF10A	pWPXL	GFP
Aequorea Victoria and Homo Sapiens	MCF10A	MRTF-A-GFP-pInducer20	MRTF-A-GFP
Aequorea Victoria, Homo Sapiens and Discosoma sp	MCF10A	H2B-mCherry-pWPXL + Ezrin-GFP-pWPXL	H2B-mCherry Ezrin-GFP
Discosoma sp and S. Cerevisiae	MCF10A	LifeAct-mCherry-pWPXL	LifeAct-mCherry
Aequorea Victoria and Homo Sapiens	MCF10A	ΔN-MRTF-A-GFP-pInducer20	ΔN-MRTF-A-GFP
Aequorea Victoria, Homo Sapiens and Discosoma sp	MCF10A	H2B-GFP-pWPXL + LifeAct-mCherry-pWPXL	H2B-GFP LifeAct-mCherry
Aequorea Victoria and Homo Sapiens	MCF10A	3Da.luc-MRTF-SRF-GFP-FUGW	3Da.luc-MRTF-SRF-GFP
Aequorea Victoria and Homo Sapiens	MCF10A	3Da.luc -GFP-FUGW	3Da.luc -GFP
Aequorea Victoria and Homo Sapiens	MCF10A	GFP-FUGW	GFP
Aequorea Victoria	A375-M2	pWPXL	GFP
Aequorea Victoria	A375-M2	LifeAct-GFP-pWPXL	LifeAct-GFP
Aequorea Victoria, Homo Sapiens and Discosoma sp	A375-M2	H2B-mCherry-pWPXL + LifeAct-GFP-pWPXL	H2B-mCherry + LifeAct-GFP
Aequorea Victoria and Homo Sapiens	A375-M2	MRTF-A-GFP-pInducer20	MRTF-A-GFP
Aequorea Victoria, Homo Sapiens and Discosoma sp	MCF10A	H2B-mCherry-pWPXL + MRTF-A-GFP-pIND.20	H2B-mCherry MRTF-A-GFP

3.2.4.2. Viral transduction

HEK293T transfection efficiency was confirmed using fluorescence microscopy after 24 hours of transfection. Then, 48 hours after co-transfection of the lentiviral vectors, the supernatants containing viral particles were harvested, filtered with a 0.22 μm pore size filter and added to the target cell line to transduce them. After 72 hours, target cells transduction efficiency was confirmed using fluorescence microscopy. Consequently, transduced target cells were selected either by FACS-based cell sorting for the pWXPL or FUGW lentiviral plasmids system or by 0.25 μg/ml puromycin selection for the pInducer20 lentiviral system. In addition, expression of MRTF-A-GFP from pInducer20 was induced by 333 ng/ml doxycycline.

3.2.5. Cell impedance analysis

Cell impedance quantification in A375-M2 melanoma cells was performed in 96-well E-plates (Roche Diagnostics), which were previously coated with the indicated collagen concentration and cells were seeded on top at the indicated cell densities. Next, impedance-based real time detection was conducted using the xCELLigence system Real-Time Cell Analyzer RTCA-MP (Roche Diagnostics). Analysis was performed recording the cell index values (CI) every 15 min for 24 h and normalization was done using the RTCA Software 1.2 (Roche Diagnostics). The impedance readout shows arbitrary cell index-values which are normalized to 1 at the indicated time points. The normalized values are calculated using the following equation: Normalization of cell index $(NClti) = Clti/Clnml\_time$, where *Clti* is the cell index at a given time point divided by the cell index at the normalization time point (*Clnml_time*). Furthermore, background impedance caused by the collagen and the cell medium was determined in each well before seeding the cells. Here, cell impedance measurement allows us to monitor different cell processes such as cell adhesion (Rees and Thomas 2015).

3.3. DNA cloning methods

3.3.1. Amplification of DNA via Polymerase Chain Reaction (PCR)

Expression constructs were generated following standard cloning methods. DNA fragments were amplified by Polymerase Chain Reactions (PCR) using 0.5 μl Hot Start II High-Fidelity DNA Polymerase in 10 μl 5x Phusion buffer (Thermo Fisher Scientific) according to the manufacturer´s instructions. Moreover, the PCR reaction contained 200 ng DNA template, 100 nM of forward and reverse primer, and optionally 0.5-1.5 μl DMSO. Then, the PCR tube was filled up to a total volume of 50 μl with ddH$_2$O. The PCR reaction was performed using a Thermocycle (Biometra) with the program described in Table 10.

Table 10: PCR program

	Steps	Temperature (°C)	Time (sec)
1	initial denaturation	95°C	3 min
2	denaturation	95 °C	30 sec Steps 2-4 (30 cycles)
3	primer annealing	60°-72 °C	30 sec
4	elongation	72 °C	30 sec/ 1kb
5	final extension	72°	3 min
6	storage	+4°C	

The DNA template was always obtained from existing plasmids. The different pre-existing plasmids and expression vectors used on this study are listed and described in Table 11.

Table 11: Expression plasmids used in this work

Plasmid	Reference	Characteristics
pGL3D.AFOS	R. Treisman (The Francis Crick Institute, London, UK) (Mohun, Garrett, and Treisman 1987)	pGL3-basic vector with 3-main SRF binding sites of the c-Fos promoter, retrieved from the TATA box of a *Xenopus laevis* actin genome. It mediates SRF-dependent expression of firefly-luciferase.
pRL-TK	Promega	Internal control for reporter gene assays. *Herpes simplex* Thymidine kinase promotor mediates *Renilla reniformis* luciferase-expression.
pInducer20		Mammalian expression. Lentiviral plasmid. Ampicillin resistance. CMV promoter.
pWPXL		Mammalian expression. Lentiviral plasmid. Ampicillin resistance. EF-1α promoter.
pMD2.G	J. Swiercz (Max Planck Institute for Heart and Lung Research, Bad Nauheim, Germany)	Mammalian expression. Lentiviral envelope expressing plasmid. Ampicillin resistance.
psPAX2	J. Swiercz (Max Planck Institute for Heart and Lung Research, Bad Nauheim, Germany)	Mammalian expression. Lentiviral packaging plasmid. Ampicillin resistance.
H2B-mCherry-pWPXL		Nuclear marker histone fusion protein H2B in a lentiviral vector.
LifeAct-mCherry-pWPXL	M. Sixt (IST, Klosterneuburg, Vienna)	LifeAct probe expressed in a lentiviral vector.
ΔN-MRTF-A-GFP-pInducer20	Cloned by C. Baarlink (Institute of Pharmacology, Marburg)	This constitutively active ΔN-MRTF-A construct (Miralles et al. 2003) cannot bind G-actin due to a lack of RPEL motifs. This vector was labelled with GFP and inserted in an inducible lentiviral vector.

MRTF-A-GFP-pInducer20	Cloned by D. Brandt (Institute of Pharmacology, Marburg)	Full length MRTF-A expressed in an inducible lentiviral vector.
3-RPEL-2-GFP-pWPXL	Cloned as explained at Table 12.	RPEL domain from the MRTF-A sequence constitutively expressed in a lentiviral vector.
Ezrin-GFP-pWPXL	Cloned as explained at Table 12. (Crepaldi et al. 1997)	Ezrin *wild type* form tagged to GFP constitutively expressed in a lentiviral vector.
Ezrin-T567A-GFP-pWPXL	Cloned as explained at Table 12. (Gautreau, Louvard and Arpin, 2000)	Ezrin non-phosphorylatable mutant T567A tagged to GFP constitutively expressed in a lentiviral vector.
Ezrin-mCherry-pWPXL	Cloned as explained at Table 12.	Ezrin *wild type* form tagged to mCherry constitutively expressed in a lentiviral vector.
3Dafos.Luc-T2A-GFP-FUGW	Cloned as explained at Table 12.	Lentiviral luciferase promoter SRF reporter gene expressing vector.
hUbC-Luc-T2A-GFP-FUGW	Cloned as explained at Table 12.	Lentiviral luciferase reporter gene vector with the hUbC promoter instead of the SRF firefly promoter.
Luc-T2A-GFP-FUGW	Cloned as explained at Table 12.	Lentiviral luciferase reporter gene expressing vector with no promoter.

Lentiviral expression vectors pWPXL-based for stable expression of fluorescently tagged 3RPEL-2GFP, Ezrin-GFP, Ezrin-T567A-GFP, Ezrin-mCherry, H2B-GFP, H2B-mCherry, LifeAct-mCherry, LifeAct-GFP and the pInducer20-based doxycycline inducible vector (Meerbrey et al. 2011) for MRTF-A-GFP and ΔN-MRTF-A-GFP were cloned using standard PCR techniques.

Lentiviral luciferase reporter gene vectors FUGW-based expressing the firefly luciferase promoter pGL3D.AFOS to measure SRF luciferase activity were cloned to generate a stable cell line. The firefly coding sequence pGL3D.AFOS (Geneste, Copeland, and Treisman 2002) was cloned into the lentiviral vector FUGW by inserting either the GL3D.AFOS promoter, the hUBc promoter or by removing both promoters as a negative control vector, respectively (Figure 18). The SRF luciferase promoter was cloned into the lentiviral vector FUGW maintaining the hUBC promoter as hUBc-driven construct or cloned with no promoter deleting the luciferase promoter and the hUBc promoter as a promoter free construct. For all luciferase reporter gene expressing cloned vectors, the luciferase reporter gene was cloned linked to a GFP by a self-cleavable T2A peptide in order to FACS sort the positive transduced cells. The pGL3D.AFOS vector presents the cFos promoter and three copies of the serum response element (SRE), serving for the SRF-dependent expression of the firefly luciferase.

Promoter free   hUbC-driven   CArG-(MRTF/SRF)-driven
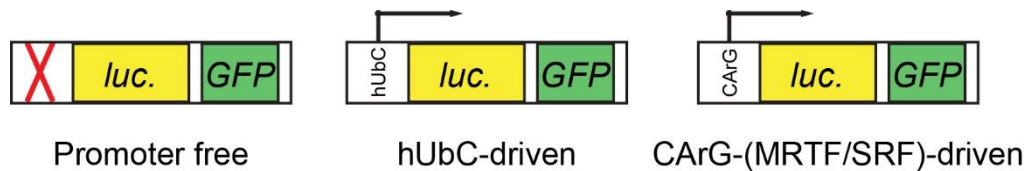
Figure 18: The SRF luciferase reporter constructs. The promoter-free construct was generated by omitting either the insertion of a GL3D.AFOS promoter or a hUbC promoter into the FUGW lentiviral vector serving as non-inducible control plasmid for the SRF luciferase reporter assays. The hUbC-driven construct was cloned into FUGW conserving its own hUbC promoter. The CArG-(MRTF/SRF)-driven construct was cloned inserting the GL3D.AFOS promoter into the lentiviral FUGW vector. All constructs were cloned linked to a GFP sequence. This image was adapted from (Soto Hinojosa et al. 2017).

The following primer oligonucleotides were used for the generation of the mentioned constructed above (Table 12):

Table 12: Primers sequences for the generation of recombinant DNA

Construct	Sequence (5' -> 3')	Backbone vector Restrictions sites
Ezrin-GFP		pWPXL
fwd primer	GCGCGCGTTTAAACTAATGCCGAAACCAATCAATGTCCGA	PmeI
rev primer	GCGCGCACGCGTCTTGTACAGCTCGTCCATGCCGAGAGTG	MluI
Ezrin-T567A-GFP		pWPXL
fwd primer	GCGCGCGTTTAAACTAATGCCGAAACCAATCAATGTCCGA	PmeI
rev primer	GCGCGCTTCGAACTTGTACAGCTCGTCCATGCCGAGAGTG	BstBI
Ezrin-mCherry		H2B-mCherry-pWPXL
fwd primer	GCGCGCGTTTAAACTAATGCCGAAACCAATCAATGTCCGA	PmeI
rev primer	GCGCGCACGCGTCTTGTACAGCTCGTCCATGCCGAGAGTG	MluI
3-RPEL-2-GFP		pWPXL
fwd primer	GCGCGCGTTAAACATGCTGCCCCCTTCCGTCATTGCTGTGAATGG	PmeI
rev primer	GCGCGCACGCGTCTTGTACAGCTCGTCCATGCCGAGAGTG	MluI
3Dafos.Luc-T2A-GFP		FUGW
fwd primer	GCGCGCTTAATTAACATTTCACACAGGAAACAGCTATGAC	PacI
rev primer	GCGCGCGAATTCTTACTTGTACAGCTCGTCCATGCCGA	EcoRI
hUbC-Luc-T2A-GFP		FUGW

fwd primer	GCGCGCGGATCCCATGGAAGACGCCAAAAACATAAAG AA	BamHI
rev primer	GCGCGCGAATTCTTACTTGTACAGCTCGTCCATGCCGA	EcoRI
Luc-T2A-GFP		FUGW
fwd primer	GCGCGCTTAATTAAATGGAAGACGCCAAAAACATAAA GAA	PacI
rev primer	GCGCGCGAATTCTTACTTGTACAGCTCGTCCATGCCGA	EcoRI

3.3.2. Agarose gel electrophoresis and purification of the PCR products

The PCR products were mixed with DNA loading dye, the 6x PCR sample loading buffer (Thermo Scientific), and subsequently loaded to 1% agarose gel which contained 1x TAE buffer with 10 µg/µl ethidium bromide. The DNA fragments were separated by running the gel in a DNA electrophoresis chamber (Bio-Rad) using a constant voltage (100 V). Later, the amplified DNA was detected under UV light and visualized with the INFINITY gel documentation system (Peqlab). The amplified DNA fragments of interest were then cut out of the agarose gel and purified using the NucleoSpin gel and PCR clean-up kit (Macherey-Nagel) according to the manufacturer´s instructions.

3.3.3. Restriction digest and DNA ligation

After PCR product purification, the purified PCR fragments and the respective cloning vectors were digested using DNA restriction enzymes for 2 hours at 37 °C in accordance with the manufacturer´s protocol. The different restriction endonucleases used on this study are shown in Table 13. All the restriction enzymes were purchased either from Thermo Scientific or New England Biolabs (NEB) as indicated. After digestion, the DNA insert and the digested vector were run on an agarose gel and the DNA was purified as previously described. Thereafter, DNA ligation was conducted in a total volume of 20 µl for 20 minutes at room temperature using 1 µl of T4 Ligase (Thermo Scientific) together with 2 µl Ligase buffer (Thermo Scientific) at a ratio of 1:4 between the digested vector and the DNA insert, respectively.

Table 13: Restriction enzymes used for this study

Restriction endonucleases	Reaction Buffer	Supplier
BstBI	Buffer B	Thermo Scientific
PmeI		
PmeI	CutSmart buffer	NEB
MluI		
PacI	CutSmart buffer	NEB
EcoRI		

BamHI	Tango buffer	Thermo Scientific
EcoRI		

3.3.4. Transformation of recombinant vector DNA into bacteria

DH5α bacteria cells were transformed with recombinant DNA by adding 6 µl of the ligation reaction to 45 µl bacterial cells on ice for 30 minutes. Then, a 45 seconds heat shock at 42 °C was applied and the cells kept on ice for 5 minutes. Next, the samples were plated on LB agar plates with antibiotic (either ampicillin or kanamycin depending on the vector resistance) and incubated at 37 °C overnight.

The following day, bacterial colonies were collected and incubated in 4 ml LB medium containing antibiotics at 37 °C overnight. DNA plasmids were isolated using the NucleoSpin Plasmid Miniprep Kit (Macherey-Nagel) according to the manufacturer´s protocol. Positive clones were selected after running a test digestion for all the clones. In order to confirm our cloned construct, the isolated DNA plasmids were sent for DNA sequencing (Macrogen) and analyzed with the DNA Strider software.

3.4. Microscopy

Microscopic imaging was performed using the confocal laser scanning microscopes LSM 700 and LSM 800 (Carl Zeiss) equipped with a 63x 1.4 NA and a 40x oil objective (Carl Zeiss). The images were later on analyzed using ZEN software (Carl Zeiss) and processed using Image J/Fiji software (National Institute of Health).

3.4.1. Immunofluorescence

Cells were seeded and grown on glass coverslips (Thermo Scientific) in 6-well plates (Sarstedt). For immunofluorescence, cells were fixed with 4% formaldehyde in PBS for 10 minutes at room temperature. After washing the coverslips three times with PBS, cells were permeabilized using 0.03% Triton-X-100 in PBS (PBS-T) or 0.05% Tween in PBS for 10 minutes at room temperature. Then, cells were blocked using 5% BSA in PBS for 1 hour at room temperature. Subsequently, samples were incubated with the primary antibody diluted in the blocking solution overnight at 4 °C followed by three PBS washing steps. The secondary antibody was also diluted in the blocking solution and incubated with the coverslips for 1 hour at room temperature. If required, nuclei were stained using DAPI (Sigma-Aldrich) at 1:10000 for 20 min at room temperature and F-actin was labelled using Alexa Fluor 555-phallodin, Alexa Fluor 488-phalloidin or Alexa Fluor 647-phalloidin (Invitrogen) at 1: 500 overnight at 4 °C or at 1:200 for 1h at room temperature.

After three final washing steps with PBS, the coverslips were mounted on the glass slides using fluorescent mounting media (DAKO).

3.4.2. Live Cell Imaging

Time-lapse microscopy of the fluorescence GFP or mCherry tagged proteins was performed at 37 °C in a 5% CO_2-humidified incubation chamber (Pecon, CO_2 module S1). Images were acquired with the LSM 700 and the LSM 800 confocal microscopes (Carl Zeiss) using the time series, Z-stack and tile scan setting of the ZEN software (Carl Zeiss). Quantitative analysis of the images was done using the ZEN software (Carl Zeiss) and ImageJ/Fiji software (National Institute of Health).

To induce plasma membrane (PM) blebbing and subsequent entosis, MCF10A cells were seeded on 35-mm glass bottom dishes (In vitro Scientific) which were previously coated at room temperature with 12% poly-HEMA wt/wt solution diluted 1/4 in ethanol to prevent cellular attachment as previously described by (Overholtzer et al. 2007). Whereas to study amoeboid blebbing invasion, 8-well μ-slide (Ibidi) were coated with either 2.4 μg/ml Collagen (Advanced Biomatrix) or 2.5 μg/ml Matrigel (Corning) according to the manufacturer´s instructions, and A375-M2 cells were seeded in DMEM medium on top of the matrix to monitor them over a time course of 16 hours.

To perform live serum stimulation assays, MCF10A cells were starved overnight in a 0.5% FCS containing cell medium and 20% serum was added directly to the cells under the microscope to follow the effects of the stimulation over time.

When indicated, cells were treated with the following drugs: the myosin II inhibitor (S)-nitro-blebbistatin (100 μM, Cayman Chemical), the ROCK inhibitor Y-27632 (10 μM, Sigma-Aldrich), the transcription inhibitor Actinomycin D (50 μg/ml, Santa Cruz Biotechnology) and the protein translation inhibitor Cycloheximide (100 μg/ml, Sigma-Aldrich), which were applied directly to the cells while scanning.

If necessary, cells were pre-seeded on glass bottom dishes (In vitro Scientific) and transfected with the DNA plasmids of interest using Lipofectamine LTX Transfection Kit (Life Technologies) 24 hours before analysis. To image cells silenced by siRNAs, transfection using Lipofectamine RNAiMax Transfection Kit (Life Technologies) was done 72 hours before imaging.

3.5.   Bleb-dependent invasion assays

3.5.1. Entosis assays

Entosis experiments were performed as previously described (Purvanov et al. 2014; Soto Hinojosa et al. 2017). MCF10A cells were grown in a 6-well plate and trypsinized to plate them at cell densities of 300.000-400.000 per well on Costar Ultra-low cluster plates (Corning) preventing cellular attachment. Cells were incubated for 4h at 37°C, then MCF10A cells were fixed directly in suspension using 8% formaldehyde in PBS for 10 minutes at room temperature. After washing the cells, the cell pellet was resuspended in PBS and seeded on top of 12-mm coverslips (Sarstedt) on a heating block at 60 °C for 5-10 minutes. Then, fixed cells on coverslips were washed three times with PBS and permeabilized using 0.05% Tween in PBS for 10 minutes at room temperature. For visualization of entotic events, cells were incubated with Alexa Fluor 555-phalloidin (Invitrogen) or Alexa Fluor 488-phalloidin (Invitrogen) at 1: 500 in PBS overnight at 4 °C to label F-actin and DAPI (Sigma-Aldrich) to label nuclei was used at 1:10 000 for 20 minutes at room temperature. When necessary, after permeabilization, cells were blocked using 5% BSA in PBS-T for 1 hour at room temperature followed by the incubation with the primary antibodies overnight as described in the Immunofluorescence protocol (Section 3.4.1).

To quantify entotic events, images were acquired with the LSM 700 and the LSM 800 confocal laser scanning microscopes (Carl Zeiss) using the Z-stack setting of the ZEN software (Carl Zeiss). Entotic cells and the total number of cells were quantified using the ZEN software (Carl Zeiss) and analyzed with ImageJ/Fiji software (National Institute of Health). For all entosis quantifications, at least 600 cells were quantified from 8 different visual fields for each coverslip and assays were performed at least three times to statistically analyse the data using Prism 6 (GraphPad Software).

3.5.2. 2D invasion assays on a matrix

To study amoeboid blebbing invasion, A375-M2 melanoma cells were seeded on top of a matrix in a 8-well μ-slide (Ibidi) which was previously coated either with fibrillar bovine Collagen (2.4 µg/ml, Advanced Biomatrix) diluted with 10X MEM and HEPES buffer or with Matrigel (2.5 µg/ml, Corning) diluted in DMEM medium and then incubated for 30 minutes at 37 °C before plating the cells. After seeding the cells on the matrix for 1 hour at 37 °C in a 5% CO_2 atmosphere, A375-M2 cells were tracked over a time period of 16 hours with the time-series and Z-stack setting of the ZEN software at the LSM 700 confocal microscope using the 40X oil objective (Carl Zeiss) in a 5% CO_2 incubation system (Pecon, CO_2 module S1). For analysis of cell morphology, percentage of elongated or rounded cells was assessed after plating the cells on a matrix for 16

hours using ImageJ/Fiji software (National Institute of Health). Other parameters like cell roundness was also evaluated using ImageJ/Fiji software (National Institute of Health).

3.6. RNA analysis

The analysis of the siRNA knockdown efficiency and the mRNA transcript level expressed for actin-MRTF/SRF target genes were based on the extraction of RNA from the cells, followed by synthesis of cDNA and quantified by real time PCR (qPCR) as described in the Figure 19.
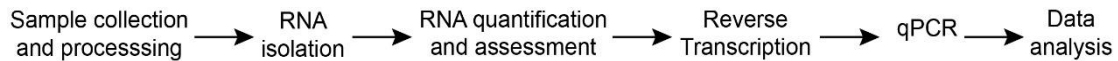
Figure 19: qPCR gene expression experimental workflow.

3.6.1. RNA isolation from cells

For total RNA extraction, cells were washed with PBS and directly lysed in the 6-well plate by adding 1 ml of Trizol reagent (Peqlab) for each well according to the manufacturer´s instructions. Then, cells were collected in a 1.5 ml eppendorf tube, incubated for 5 minutes at room temperature to allow complete dissociation of nucleoprotein complex and 200 µl chloroform was added, followed by 15 seconds of intensive vortexing and afterwards, samples were incubated for 10 minutes at room temperature. Phase separation was achieved by centrifugation at 12000 g for 15 minutes at 4°C. The RNA found in the upper aqueous phase was carefully transferred to a new 1.5 ml eppendorf tube and mixed with 500 µl isopropanol to precipitate the RNA. After 10 minutes incubation at room temperature, samples were centrifuged at 12 000g for 15 minutes at 4 °C to pellet the RNA. Finally, the RNA pellet was washed with 75% ethanol and pelleted at 12000 g for 5 minutes at 4°C, then dried at room temperature and dissolved in 20 µl RNase free H_2O. Samples were stored at -80 °C. All the steps must be performed RNA-free until cDNA is obtained on the next phase.

3.6.2. Reverse Transcription of total RNA

Reverse transcription was performed using reverse transcriptase enzymes to convert RNA into their complementary DNA (cDNA). After RNA extraction from the cells, 500 ng RNA in a total volume of 10 µl were incubated with 1 µl of Random Hexamer Primer (100 µM, Thermo Scientific) for 5 minutes at 65 °C using a Thermal Cycler (Biometra). This step was followed by PCR with a master mix containing: 2 µl 10 mM dNTPs (Promega), 1 µl RiboLock Ribonuclease Inhibitor (Thermo Scientific), 1 µl RevertAid Reverse Transcriptase (Thermo Scientific) and 6 µl 5x Reverse Transcriptase buffer (Thermo Scientific). The PCR reaction was filled up to a final volume of 19 µl. This master mix was gently mixed and 19 µl were pipetted into each RNA/primer reaction tube on ice. At the end, the samples were transferred to the Thermal Cycler Gene Amp

PCR System 9700 (Applied Bioystems) to start the PCR for cDNA preparation with the following program:

Table 14: PCR program for cDNA synthesis

Steps	Temperature (°C)	Time (sec)
1	25°C	10 min
2	42 °C	60 min
3	70 °C	10 min
4	+4°C	

3.6.3. Quantitative real time PCR (qPCR)

After cDNA synthesis, the quantitative real time PCR (qPCR) was performed with Real Time Quantitative Thermal Cycler (Bio-Rad) using a reaction mixture with SYBR Green as a fluorescent dye (Bio-Rad).

qPCR is based on the same principle as conventional PCR and allows the quantification of the final DNA after each amplification step. The total amount of PCR product is detected by measuring the fluorescence intensity at the end of each cycle. For the PCR reactions, first the cDNA from the reverse transcription product was diluted 1:10 and 5 µl of the cDNA were directly pipetted to the 96-well qPCR plate. Then, a master mix reaction was prepared for each primer pair containing (per sample): 12.5 µl SYBR-Green (Bio-Rad), 1 µl forward primer and reverse primer (100 nM, Sigma-Aldrich), and 9 µl RNAse-free H_2O. A list of the qPCR primers sequences (Sigma-Aldrich) used in this work is shown in Table 15 and the qPCR program (Bio-Rad) used is described in Table 16.

Table 15: qPCR primers sequences

Name	Sequence 5'-->3'
TATA-binding protein fwd	5'-TGCACAGGAGCCAAGAGTGAA-3'
TATA-binding protein rev	5'-CACATCACAGCTCCCCACCA-3'
hSRF fwd	5'-CAGATCGGTATGGTGGTCGG-3'
hSRF rev	5'-GTCAGCGTGGACAGCTCATA-3'
hEzrin fwd	5'-TAAGGGTTCTGCTCTGACTCCA-3'
hEzrin rev	5'-GCTCTGCATCCATGGTGGTAA-3'
hMRTF-A fwd	5'-CATGAGTCCCAGGGTTCTGT-3'
hMRTF-A rev	5'-ACTTGGCAGTGGGGATAGTG-3'
hMRTF-B fwd	5'-ACATTCGCCCTTTCTTGCAGT-3'
hMRTF-B rev	5'-TCCGAGATTGCCATCTTATTGTC-3'
hRadixin fwd	5'-CCATATTGCCGAGCTGTCTG-3'
hRadixin rev	5'-GGCAAATTCCAGCTCAGCAT-3'
hMoesin fwd	5'-ATCCAAGCCGTGTGTACTGC-3'
hMoesin rev	5'-AAATAGCTGCTTCCCGGTGG-3'
hCYR61 fwd	5'-GTGACGAGGATAGTATCAAGGACC-3'

hCYR61 rev	5'-ATTTCTGGCCTTGTAAAGGGTTG-3'
h_c-Fos fwd	5'-CTCTCTTACTACCACTCACCCGC-3'
h_c-Fos rev	5'-GGTCCGTGCAGAAGTCCTGCG-3'
hIntegrin B1 fwd	5'-CCGCGCGGAAAAGATGAA-3'
hIntegrin B1 rev	5'-ACATCGTGCAGAAGTAGGCA-3'
hMyosin fwd	5'-TCCCCGCTGGGAATGGTC-3'
hMyosin rev	5'-CTTATCGGCAGCTTGCTGTG-3'
hMMP-9 fwd	5'-CGACGTCTTCCAGTACCGAG-3'
hMMP-9 rev	5'-TTGTATCCGGGCAAACTGGCT-3'
hmDia1 fwd	5'-GTCAGGCTTGCGGGATATG-3'
hmDia1 rev	5'-TTCAGCACCAAATGTTTGCAC-3'
hRac-1 fwd	5'-CACCGAGCACTGAACTTTGC-3'
hRac-1 rev	5'-CGGGAGGCTGTTCTGCTTTA-3'
hRhoA fwd	5'-GTCCACGGTCTGGTCTTCAG-3'
hRhoA rev	5'-CAGCCATTGCTCAGGCAAC-3'
hMLC2 fwd	5'-TGTCAGGCAGATCTGTGACG-3'
hMLC2 rev	5'-GGTTATACCTCCGTGCCAGG-3'

Table 16: qPCR program

	Step	Temperature (°C)	Time
1	Initial denaturation	95	3 min
2	Denaturation	95	10 s Steps 2-4 40 cycles
3	Annealing	60	30 s
4	Elongation	72	30 s
5	Final elongation	95	2 min
6	Melting curve	55→ 95	10 s

Gene expression analysis was then evaluated by determining the ratio between the amount of target gene of interest and an endogenous reference gene which is equally expressed in all samples. Relative mRNA levels were quantified using the delta cycle threshold (ΔΔCT) method normalized to the TATA-binding protein (TBP) cDNA. To calculate the fold change in the target gene relative to the TBP control gene is determined by the following equation:

Fold change = $2^{-\Delta(\Delta CT)}$

where $\Delta CT = Ct_{\text{target gene}} - Ct_{\text{TBP}}$ and $\Delta(\Delta CT) = \Delta Ct_{\text{interest cDNA}} - \Delta Ct_{\text{control cDNA}}$

3.7.   Protein analysis

3.7.1. Western Blotting

Proteins were separated by sodium dodecyl sulfate polyacrylamide gel electrophoresis (SDS-PAGE) according to their molecular weight with the Mini-PROTEN Tetra Cell System (Bio-Rad). Sample preparation started with the cell lysis step by adding 2x Laemmli Buffer (Table 4) directly to the cells to denature their proteins. After protein denaturation, cell lysates were then

collected in a 1.5 ml Eppendorf tube and boiled for 10 minutes at 95 °C and subsequently lysates were centrifuged at 12 000 g for 10 minutes. Afterwards, samples were immediately loaded onto an SDS-PAGE gel or stored at -20°C. To run SDS-polyacrylamide gels, separating gels were cast in different concentrations of 6%, 8%, 10% or 15% according to the protein size and 6% for the stacking gel. Then, cell lysate samples and the Page-ruler pre-stained protein size ladder (Thermo Scientific) were loaded into the wells and SDS-polyacrylamide gels were run using constant voltage (80 V for stacking gel and 120 V for separating gel) to electrophoretically separate the proteins. Next, the separated proteins were transferred to a 0.45 µm nitrocellulose blotting membrane (GE Healthcare) using the Mini Trans-Blot Electrophoretic Cell system (Bio-Rad) filled with the Western blot transfer buffer (Table 4) applying constant 350 mA for 90 minutes on ice. After protein transfer, the nitrocellulose membranes were incubated in blocking buffer (Table 4) for 1 hour at room temperature. This blocking step was followed by incubating the different primary antibodies (Table 17) diluted in the blocking buffer with the membranes on a shaker overnight at 4°C. After washing the membranes three times with TBST buffer (Table 4) for 10 minutes, the secondary HRP-conjugated antibodies diluted (Table 17) in the blocking buffer were incubated for 1 hour at room temperature. Membranes were washed three more times with TBST before developing them.

Enhanced chemiluminescence (ECL, Table 4) was used to detect the antibody-labelled protein bands on Medical X-ray films (Kodak Film) which were exposed on top of the membrane at different time points in a dark room and developed with the X-ray film processor (Medical Index). The primary and secondary antibodies dilutions used on this work are listed in the Table 17:

Table 17: Antibodies used for Western Blot

Primary Antibody	Dilutions
Goat anti-MRTF-A (C-19)	1:200
Rabbit anti-SRF (G-20)	1:1000
Mouse anti-Ezrin	1:1000
Rabbit anti-MRTF-B	1:1000
Rabbit anti-tubulin	1:5000
Rabbit anti-Rac-1	1:500
Rabbit anti-phospho-myosin light chain 2	1:500
Mouse anti-mDia1	1:1000
Mouse anti-Integrin β1	1:1000
Mouse anti-GFP	1:1000
Secondary Antibody	
Goat anti-rabbit IgG HRP	1:5000
Sheep anti-mouse IgG HRP	1:5000
Anti-goat IgG HRP	1:5000

Donkey anti-goat IgG HRP	1:10000

3.7.2. Reporter gene analysis

MRTF/SRF luciferase reporter assay was assessed for reporter gene analysis where the transcriptional activity of the reporter gene under control of the SRF promoter can be measured. In this work, cells were either transiently transfected with the reporter gene constructs pRL-TK (Promega) and the expression vector pGL3D.AFOS (R. Treisman, The Francis Crick Institute, London, UK) (Mohun, Garrett, and Treisman 1987) or a stable cell line was generated using the FUGW lentiviral system where the SRF promoter, 3D.Aluc (Geneste, Copeland, and Treisman 2002), from the pGL3D.AFOS vector was previously cloned into the lentivirus as explained at the Section 3.3.1.

The reporter pGL3D.AFOS vector presents the c-Fos promoter and three copies of the serum response element (SRE) allowing the SRF-dependent expression of the Firefly luciferase. The co-transfected control vector pRL-TK (Promega) shows Renilla luciferase expression under the control of the viral thymidine kinase promoter. Firefly luciferase activity was normalized to the control reporter pRLTK Renilla luciferase expression.

To generate a stable MCF10A cell line under the control of the MRTF-SRF promoter, lentiviral luciferase reporter gene constructs (Figure 18) were cloned using the FUGW (D. Oliver, University of Marburg, Germany) lentiviral system where the MRTF-SRF promoter 3D.Aluc was linked to GFP and inserted at the FUGW vector replacing its promoter as explained in detail at the section 3.3.1.

Transiently transfected cells or stable cells expressing the SRF luciferase promoter were treated under the desired conditions for each assay and then SRF luciferase activity was quantified (Figure 20). For that, cells were lysed with 200 µl Triton lysis buffer (Baker and Boyce 2014) on ice and collected in 1.5 ml Eppendorf tube, followed by a 10 minutes centrifugation at 13 000 rpm at 4°C. To measure the luciferase activity, first 50 µl Firefly assay buffer (Baker and Boyce 2014) were added to 10 µl of cell lysate, and the first measurement was assessed using a Luminoskan TM Ascent Microplate Luminometer (Thermo Scientific) with the Ascent Software (Thermo Scientific). A second measurement was carried out by adding 75 µl Renilla assay buffer (Baker and Boyce 2014) to the previous wells and finally, the firefly values were normalized to the renilla signal.
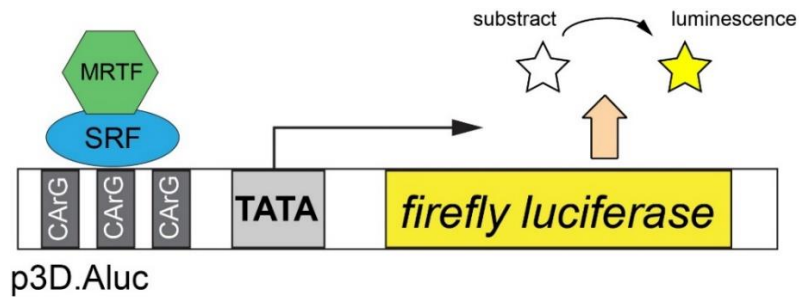
Figure 20: MRTF-SRF luciferase reporter gene expression. This scheme represents the MRTF-SRF driven luciferase reporter gene. SRF reporter gene assays were performed by measuring firefly luciferase activity in cells under the control of the MRTF/SRF luciferase reporter. This reporter gene contains the SRF promoter from the pGL3D.AFOS vector. This image was adapted from (Soto Hinojosa et al. 2017).

3.8. Statistical analysis

The statistical analysis of the data was done using Prism 6 (GraphPad Software). Data analysis is shown as mean ± SD and data distribution was assumed to be normal. Statistical significance was assessed as indicated for each experiment either with the unpaired Student´s t test for the comparison of two conditions or the ANOVA test for the comparison of several conditions. Statistical differences were judged as significant at *, $P < 0.05$; **, $P < 0.01$; ***, $P < 0.001$; and ****, $P < 0.0001$.

4. Results

4.1. Transcriptional regulation of the MRTF/SRF pathway during PM blebbing

Non-apoptotic plasma membrane blebbing is enhanced by matrix deadhesion and as a consequence, cells will potentially undergo bleb-associated cell motility such as entotic invasion and amoeboid blebbing invasion (Figure 31 A). Hence, our aim was to elucidate the underlying signaling pathway controlling plasma membrane (PM) blebbing (Figure 21 A) and further the bleb-dependent mode of invasion known as entosis (Figure 21 B).

Live cell imaging allowed us to investigate the regulation of actin dynamics during plasma membrane blebbing. Thus, characterization and further analysis of bleb dynamics was performed to study the bleb cycle in detail (Figure 21 A) and the importance of non-apoptotic PM-blebbing for bleb-associated cell motility, such as entotic cell-in-cell invasion (Figure 21 B). To examine sustained PM blebbing and subsequent entosis, human breast epithelial MCF10A cells were seeded on poly-HEMA coated dishes, which are known to induce blebbing and entosis by preventing cellular attachment (Overholtzer et al. 2007).
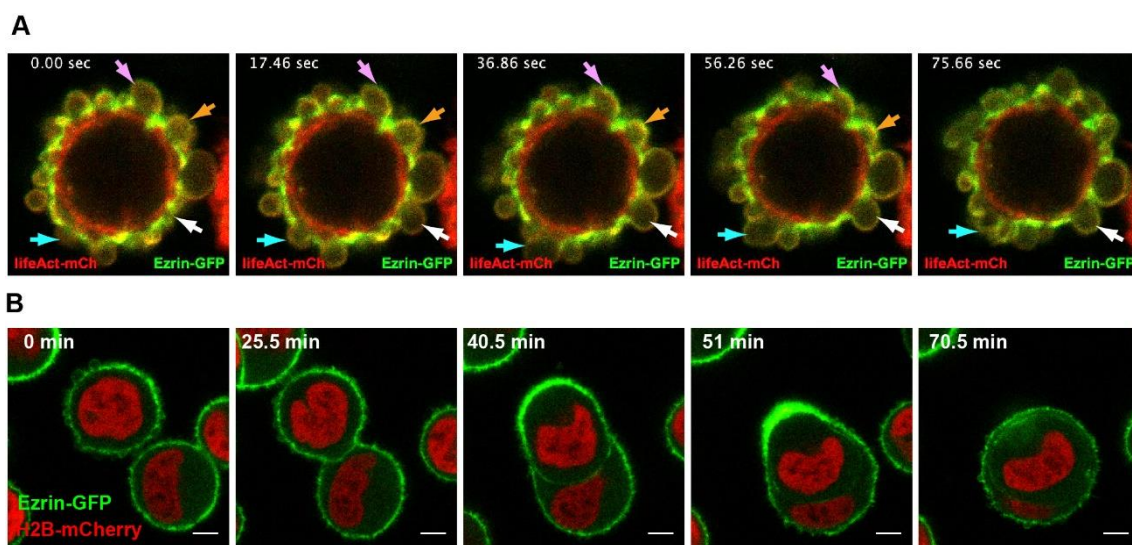
Figure 21: Characterization of plasma membrane blebbing. (A) Bleb cycle in the human breast epithelial cell line MCF10A co-expressing LifeAct-mCherry (red) to label the actin cytoskeleton and the ERM protein Ezrin-GFP (green). Arrows indicate the bleb cycle for individual blebs over time. **(B)** MCF10A cells in suspension stably co-expressing the nuclear marker H2B-mCherry (red) with Ezrin-GFP (green) were monitored to analyze blebbing and subsequent entotic invasion. This time series reveals the importance of plasma membrane blebbing as the driving force for entosis. Scale bars, 5 μm.

4.1.1. Plasma membrane blebbing is affected in the absence of SRF

To study the impact of the MRTF/SRF signaling pathway on plasma membrane blebbing, our first approach was to analyze the effects of Serum Response Factor (SRF) in cells undergoing PM-blebbing. Therefore, bleb dynamics were evaluated upon interfering with MRTF/SRF in human epithelial breast cells MCF10A. First, control or SRF-silenced MCF10A cells stably expressing GFP (Figure 22 C) were plated on poly-HEMA-coated dishes to induce PM blebbing and imaged over time to examine bleb dynamics (Figure 22 A). Here, we observed that SRF-depleted cells showed a different blebbing phenotype, in which blebs were bigger and the bleb cycle was slower compared to the control cells (Figure 22 A-B), suggesting that bleb dynamics are affected in the absence of SRF.

Different parameters were analyzed in order to quantify the observed PM-blebbing phenotype in the absence of SRF, including the bleb cycle dynamics, the bleb size and the ratio of blebbing and non-blebbing cells. The maximum bleb expansion length was measured and indeed, our data showed that SRF-depleted MCF10A cells produced bigger blebs than control cells in suspension (Figure 22 D). Then, we focused on bleb dynamics and followed in detail the bleb cycle for individual blebs over time quantifying expansion and retraction times. Interestingly, our data showed that bleb retraction is significantly prolonged in the absence of SRF (Figure 22 B and E). As a consequence, the total bleb cycle time was increased in SRF-depleted cells, whereas bleb expansion remained unaffected in the absence of SRF (Figure 22 B and E). Consistent with this, we found that SRF-depleted cells presented less blebbing activity compared to cells treated with control siRNA (Figure 22 F). Overall these data suggest that functional non-apoptotic PM blebbing is impaired in the absence of SRF, indicating that SRF is required for efficient bleb retraction and dynamic PM blebbing.
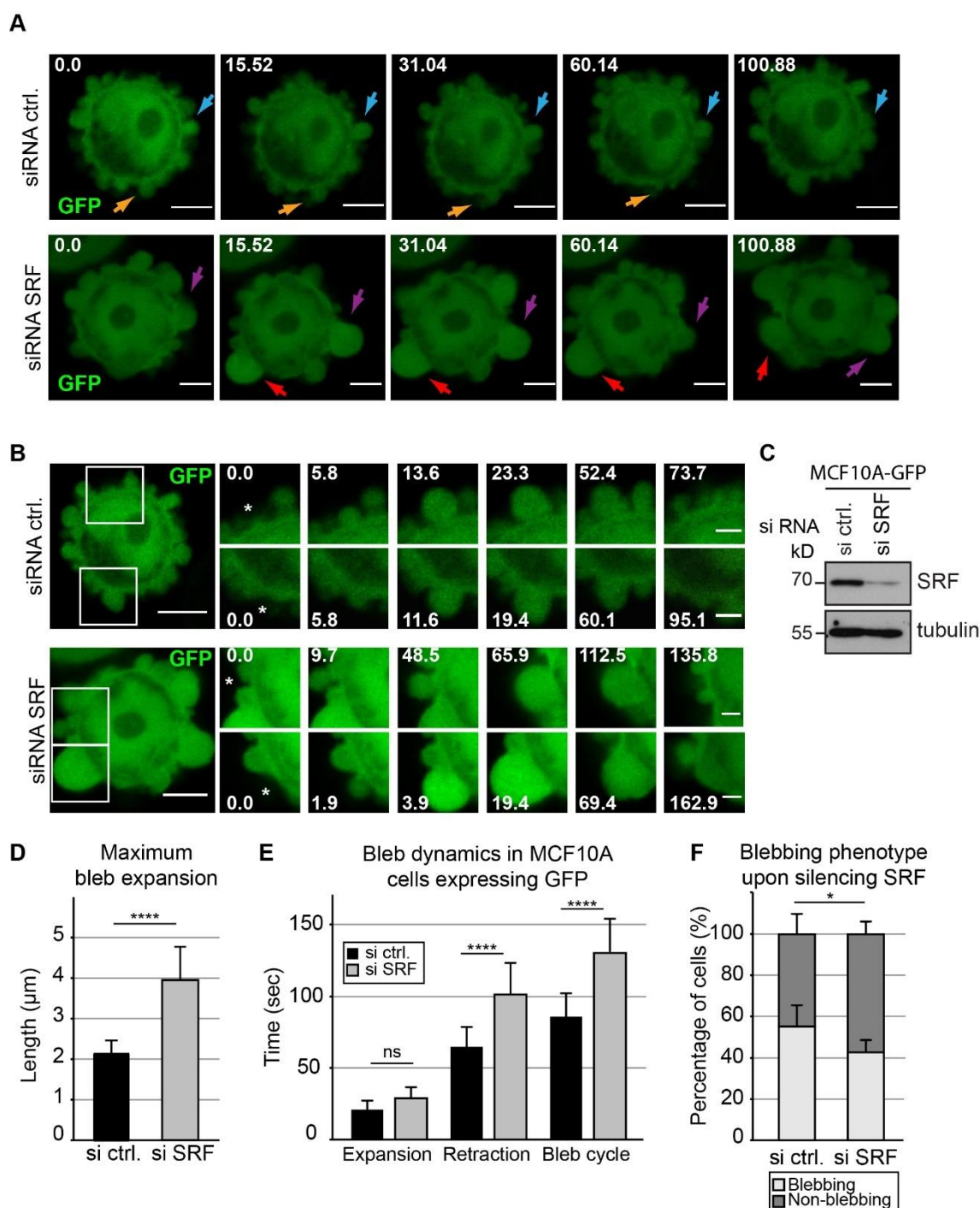
Figure 22: Non-apoptotic blebbing phenotype is impaired in SRF-depleted cells. (A) Time-lapse imaging of MCF10A cells stably expressing GFP (green) transfected with control or SRF siRNAs and seeded on poly-HEMA coated dishes to analyze bleb dynamics. Arrows indicate the bleb cycle for individual blebs over time. Time is indicated in seconds. Scale bars, 5 μm. **(B)** Live MCF10A cells stably expressing GFP, treated with the indicated siRNAs plated on poly-HEMA culture dishes to monitor rapid plasma membrane blebbing. Time is indicated in seconds. Areas marked by white boxes are shown magnified over time to highlight expansion and retraction of individual blebs (indicated by asterisks). Scale bars, 5 μm (overview) and 2 μm (magnification). **(C)** Western Blot demonstrating SRF knockdown efficiency in MCF10A cells stably expressing GFP. Tubulin served as loading control. **(D)** MCF10A cells stably expressing GFP

transfected with indicated siRNAs were monitored over time to quantify the maximum bleb expansion length for individual blebs. Errors bars indicate SD and asterisks indicate statistical significance (****, P < 0.0001). **(E)** Quantification of bleb dynamics in blebbing cells stably expressing GFP. MCF10A cells treated with indicated siRNAs to quantify time for expansion, retraction and total bleb cycle of individual blebs. At least 60 blebs and 15 cells per condition were measured. Errors bars indicate SD and asterisks indicate statistical significance (****, P < 0.0001). ns indicates no significance (P ≥ 0.05). **(F)** Blebbing phenotypes were quantified in MCF10A cells stably expressing GFP treated with indicated siRNAs. At least 100 cells were quantified for each condition from 6 independent experiments. Errors bars indicate SD and asterisks indicate statistical significance (*, P < 0.05).

4.1.2. Cortical contractility and PM blebbing regulate nucleocytoplasmic MRTF-A shuttling

Myocardin-related transcription factor A (MRTF-A) is a well-known actin-regulated transcriptional coactivator of Serum Response Factor (SRF). Given our previous observation suggesting a potential link between SRF transcription and regulation of bleb dynamics, we next investigated the effects of the SRF transcriptional coactivator MRTF-A in continuous plasma membrane blebbing.

Subcellular MRTF-A localization is dependent on the G-actin concentration, and for instance the formation of F-actin contributes to less G-actin, which results in nuclear MRTF-A translocation. Nuclear MRTF-A accumulation is promoted upon release of G-actin, which can occur due to actin polymerization leading to SRF-dependent gene expression (Vartiainen et al. 2007; Baarlink, Wang, and Grosse 2013; Mouilleron et al. 2011). Serum stimulation was shown to trigger nuclear MRTF-A accumulation inducing nuclear actin polymerization (Miralles et al. 2003; Baarlink, Wang, and Grosse 2013). Therefore, we confirmed endogenous MRTF-A nuclear accumulation in response to serum stimulation in human MCF10A cells (Figure 23 B) reproducing the results observed in mouse fibroblast NIH3T3 cells (Miralles et al. 2003). Thus, our data indicate that the serum response also mediates nucleocytoplasmic MRTF-A shuttling in MCF10A cells.
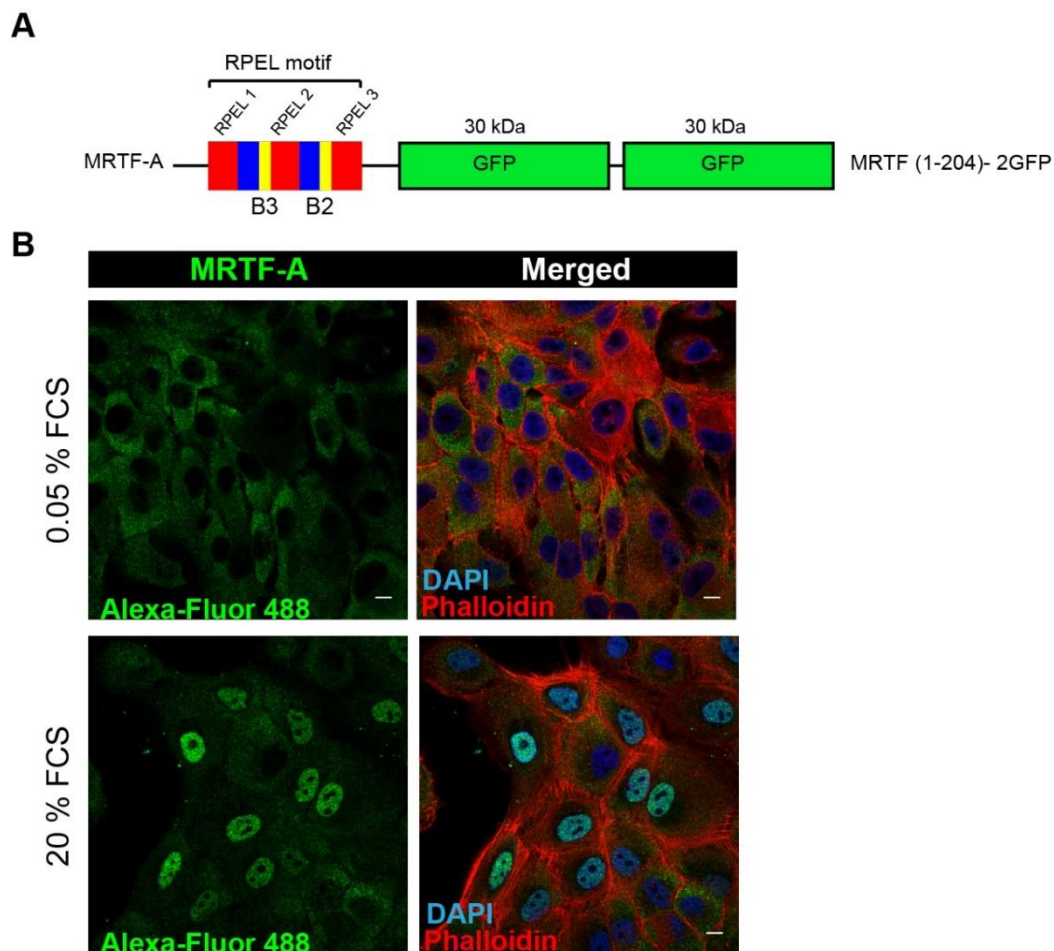
Figure 23: Serum induces nucleocytoplasmic MRTF-A shuttling in MCF10A cells. (A) Schematic representation of the MRTF-A RPEL domains tagged to two GFPs. The RPEL motif has been shown to be sufficient to allow nucleocytoplasmic MRTF-A shuttling upon serum stimulation. **(B)** Immunolabelling of endogenous MRTF-A (green), nuclei (DAPI, blue) and F-actin (Phalloidin, red) of MCF10A cells under starving conditions or upon 15 minutes of 20% serum (FCS) stimulation as indicated. Scale bars, 10 μm.

We next evaluated whether non-apoptotic plasma membrane blebbing affects MRTF-A subcellular distribution. MCF10A cells stably expressing MRTF-A were generated via viral transduction using either the MRTF-A RPEL domain or the full-length MRTF-A. The RPEL motif of MRTF-A has been reported to be sufficient to control nucleocytoplasmic shuttling of MRTF-A upon serum stimulation (Guettler et al. 2008). Hence, the full-length MRTF-A or the RPEL domain were linked to one or two GFP sequences into a lentiviral vector to generate a stable MCF10A cell line inducibly expressing the full-length MRTF-A-GFP or constitutively expressing RPEL-2GFP, respectively (Figure 23 A).

To analyze MRTF-A subcellular localization during induced plasma membrane blebbing, MCF10A cells stably expressing either the RPEL domain or full length MRTF-A were plated on poly-HEMA culture dishes to induce matrix deadhesion, which in turn triggers blebbing activity (Figure 24

A). Cells were imaged with a confocal microscope to monitor MRTF-A localization over time during PM blebbing. Notably, we observed that dynamic nucleocytoplasmic MRTF-A shuttling is blebbing dependent, whereby blebbing cells present nuclear MRTF-A and non-blebbing cells show cytoplasmic MRTF-A localization (Figure 24 B and D). Surprisingly, this rapid dynamic process shows cells initiating blebbing activity with nuclear MRTF-A accumulation and within minutes cells eventually stop blebbing leading to MRTF-A translocation to the cytoplasm (Figure 24 B and D, arrows indicate shuttling). To verify our findings, the subcellular distribution of MRTF-A or RPEL domain was quantified in blebbing cells and compared with non-blebbing cells. Consistently, quantification results showed blebbing cells with mostly predominant nuclear MRTF-A accumulation, while non-blebbing cells presented cytoplasmic or pan-cellular MRTF-A localization (Figure 24 C and E). These data reveal a striking correlation between PM blebbing and dynamic nuclear MRTF-A accumulation, indicating that nucleocytoplasmic MRTF-A translocation depends on blebbing activity.

To further investigate a link between the contractile actin cortex and MRTF-A localization in induced PM blebbing, Blebbistatin was used to disrupt blebbing activity. This drug is a small molecule inhibitor of non-muscle myosin IIA known to block plasma membrane blebbing (Cheung et al. 2002; Straight et al. 2003; Limouze et al. 2004; Guillaume T Charras et al. 2006; Norman, Sengupta, and Aranda-Espinoza 2011). Drug treatment with Blebbistatin resulted in complete MRTF-A translocation to the cytoplasm within 30 minutes (Figure 25 A). Subcellular MRTF-A localization was then quantified to validate our data in response to 100 µM Blebbistatin treatment for 30 minutes. The results show that cells blebbing activity ceased triggering MRTF-A export to the cytoplasm (Figure 25 B).

We report here that PM blebbing together with the contractile actin cortex control dynamic MRTF-A nucleocytoplasmic translocation, which in turn suggest that MRTF/SRF might be involved in sustained long-term PM blebbing.
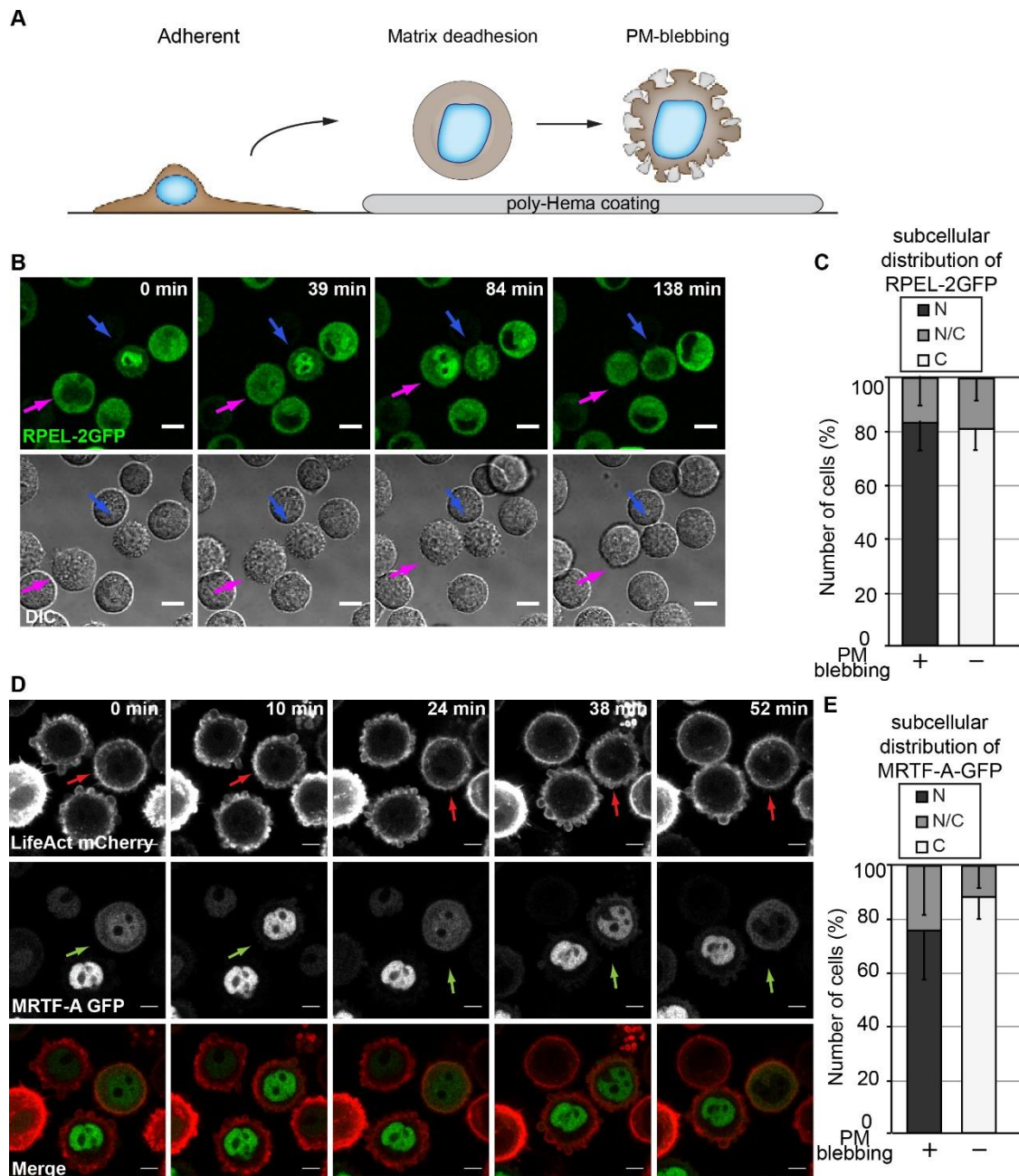
Figure 24: Plasma membrane blebbing triggers dynamic nuclear MRTF-A accumulation. (A) This cartoon illustrates the work flow to study bleb dynamics. Adherent MCF10A cells are detached and subsequently plated on poly-HEMA coated dishes preventing cellular attachment. As a result of a lack of matrix adhesion, plasma membrane blebbing is eventually induced. **(B)** Live MCF10A cells stably expressing RPEL-2GFP (green) plated on poly-HEMA were monitored over time to analyze RPEL subcellular localization. Differential interference contrast (DIC) was added for each frame to visualize plasma membrane blebbing. Arrows indicate RPEL-2GFP shuttling cells. Scale bars, 10 µm. **(C)** Quantification of RPEL-2GFP subcellular localization for blebbing and non-blebbing MCF10A cells stably expressing RPEL-2GFP plated on poly-HEMA. At least 100 cells from four independent experiments were quantified. Localization was defined as predominantly cytoplasmic (C), pancellular (N/C), or nuclear (N). Error bars indicate SD. **(D)** Time-lapse imaging of MCF10A cells stably co-expressing MRTF-A-GFP (green) together with LifeAct-mCherry (red)

76

seeded on poly-HEMA coated dishes to monitor MRTF-A-GFP subcellular localization over time. LifeAct-mCherry expression labelling the actin cytoskeleton allows visualization of blebs. Arrows indicate a cell with dynamic nucleocytoplasmic MRTF-A shuttling. Scale bars, 5 μm. **(E)** Quantification of subcellular distribution of MRTF-A-GFP in blebbing and non-blebbing MCF10A cells stably expressing GFP-tagged MRTF-A on poly-HEMA as in **C.** At least 180 cells from six independent experiments were quantified. Localization is defined as described in **C.** Error bars indicate SD.
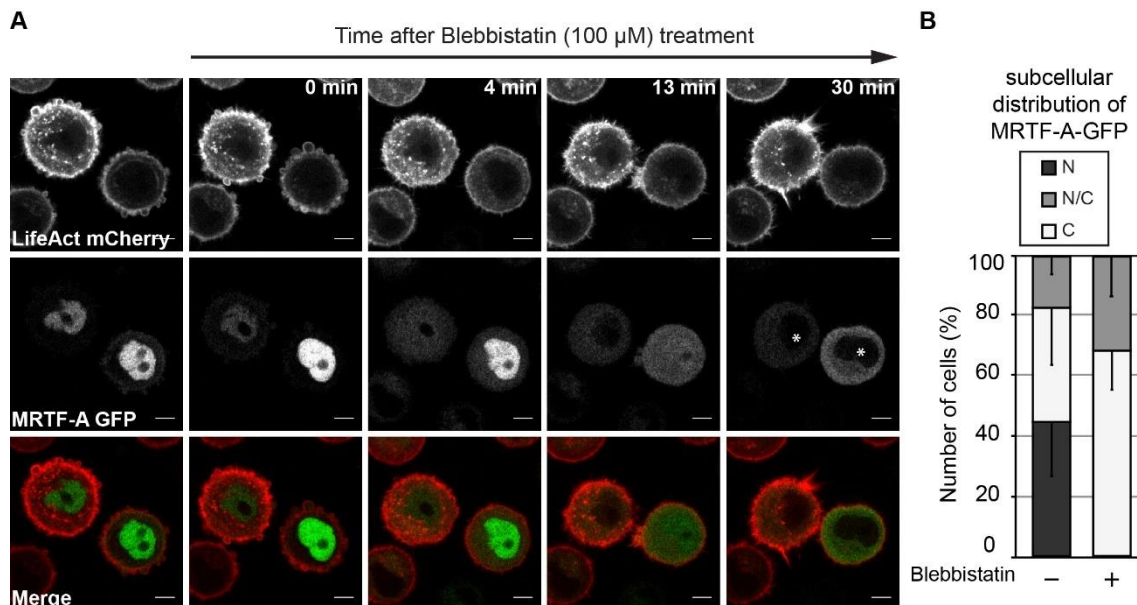
Figure 25: Blebbistatin treatment blocks blebbing activity leading to MRTF-A cytoplasmic export. (A) Time-lapse imaging of MCF10A cells stably co-expressing MRTF-A-tagged GFP (green) and LifeAct-tagged mCherry (red) plated on poly-HEMA were treated with the non-muscle myosin IIa inhibitor Blebbistatin (100 μM) at 0 min and MRTF-A-GFP subcellular distribution was monitored over time as indicated. LifeAct-mCherry is included to visualize plasma membrane blebbing and reveals inhibition of blebbing activity. Asterisks indicate cells with cytoplasmic export of MRTF-A. Scale bars, 5 μm. **(B)** Quantification of MRTF-A-GFP subcellular distribution after treatment with 100 μM Blebbistatin for 30 minutes in MCF10A cells compared to non-treated cells. At least 200 cells from six independent experiments were quantified. Localization was defined as cytoplasmic (C), pancellular (N/C), or nuclear (N). Error bars indicate SD.

4.1.3. MRTF/SRF transcriptional activity is induced by sustained PM blebbing

These findings suggested that the MRTF/SRF pathway appears to play a role in PM blebbing. Our next goal was to investigate the direct link between induced continuous blebbing and MRTF/SRF transcription. Therefore, we examined whether matrix deadhesion induced PM blebbing directly stimulates MRTF/SRF activity and if SRF transcription is affected upon PM blebbing. Consistent with our previous experimental model, plasma membrane blebbing was induced by plating the cells on poly-HEMA coated culture dishes to prevent cellular adhesion. Consequently, cells will remain in suspension and present blebbing activity, and eventually entotic events will take place (Figure 24 A).

SRF luciferase reporter genes assays were assessed to test our hypothesis and understand whether sustained long-term plasma membrane blebbing conditions regulate actin-mediated MRTF/SRF transcriptional activity. For that, the SRF reporter gene tagged to GFP was cloned into the lentiviral vector FUGW and then MCF10A cells were transduced to stably express the SRF reporter gene linked to GFP. The luciferase reporter gene construct was originally closed under the control of the SRF promoter 3D.Aluc (Geneste, Copeland, and Treisman 2002) generating the SRF luciferase reporter gene, which allows us to measure accumulation of luciferase protein under the SRF promoter by luminescence measurement.

Serum stimulation assays were performed to validate the MCF10A cell lines stably expressing the SRF-luciferase reporter. As expected, the negative control cell line without a promoter showed no SRF luciferase activity (Figure 26 A), whereas the cell line expressing the hUBc promoter from the lentiviral FUGW showed constitutively active SRF luciferase activity either with or without serum stimulation (Figure 26 A). Importantly, the CArG-(MRTF/SRF)-driven cell line showed a remarkable increase of luciferase activity in response to serum (Figure 26 A) allowing the determination of the activity of the MRTF/SRF transcriptional pathway by luminometric quantification of the luciferase protein.

We next aimed to investigate whether sustained long-term blebbing enhances SRF luciferase activity. To test this hypothesis, we evaluated SRF induction in MCF10A cells stably expressing SRF luciferase reporter cultured on poly-HEMA for longer periods of time. Our data showed a notable increase of SRF luciferase activity upon induced sustained long-term PM blebbing over time under these conditions (Figure 26 B), suggesting that SRF luciferase activity is stimulated in response to continuous dynamic PM-blebbing activity. Consistent with this, qPCR-based analysis of SRF transcript levels were assessed to confirm our observations and, similarly, we found that SRF is upregulated upon induced PM-blebbing (Figure 26 C), indicating MRTF/SRF activity in response to blebbing, since SRF is a target gene of its own transcriptional activity (Esnault et al. 2014). Taken together, these data suggest that long-term non-apoptotic PM blebbing is coupled to nuclear MRTF-A shuttling, which enhances upregulation of SRF expression on a transcript as well as protein level.
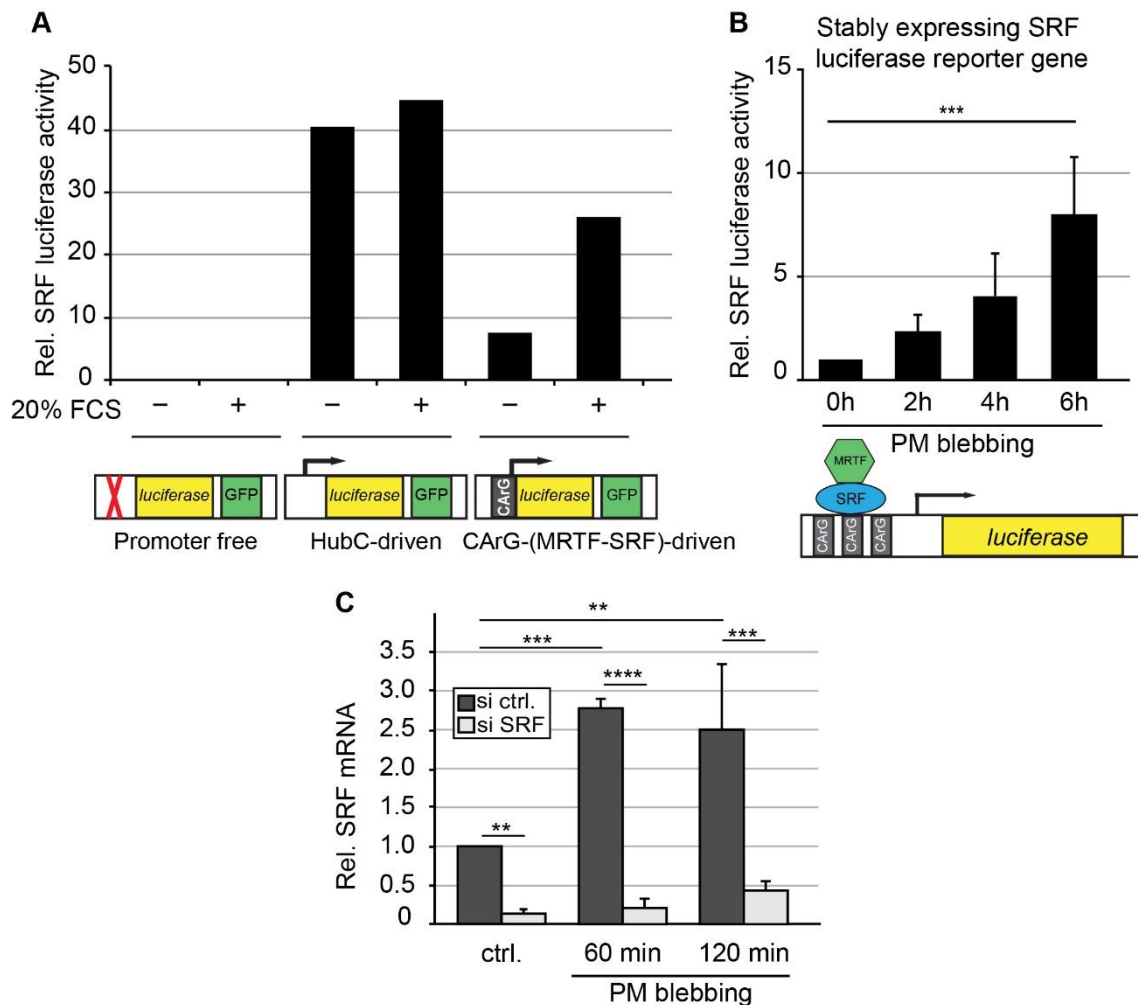
Figure 26: Sustained long-term PM blebbing enhances MRTF/SRF activity. (A) To validate the MCF10A cell lines stably expressing different luciferase reporter constructs, cells were either serum deprived for 24h followed by stimulation with 20% serum for 7h or serum deprived for a total time of 31h. Then, the amount of firefly luciferase was measured luminometrically to assess relative levels of SRF luciferase activity. Results are shown from one experiment. **(B)** The amount of firefly luciferase was measured in MCF10A cells stably expressing the SRF luciferase reporter, seeded on poly-HEMA for indicated periods of time. Results are shown as means from four independent experiments. Error bars indicate SD. Asterisks indicate statistical significance (***, P < 0.001). **(C)** Relative SRF mRNA levels were assessed by quantitative RT-PCR from MCF10A cells, which where adherent (ctrl.) or plated on poly-HEMA for the indicated periods of time to induce PM blebbing. MCF10A cells were transfected with either control or SRF siRNA prior to plating. Note SRF mRNA upregulation upon PM blebbing and validation of SRF knockdown. Results are shown as means from three independent experiments. Error bars indicate SD and asterisks indicate statistical significance (**, P < 0.01; ***, P < 0.001; ****, P < 0.0001).

4.1.4. Dynamic PM blebbing induces MRTF/SRF transcriptional activity leading to Ezrin upregulation

Given our findings that MRTF/SRF transcriptional activity is dependent on PM blebbing, we next aimed to identify the specific target genes involved in our bleb-dependent invasion model (Figure 31 A). ERM proteins are known to be involved during the bleb cycle to reassemble the actin cortex (G. Charras and Paluch 2008), thereby we investigated whether ERM proteins could be potential MRTF/SRF target genes under our sustained blebbing conditions.

Our findings so far revealed that expression of the ERM protein Ezrin is robustly upregulated on a protein and transcript level upon induced PM-blebbing (Figure 27 A-C). Hence, we evaluated whether MRTF/SRF is involved in Ezrin upregulation. For that, we employed knockdown of SRF or double knockdown of MRTF-A and B in MCF10A cells. Surprisingly, induction of Ezrin transcript levels is reduced in the absence of SRF or MRTF-A/B (Figure 27 A-B), indicating that blebbing stimulates upregulation of Ezrin in a MRTF/SRF-dependent manner.

Even though these data suggest that sustained PM blebbing induces MRTF/SRF-dependent upregulation of Ezrin expression, we further tested whether other ERM proteins and other actin-associated proteins are also potential target genes to confirm our hypothesis and determine the specificity towards Ezrin. Nonetheless, our results show that Radixin, Moesin or Myosin are neither upregulated by induced PM-blebbing nor are dependent on the MRTF/SRF signaling pathway (Figure 27 D-F) demonstrating Ezrin exclusivity. Thus, MRTF/SRF induction upon induced PM-blebbing appears to be specific for the metastatic ERM protein Ezrin.
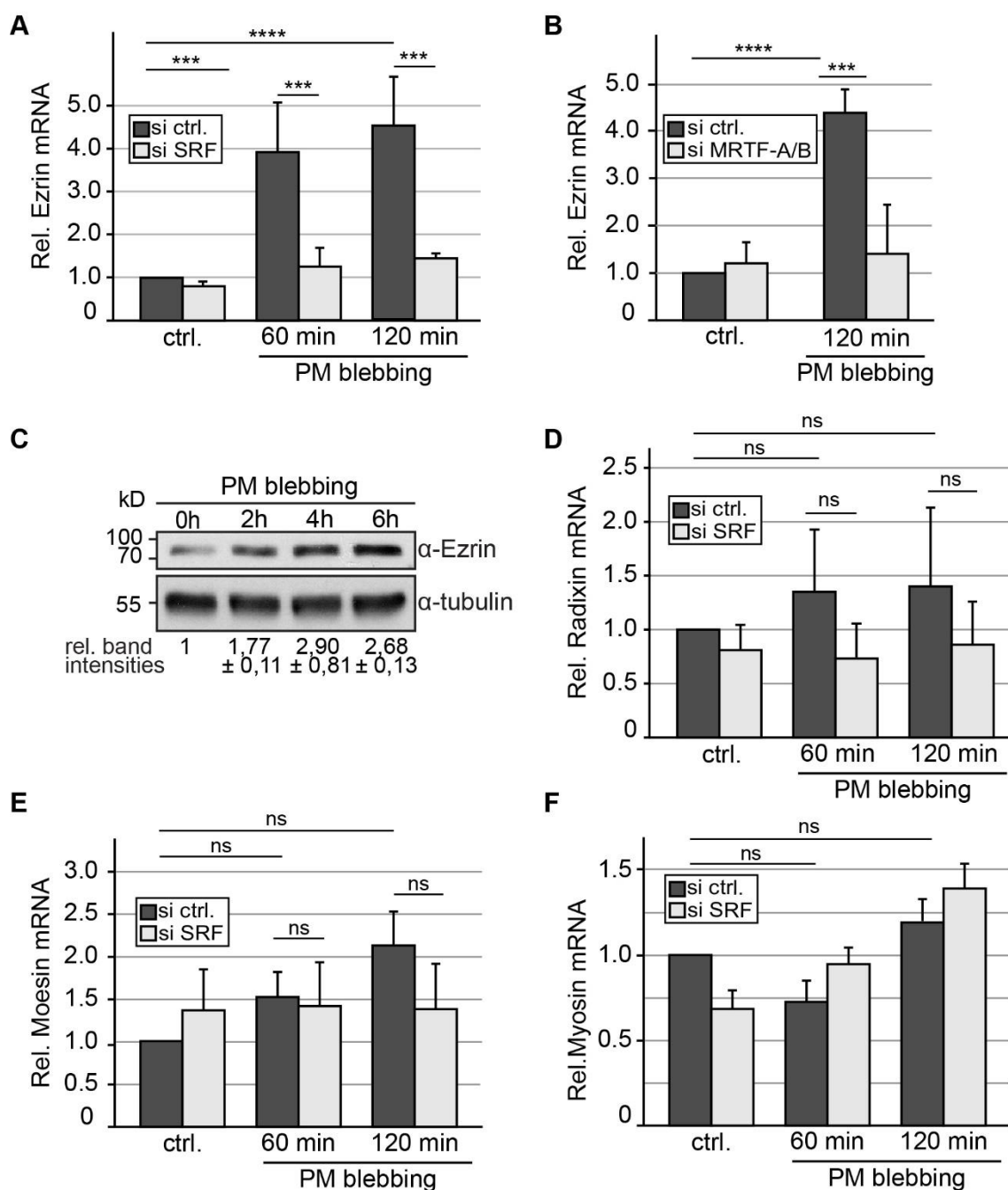
Figure 27: PM blebbing triggers MRTF/SRF-dependent upregulation of the ERM Ezrin. (A, B, D, E, F) Relative mRNA levels from MCF10A cells either attached (ctrl.) or plated on poly-HEMA culture dishes to induce blebbing for the indicated periods of time were assessed by quantitative RT-PCR. Errors bars indicate SD and asterisks indicate statistical significance (ns, $P \geq 0.05$; ***, $P < 0.001$; ****, $P < 0.0001$). **(A)** Relative Ezrin mRNA levels from MCF10A cells transfected with control or SRF siRNA were compared by quantitative RT-PCR. Results are shown as the mean from three independent experiments. **(B)** Relative Ezrin mRNA levels from MCF10A cells transfected with control or combined siRNAs against MRTF-A and MRTF-B were compared. Results are shown as the mean from three independent experiments. **(C)** Western blot analysis showing Ezrin protein expression in MCF10A cells plated on poly-HEMA to induce plasma membrane blebbing for indicated durations. Tubulin served as loading control. Western blot band intensities were densitometrically quantified from two independent experiments using ImageJ. **(D-F)**

Relative mRNA levels of Radixin **(D)**, Moesin **(E)** and Myosin **(F)** from MCF10A cells transfected with control or SRF siRNA were compared. Results are shown as the mean from three independent experiments.

To further verify that Ezrin is upregulated in a MRTF/SRF-dependent manner during blebbing, the prototypic serum stimulation assay was tested in MCF10A cells. At first, we confirmed that the well-known SRF-inducible immediate early target genes Fos and CYR61 (O'Brien et al. 1990; Müller et al. 1984) were enhanced in response to serum stimulation in human MCF10A cell system (Figure 28 A). Our data indicate that Ezrin mRNA levels are upregulated upon serum stimulation, while Radixin and Moesin are not affected (Figure 28 B).
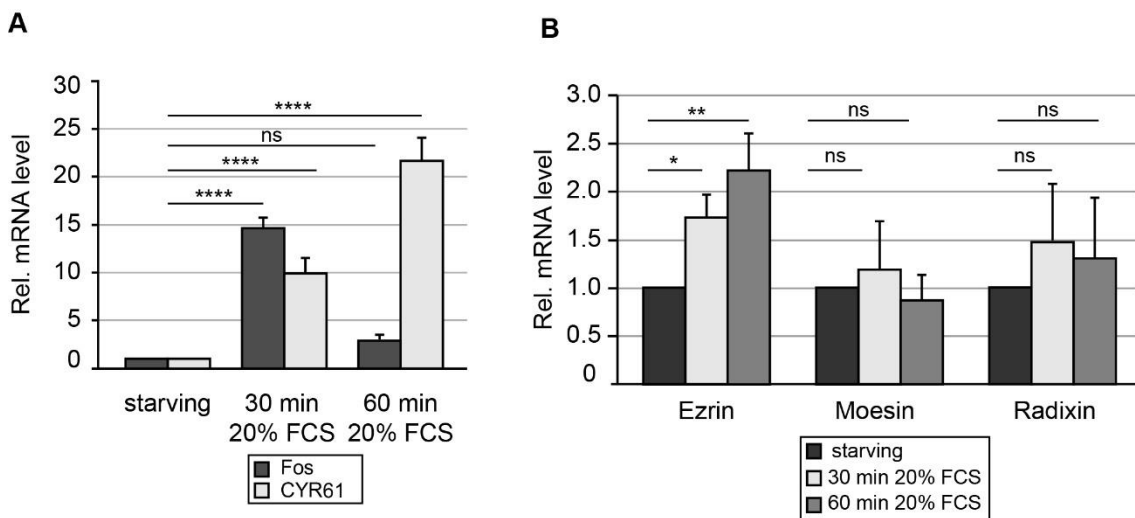
Figure 28: Serum stimulation leads to upregulation of the ERM protein Ezrin. (A) Relative mRNA levels of Fos and CYR61 were assessed by quantitative RT-PCR from MCF10A cells maintained under serum deprivation conditions with 0.05% FCS for 24h, followed by serum stimulation using 20% horse serum for the indicated periods of time. Results are shown as the mean from three independent experiments. Error bars indicate SD and asterisks indicate statistical significance (****, $P < 0.0001$). ns indicates no significance ($P \geq 0.05$). **(B)** Relative mRNA levels of Ezrin, Radixin and Moesin were assessed from MCF10A cells in serum-deprived conditions for 24h and then stimulated either with or without serum for the indicated periods of time. Results are shown as the mean from three independent experiments. Error bars indicate SD and asterisks indicate statistical significance (*, $P < 0.05$; **, $P < 0.01$). ns indicates no significance ($P \geq 0.05$).

Next, we were interested to confirm that plasma membrane blebbing and not matrix deadhesion *per se* is the condition that triggers nuclear accumulation of MRTF-A upon plating cells on poly-HEMA coated dishes. Therefore, MCF10A cells were detached and plated on poly-HEMA to stimulate blebbing and treated either with the ROCK inhibitor Y27632 or the myosin II-A drug Blebbistatin. Treatment with Blebbistatin is known to block blebbing activity and the ROCK inhibitor drug has been described to interfere with entosis (Purvanov et al. 2014). As a

result of drug treatments, relative SRF and Ezrin mRNA transcript levels were unaffected upon PM-blebbing (Figure 29 A-B). Thus, preventing blebbing inhibits SRF and Ezrin transcriptional upregulation, which confirms our hypothesis that matrix deadhesion triggers blebbing-inducing MRTF/SRF-mediated upregulation of Ezrin. Together these findings reveal that matrix deadhesion induces cellular blebbing, which in turn enhances MRTF/SRF-dependent upregulation of the specific ERM protein Ezrin.

A

B
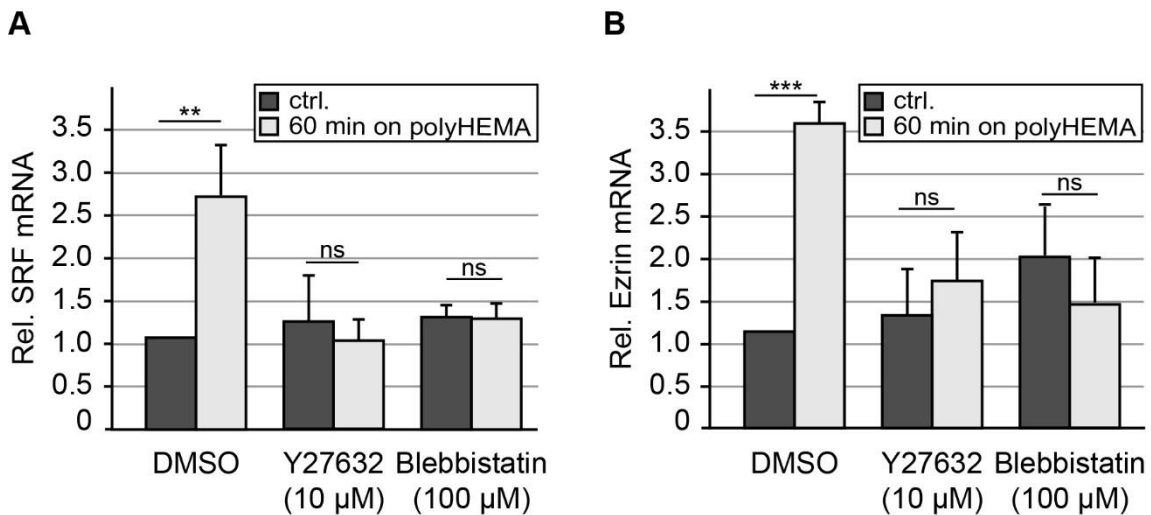
Figure 29: Detachment-induced upregulation of SRF and Ezrin depends on PM blebbing. Relative mRNA levels of SRF **(A)** and Ezrin **(B)** were assessed by quantitative RT-PCR from MCF10A cells cultured in attached conditions (ctrl.) or plated on poly-HEMA for 60 min. Cells were treated either with 10 µM ROCK inhibitor Y27632, 100 µM Blebbistatin or 0.1% DMSO (ctrl.) for 60 min. Results are shown as the mean from three independent experiments. Error bars indicate SD and asterisks indicate statistical significance (**, $P < 0.01$; ***, $P < 0.001$). ns indicates no significance ($P \geq 0.05$).

4.1.5. Effects of the MRTF/SRF transcriptional pathway on formin mDia1

Previous work from our laboratory has reported the importance of the Diaphanous formin mDia1 downstream of Rho for bleb-associated cancer invasion (Thomas M Kitzing et al. 2007), as well as for functional non-apoptotic plasma membrane blebbing driving entotic cell-in-cell invasion (Purvanov et al. 2014).

Therefore, we hypothesized that the actin nucleation factor mDia1 may also play a role in the MRTF/SRF transcriptional pathway. Hence, we assessed the protein and transcript levels of mDia1 in SRF-depleted MCF10A cells. However, expression levels of formin mDia1 were not affected in the absence of SRF (Figure 30 A-B), indicating that SRF silencing does not alter expression of the formin mDia1.

A

B
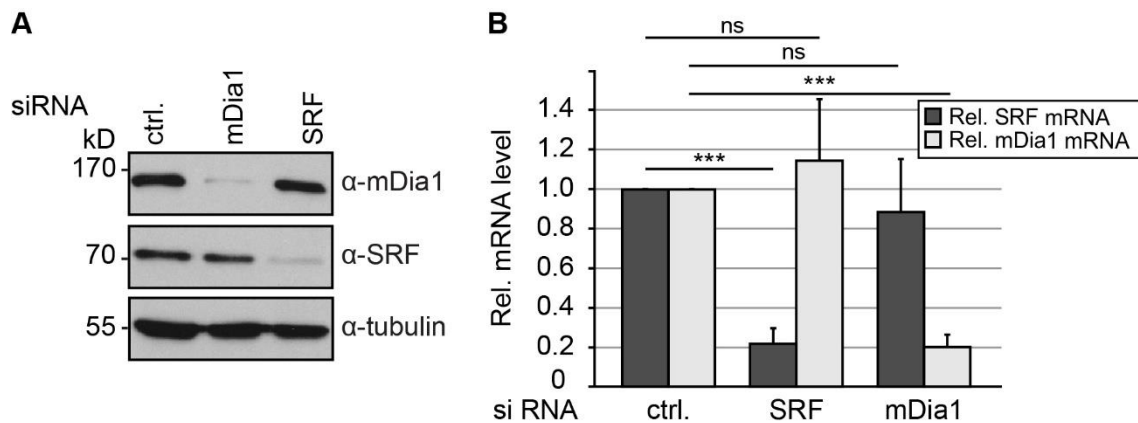
Figure 30: The MRTF/SRF pathway has no effect on formin mDia1 expression. (A) Western blot showing no effect on expression levels of formin mDia1 in SRF-depleted MCF10A cells and *vice versa* no influence of mDia1 depletion on protein levels of SRF. Results confirm siRNA-mediated knockdown efficiencies for SRF and mDia1 in MCF10A cells. Tubulin served as loading control. **(B)** Relative mRNA levels of SRF and mDia1 were assessed by quantitative RT-PCR from MCF10A cells treated either with control siRNA, siRNA directed against SRF or mDia1. Results are shown as the mean from three independent experiments. Error bars indicate SD and asterisks indicate statistical significance (***, P < 0. 001). ns indicates no significance (P ≥ 0.05).

4.2. The importance of MRTF/SRF transcription for entotic invasion

Given the crucial role of blebbing in driving entotic invasion (Purvanov et al. 2014), we next aimed to understand if MRTF/SRF transcriptional regulation is involved in bleb-associated entotic invasion.

4.2.1. Role of the ERM protein Ezrin during entotic cell-in-cell invasion

Since MRTF/SRF appears to be important in plasma membrane blebbing and to further analyze this process, we tested the impact of this pathway on entosis (Figure 31 A). Although our results identified the ERM Ezrin as a MRTF/SRF target gene, it was unclear if Ezrin expression plays a role in PM blebbing and subsequent entotic invasion. It is known that ERM proteins localize at the cell cortex and interact with the plasma membrane and the actin cytoskeleton. Interestingly, previous findings showed that membrane blebbing is Ezrin-dependent and blebbing is decreased at the Ezrin-rich uropod-like structure during amoeboid blebbing invasion (Lorentzen et al. 2011).
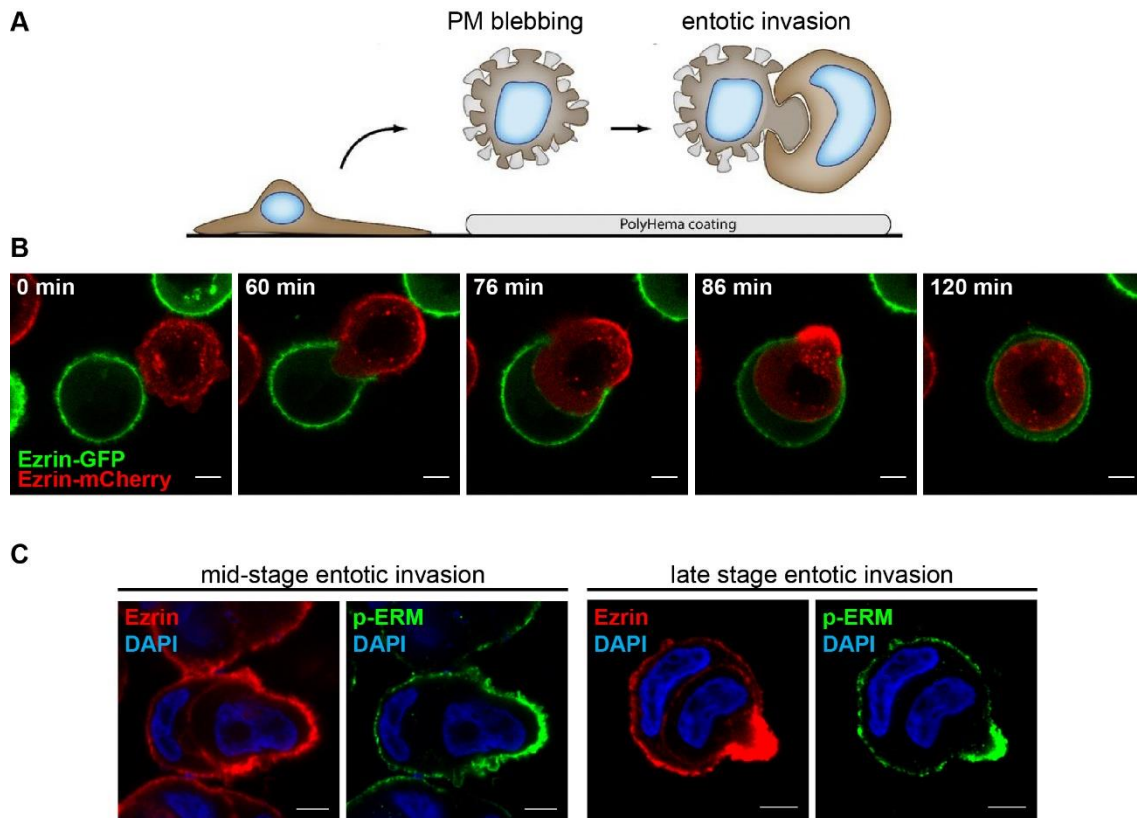
Figure 31: The ERM protein Ezrin is redistributed at the rear end of the invading cell. (A) This cartoon illustrates an experimental model to study induced plasma membrane blebbing and subsequent entotic invasion by plating cells on poly-HEMA to prevent cellular attachment. **(B)** Live MCF10A cell stably expressing the ERM Ezrin-tagged to mCherry (red) invading into another cell expressing Ezrin-tagged GFP (green) were monitored over time to visualize Ezrin distribution during cell-in-cell invasion. Note the polarized redistribution and enrichment of Ezrin-mCherry at the rear end of the invading cell. Time (min) is indicated at the upper left corner. Scale bars, 5 µm. **(C)** Immunolabelling of endogenous Ezrin (red), phospho-Ezrin/Radixin/Moesin (green) and nuclei (DAPI, blue) in MCF10A cells fixed after 4h in suspension to induce entotic invasion. Note the polar redistribution of Ezrin and p-ERM at the rear of the invading cell during cell engulfment and at the uropod-like structure phase. Scale bars, 5 µm.

To this end, we generated a MCF10A cell line stably co-expressing GFP-tagged Ezrin (green) together with the nuclear marker mCherry-tagged H2B (red) to monitor Ezrin localization over time during entotic invasion. We observed that Ezrin is redistributed and accumulated at the rear end of the invading cell during advanced stages of cell-in-cell invasion, such as cell engulfment and at the uropod-like structure (Figure 21 B and Figure 31 B). To further confirm Ezrin redistribution and enrichment at the invading cell during entosis, Ezrin-GFP and Ezrin-mCherry expressing MCF10A cells were mixed and the entosis outcome analyzed. Indeed, this dual color-assay confirmed polarized enrichment of Ezrin at the rear end of the invading cell that is driving entotic invasion (Figure 31 B).

To gain insights into Ezrin activation, we examined the activation state of Ezrin during the entotic invasion process by evaluating Ezrin's phosphorylation state. We observed that endogenous phosphorylated-ERM (pERM) colocalizes with endogenous Ezrin during entotic invasion showing a polarized enrichment of pERM at the rear of the invading cell (Figure 31 C).

4.2.2. Entotic invasion requires transcriptional activity and MRTF/SRF transcription

In order to address whether transcriptional activity plays an important role for entotic invasion, global transcription was blocked by applying 50 µg/ml Actinomycin D (Bensaude 2011) and subsequently, entosis ability was quantified. First, we verified effective inhibition of transcription using the indicated concentration and duration of Actinomycin D treatment in a serum stimulation assay, which confirms the efficiency of the inhibitor, since it robustly blocks Fos mRNA induction (Figure 32 B). Entosis assays showed a significant decrease in entotic invasion upon Actinomycin D treatment compared to non-treated MCF10A cells (Figure 32 A and C). We then blocked translation to interfere with protein synthesis using the translation inhibitor Cycloheximide and studied its effects on entosis. Treatment of MCF10A cells with 100 µg/ml Cycloheximide resulted in a complete block of entosis (Figure 32 A and C), indicating that both global transcription and translation are crucial events for entosis.

SRF and its transcriptional coactivator MRTF-A are known to regulate actin-related target genes, but also genes fundamental for cell proliferation and tumor growth (Leitner et al. 2011; Ohrnberger et al. 2015; Shaposhnikov et al. 2013). Nonetheless, whether MRTF/SRF and Ezrin affect entotic invasion was unknown. To test if Ezrin, MRTF or SRF are required for entosis, MCF10A cells were silenced with siRNAs directed against Ezrin, MRTF A/B or SRF and then, entosis assays were performed. Our data showed successful knockdown (Figure 33 A) and surprisingly, that silencing of either Ezrin, MRTF A/B or SRF lead to strongly decreased entosis (Figure 33 B), suggesting that MRTF/SRF and Ezrin are required for entotic invasion. Taken together, these results indicate that global transcriptional activity and the specific MRTF/SRF transcriptional pathway are crucial for entotic cell-in-cell invasion.

A

B **C**
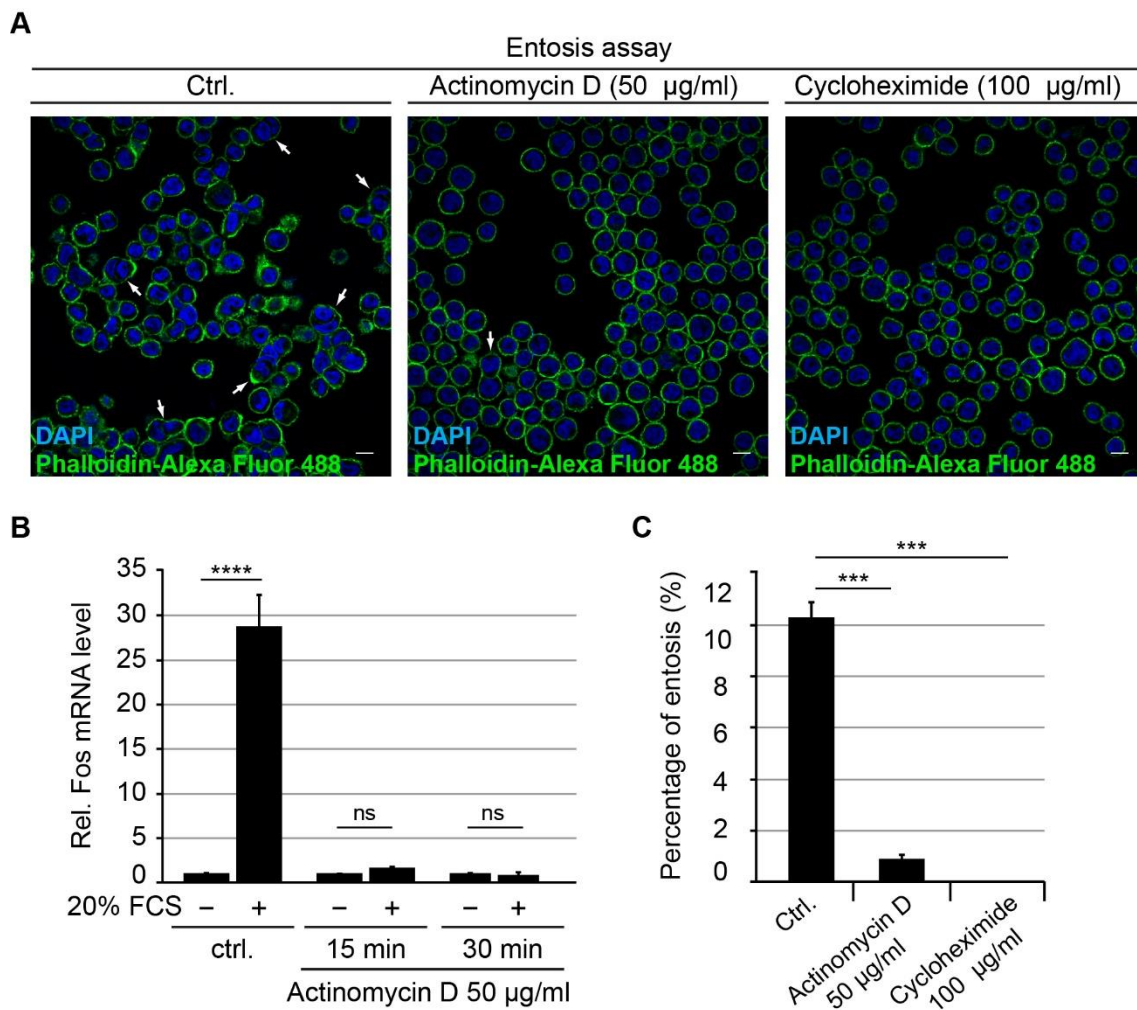
Figure 32: Global transcriptional activity and translation are essential for entotic invasion. (A) MCF10A cells plated on ultra-low attachment culture dishes to induce cell-in-cell invasion were treated either with 50 µg/ml Actinomycin D to test the effects of transcriptional inhibition or with 100 µg/ml Cycloheximide to study the effects of translational inhibition. Cells without drug treatment were used as controls. After drug treatment and 4h of culture in suspension, cells were fixed and labelled for F-actin with Phalloidin-Alexa Fluor 488 (green) and nuclei with DAPI (blue). Arrows indicate entotic events. Scale bars, 10 µm. **(B)** Relative mRNA levels of serum-inducible Fos expression were assessed by quantitative RT-PCR from MCF10A cells. Cells were serum starved for 24h and stimulated either with or without 20% FCS for 30 min, then treated with or without 50 µg/ml Actinomycin D for the indicated periods of time to confirm transcriptional inhibition. Results are shown as the mean from two independent experiments. Error bars indicate SD. Asterisks indicate statistical significance (****, $P < 0.0001$). ns indicates no significance ($P \geq 0.05$). **(C)** Quantification of entotic invasion corresponding to **A.** Entotic events were counted from three independent experiments using at least 2000 cells for each condition. Error bars indicate SD. Asterisks indicate statistical significance (***, $P < 0.001$).
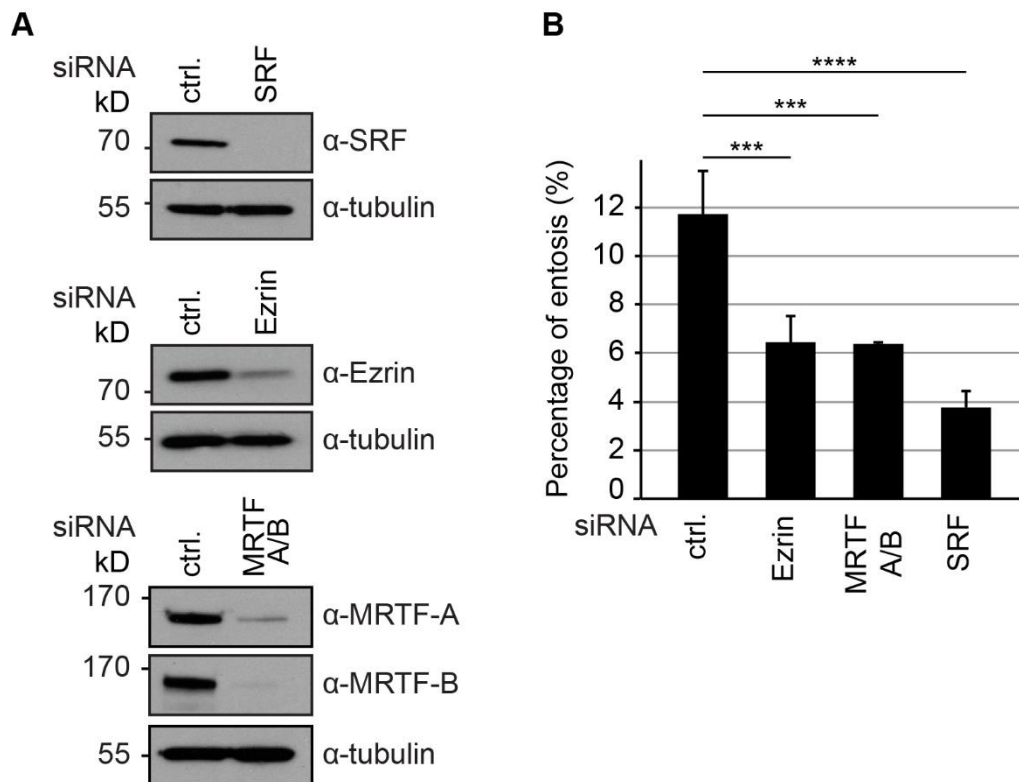
Figure 33: Cell-in-cell invasion requires MRTF/SRF and Ezrin expression. (A) Western blot showing siRNA-mediated knockdown efficiencies of SRF, Ezrin or MRTF-A together with MRTF-B in MCF10A cells. Tubulin was used as a loading control. **(B)** Entotic invasion quantification of MCF10A cells treated with indicated siRNAs for 72h before being analyzed for entosis. Entotic events were counted from three independent experiments and at least 800 cells for each condition were quantified. Error bars indicate SD. Asterisks indicate statistical significance (***, $P < 0.001$; ****, $P < 0.0001$).

Next, we elucidated the effect of MRTF-A on entotic invasion. Given the association between MRTF/SRF with entosis, we determined whether overexpressing MRTF-A could enhance entotic invasion. Constitutively active MRTF known as ΔN-MRTF was stably expressed tagged to GFP in transduced MCF10A cells and entosis ability was compared with MCF10A control cells stably expressing GFP. MCF10A cells stably expressing ΔN-MRTF-A-GFP were induced with doxycycline to trigger expression of constitutively active MRTF-A. Confocal microscopy and RT-qPCR confirmed inducible expression and nuclear localization of ΔN-MRTF-A linked to GFP construct in response to doxycycline (Figure 34 A and C). Indeed, our results showed an increase of entotic invasion in MCF10A cells stably expressing ΔN-MRTF-A (Figure 34 B), suggesting that constitutively active MRTF-A enhances entosis.
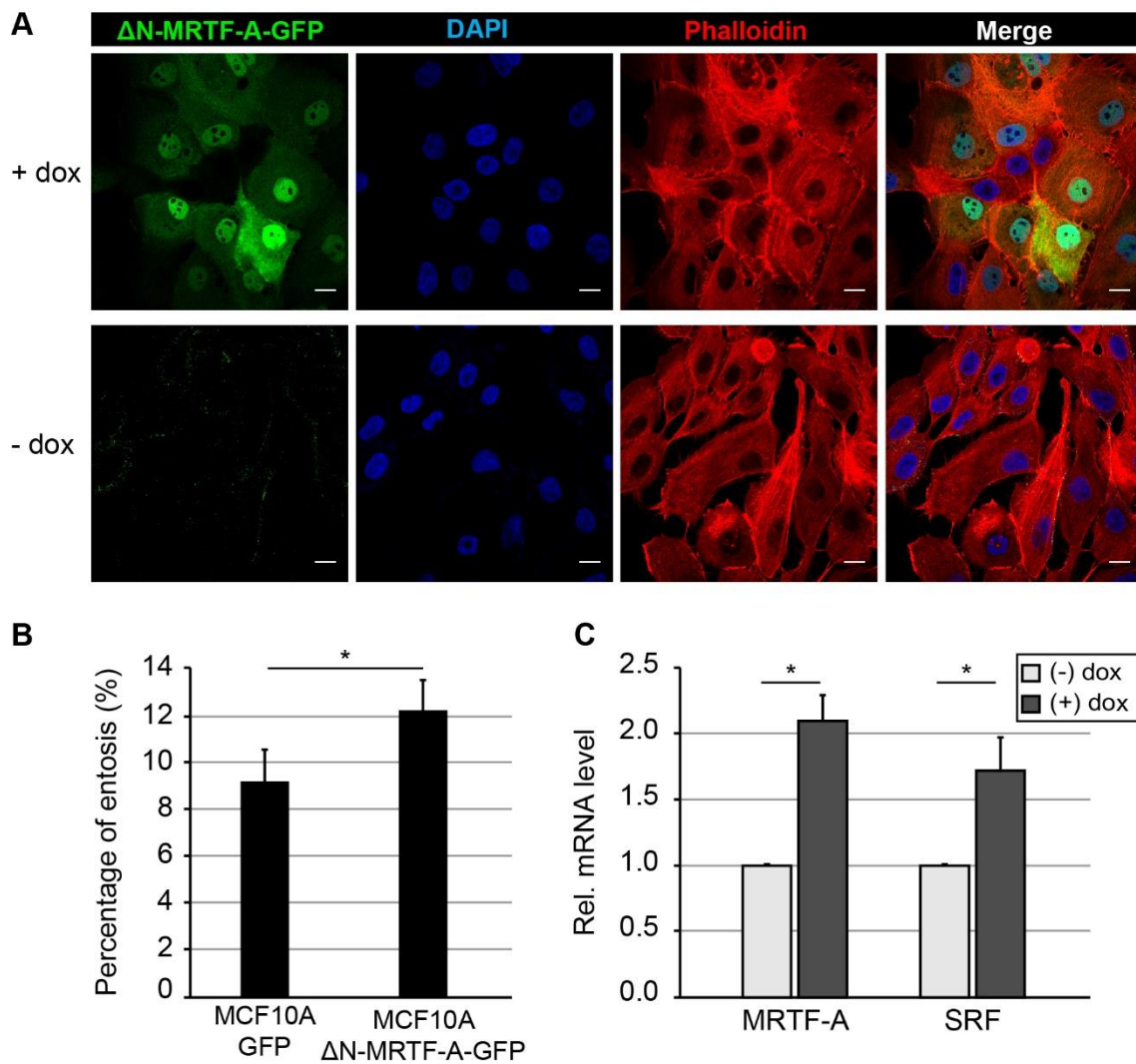
Figure 34: Constitutively active MRTF-A promotes entotic invasion. (A) Doxycycline induction of MCF10A cells stably expressing an inducible ΔN-MRTF-GFP (green) was validated with confocal imaging after adding doxycycline for 24h (+dox) to induce expression of constitutively active MRTF-A. Cells were fixed and labelled for F-actin with Rhodamine-Phalloidin 555 (red) and nuclei were stained with DAPI (blue). Scale bar, 15 µm. **(B)** Quantification of entotic invasion in MCF10A cells induced to express constitutively active MRTF-A (ΔN-MRTF-GFP) or only GFP as control cell line. Entotic events were quantified from three different experiments. Error bars indicate SD and the asterisk indicates statistical significance (*, P < 0.05). **(C)** Relative mRNA levels of MRTF-A and SRF were assessed by quantitative RT-PCR from MCF10A cells treated with or without doxycycline to validate the doxycycline-inducible ΔN-MRTF-GFP expression. Results are shown as the mean from three independent experiments. Error bars indicate SD and asterisks indicates statistical significance (*, P < 0.05).

4.2.3. The MRTF/SRF pathway is crucial in the invading cell to promote entotic invasion

We next investigated whether the invading or the host cell is affected by SRF depletion during entosis. We performed a dual-color entosis assay, in which control H2B-GFP cells (green) and SRF-depleted H2B-mCherry cells (red) were mixed and entotic events were quantified. This assay showed strongly reduced entosis in the absence of SRF in the invading cell indicating that SRF-depleted cells failed to invade host cells (Figure 35 A). However, when SRF was silenced in host cells, entosis was not altered (Figure 35 A). Hence, SRF contributes to entosis and appears to be specifically required in the invading cell, which in turn is the cell with continuous PM blebbing driving entotic invasion.

To further analyze why SRF-depleted cells fail to undergo entotic invasion, entosis events were monitored over time by live cell imaging. Interestingly, our data showed that SRF-depleted cells failed to successfully complete entotic invasion in spite of cell engulfment initiation (Figure 35 C). Additionally, entosis quantification revealed that only 20% of initiated entotic events were able to complete cell-in-cell invasion in the absence of SRF, whereas roughly 80% of siRNA treated control cells successfully finished entosis (Figure 35 B). We defined initiation of entosis by an initial protrusion of one cell into another and followed them over time to assess the proportion of completed entotic events. These data demonstrate the importance of SRF in the invading cell in driving entosis, suggesting that SRF-depleted invading cells fail to produce enough force to invade into the host cell.

We next examined MRTF-A subcellular localization during entotic invasion. MCF10A cells stably co-expressing MRTF-A-GFP (green) and the actin marker LifeAct-mCherry (red) were monitored over time during cell-in-cell invasion. Our results reveal the importance of nuclear MRTF-A localization in the invading cells before cell invasion during entotic non-apoptotic blebbing and before cell engulfment, while host cells predominantly showed cytoplasmic MRTF-A before engulfment (Figure 36 A-B). Despite prominent differences in MRTF-A localization in invading and host cells prior to engulfment, both cell types display a similar pattern of cytoplasmic or pancellular localization after engulfment (Figure 36 B). These data indicate that nuclear MRTF-A accumulation is required in the invading cell before cell engulfment in order to trigger entotic invasion.
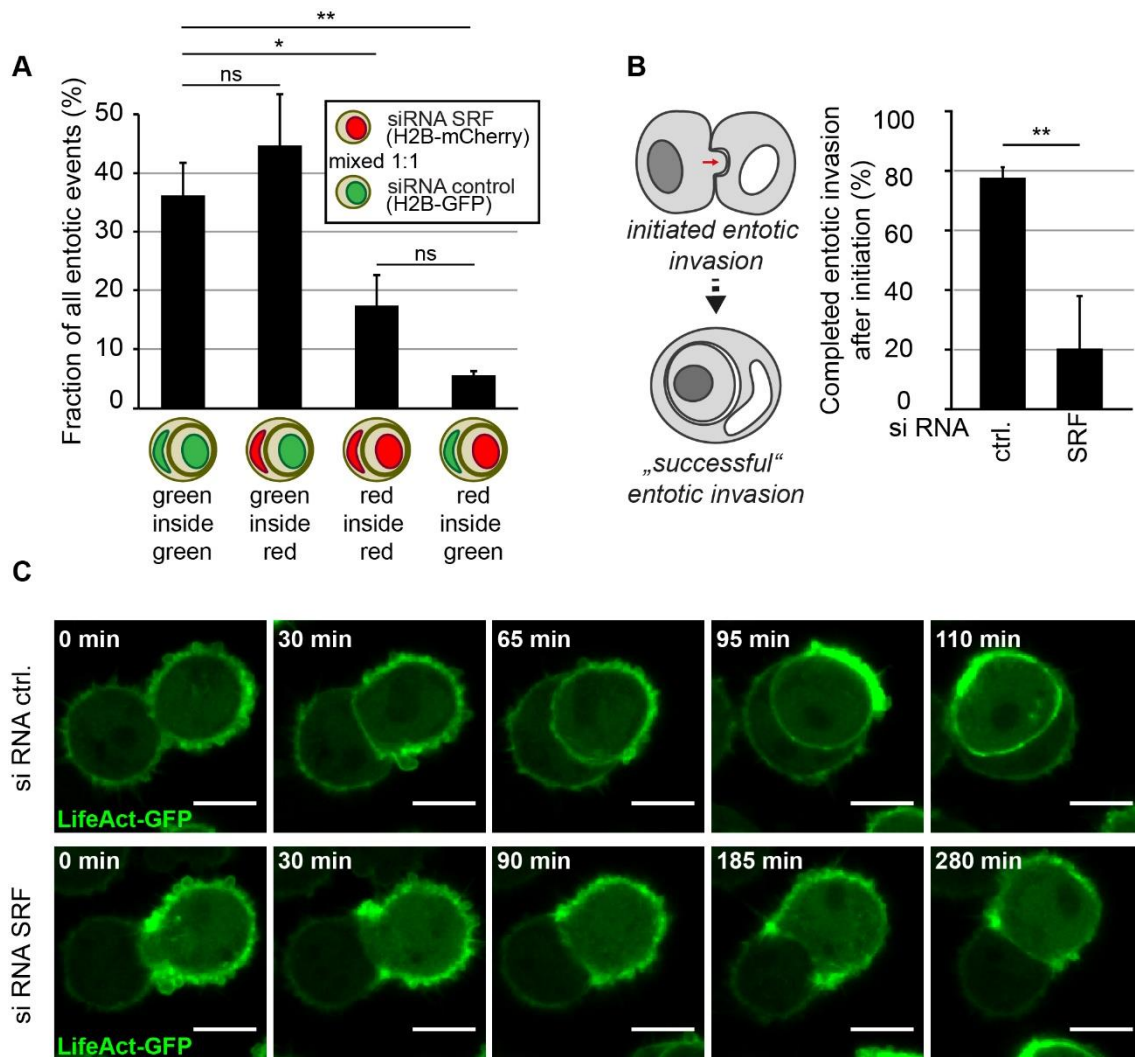
Figure 35: SRF depletion specifically affects the invading cell during entotic invasion. (A) MCF10A cells stably expressing the nuclear marker H2B-mCherry (red) were transiently transfected with SRF siRNA (H2B-mCherry) for 72h, while H2B-GFP (green) expressing cells were transfected with control siRNA for 72h. Then, equal cell numbers were mixed and plated on ultra-low attachment plates for 4h to induce cell-in-cell invasion. Entotic events were scored according to the indicated color combinations. Note the impaired invasion in SRF-silenced invading cells. At least 290 entotic events were considered from three independent experiments. Error bars indicate SD. Asterisks indicate statistical significance (*, $P < 0.05$; **, $P < 0.01$). ns indicates no significance ($P \geq 0.05$). **(B)** Quantification of completed entotic invasion events in MCF10A cells transfected with control or SRF siRNA for 72h. Numbers represent percentage of successful cell-in-cell invasion of overall events, characterized by an initial cell-in-cell protrusion. At least 40 initiated entotic invasion events were analyzed from ten independent experiments. Error bars indicate SD. Asterisk indicates statistical significance (**, $P < 0.01$). **(C)** MCF10A cells stably expressing LifeAct-GFP (green) treated with indicated siRNAs, control or SRF, were plated on poly-HEMA coated dishes and monitored over time to analyze entotic invasion. Note that SRF-depleted MCF10A cells fail to complete entotic invasion. Scale bars, 10 μm.

A

B
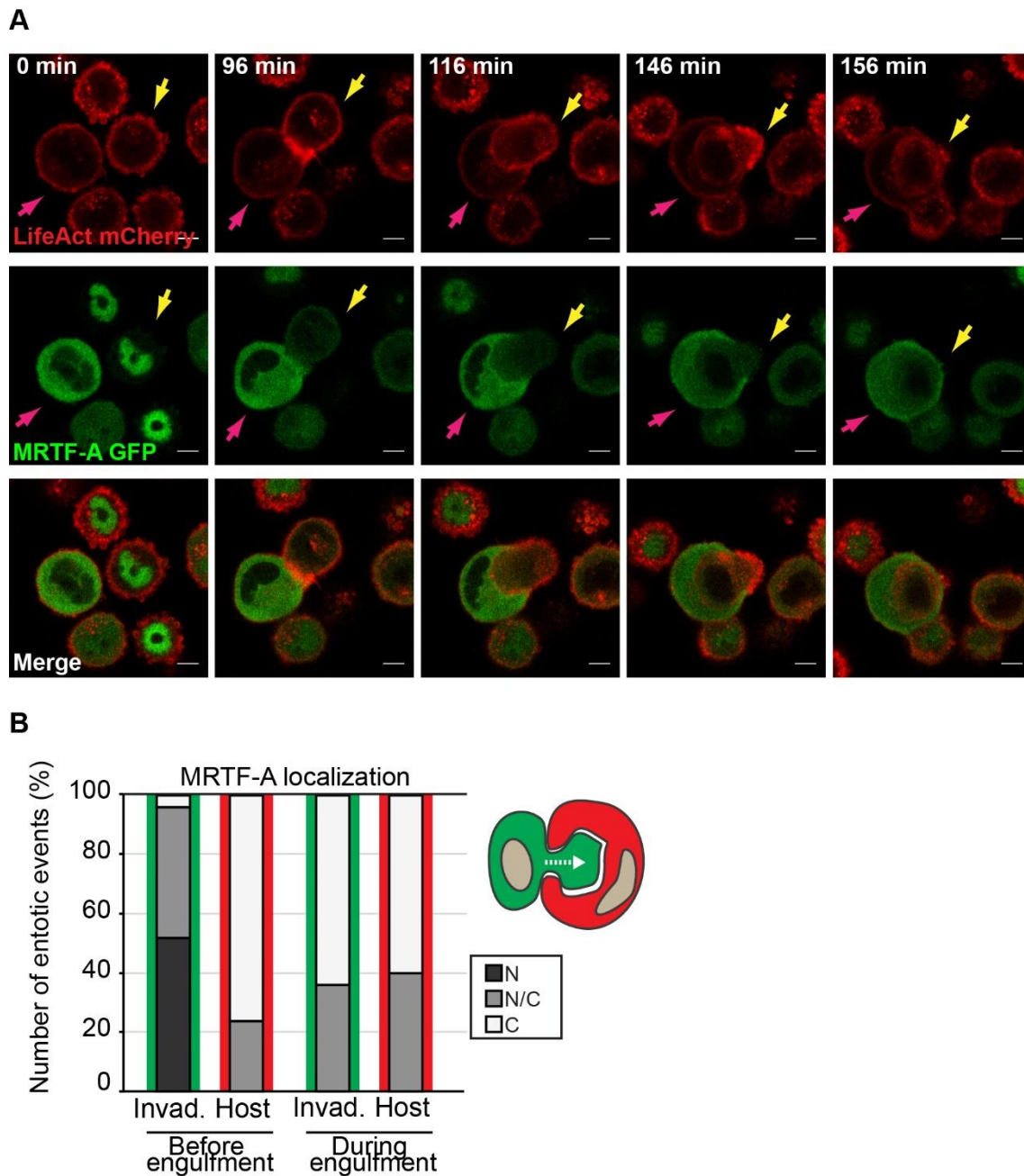
Figure 36: Invading cells show nuclear MRTF-A localization during entosis initiation. (A) Time-lapse imaging of MCF10A cells stably expressing LifeAct-mCherry (red) together with MRTF-A-GFP (green) on poly-HEMA over time to follow MRTF-A localization during the process of cell-in-cell invasion. An invading cell is marked by a yellow arrow while the pink arrow indicates the corresponding host cell in individual frames. Scale bars, 5 μm. **(B)** Quantification of MRTF-A-GFP subcellular distribution before and during cell engulfment for the invading (inner) and the host (outer) cell as seen in **A.** MRTF-A subcellular distribution was quantified as predominant nuclear (N), pancellular (N/C) or cytoplasmic (C). At least 25 entotic events were considered.

4.2.4. Expression of the ERM protein Ezrin restores PM blebbing and entosis in SRF-depleted cells

Our findings show that upregulation of the ERM Ezrin depends on the MRTF/SRF transcriptional pathway. Therefore, we assessed the importance of Ezrin on bleb dynamics. For that, *wild-type* Ezrin-GFP was stably expressed in MCF10A cells to compare bleb dynamics with stably expressing GFP cells (Figure 37 A). Then, cells were treated with siRNA against SRF or control siRNA, and bleb dynamics were further analyzed. Western blot analysis confirmed silencing of SRF for both cell lines (Figure 37 B). Interestingly, we observed that the maximum bleb expansion length was not increased in the Ezrin-GFP-expressing cells in the absence of SRF (Figure 37 C), while SRF depletion strongly affected bleb dynamics generating larger blebs in control cells expressing GFP (Figure 37 C and Figure 22 D). Furthermore, depletion of SRF did not affect bleb retraction time in blebbing cells expressing *wild-type* Ezrin-GFP (Figure 37 D) compared to the control siRNA-treated cells (Figure 37 D), even though we previously observed longer bleb retraction time in control cells stably expressing GFP (Figure 22 E). These data reveal that increased *wild-type* Ezrin expression is sufficient to rescue SRF suppression during bleb dynamics.

Our results demonstrate a novel function for Ezrin in restoring impaired plasma membrane blebbing in SRF-depleted cells, therefore we next tested the non-phosphorylatable mutant Ezrin-T567A, which is found poorly associated to the actin cytoskeleton (Gautreau, Louvard, and Arpin 2000). This inactive Ezrin variant T567A was expressed tagged to GFP in MCF10A cells to determine its effects on bleb dynamics and entosis. Expression of the inactive Ezrin-T567A affected bleb dynamics. Cells produced larger blebs and showed deficient bleb retraction and less blebbing activity (Figure 37 A, C and E). This indicates that Ezrin-T567A expression could not override the lack of SRF for efficient bleb dynamics. Taken together, these results confirm that Ezrin activity is sufficient for functional bleb dynamics validating Ezrin as a MRTF/SRF target gene.

Consistent with our data, *wild-type* Ezrin expression rescued entotic invasion in the absence of SRF (Figure 38 A), even though entosis was reduced for SRF-depleted control cells expressing GFP (Figure 38 A). Moreover, re-expression of the non-phosphorylatable mutant Ezrin T567A failed to restore entosis (Figure 38 A), indicating that *wild-type* Ezrin expression is crucial for entosis in SRF-silenced cells. We further examined the phenotype of the SRF-depleted stably expressing *wild-type* Ezrin-GFP MCF10A cells undergoing entotic invasion. We observed that entosis events occur in a similar manner regardless of SRF depletion upon ectopic Ezrin expression. Cell-in-cell invasion time was also unaffected (Figure 38 B-C). Together these

findings underline the importance of Ezrin expression to rescue bleb dynamics and subsequent entosis in the absence of SRF.
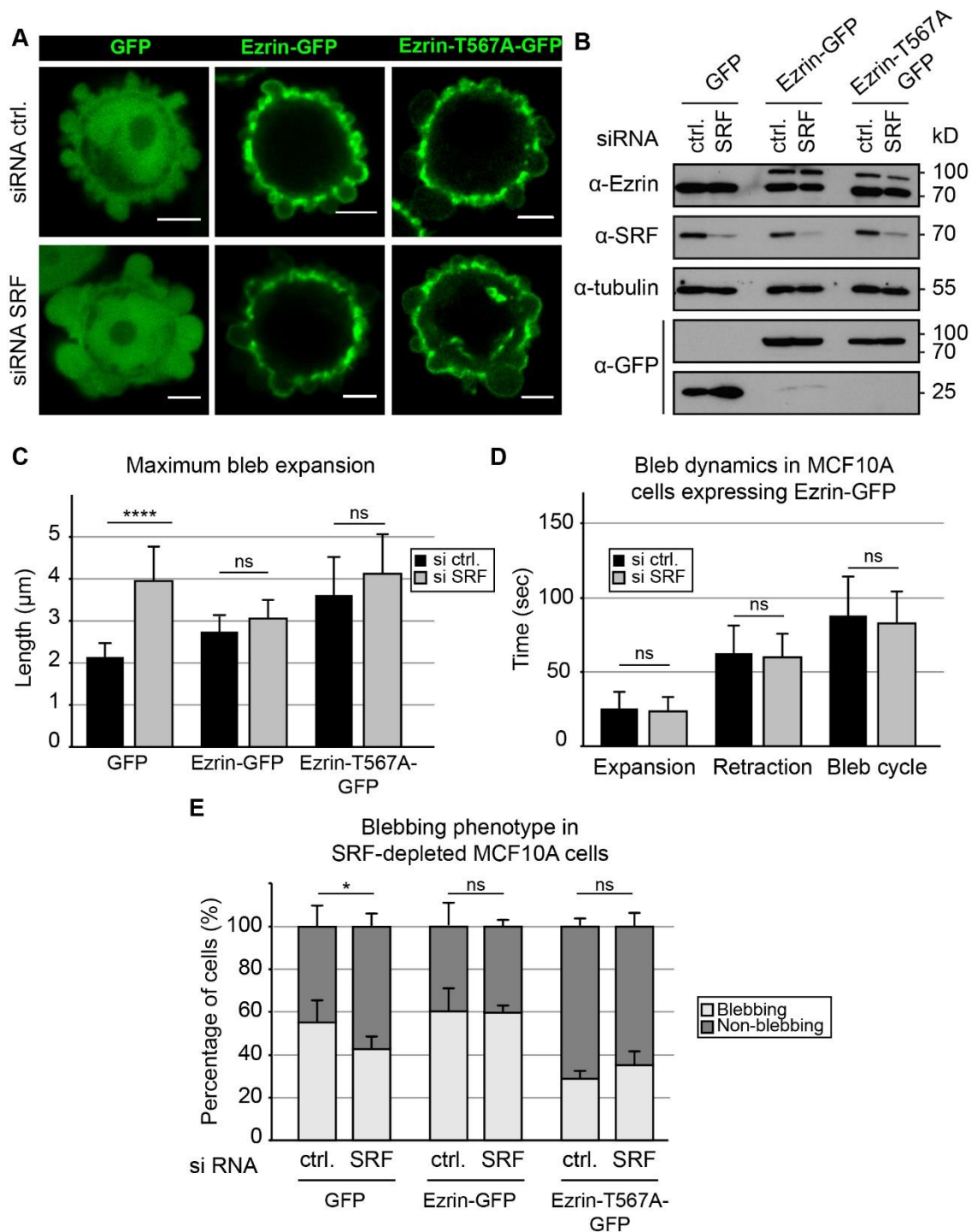
Figure 37: Expression of *wild type* Ezrin rescues bleb dynamics in SRF-depleted cells. (A) Live MCF10A cells stably expressing either GFP, *wild type* Ezrin-GFP or the inactive mutant Ezrin-T567A-GFP treated with the indicated siRNAs for 72h were plated on poly-HEMA culture dishes and imaged over time to visualize bleb dynamics. Scale bars, 5 µm. **(B)** Western blot showing SRF knockdown efficiency in MCF10A cells stably expressing GFP, Ezrin-GFP or Ezrin-T567A-GFP. Note the detection of endogenous and overexpressed Ezrin. Tubulin served as loading control. **(C)** Quantification of maximum bleb expansion

94

length of individual blebs in MCF10A cells in **A.** At least 60 blebs and 15 cells were quantified for each condition **(C-E)**. Errors bars indicate SD and asterisks indicate statistical significance (****, P < 0.0001). ns indicates no significance (P ≥ 0.05). **(D)** Live MCF10A cells stably expressing Ezrin-GFP treated with siRNAs as in **A.** were plated on poly-HEMA to induce blebbing and imaged over time to measure the time for expansion and retraction of individual blebs. Errors bars indicate SD. ns indicates no significance (P ≥ 0.05). **(E)** MCF10A cells described in **A.** were plated on poly-HEMA dishes to analyze the number of blebbing cells and non-blebbing cells. At least 100 cells were quantified for each condition from three independent experiments. Errors bars indicate SD and the asterisk indicates statistical significance (*, P < 0.05). ns indicates no significance (P ≥ 0.05).

A

B

MCF10A Ezrin-GFP	si ctrl.	si SRF
	time (min)	time (min)
1	84	60
2	100	132
3	124	84
4	88	72
5	96	96
6	164	48
7	64	84
8	128	60
9	80	64
10	52	168
Mean	98 ± 33,05	86,8 ± 37,14

C
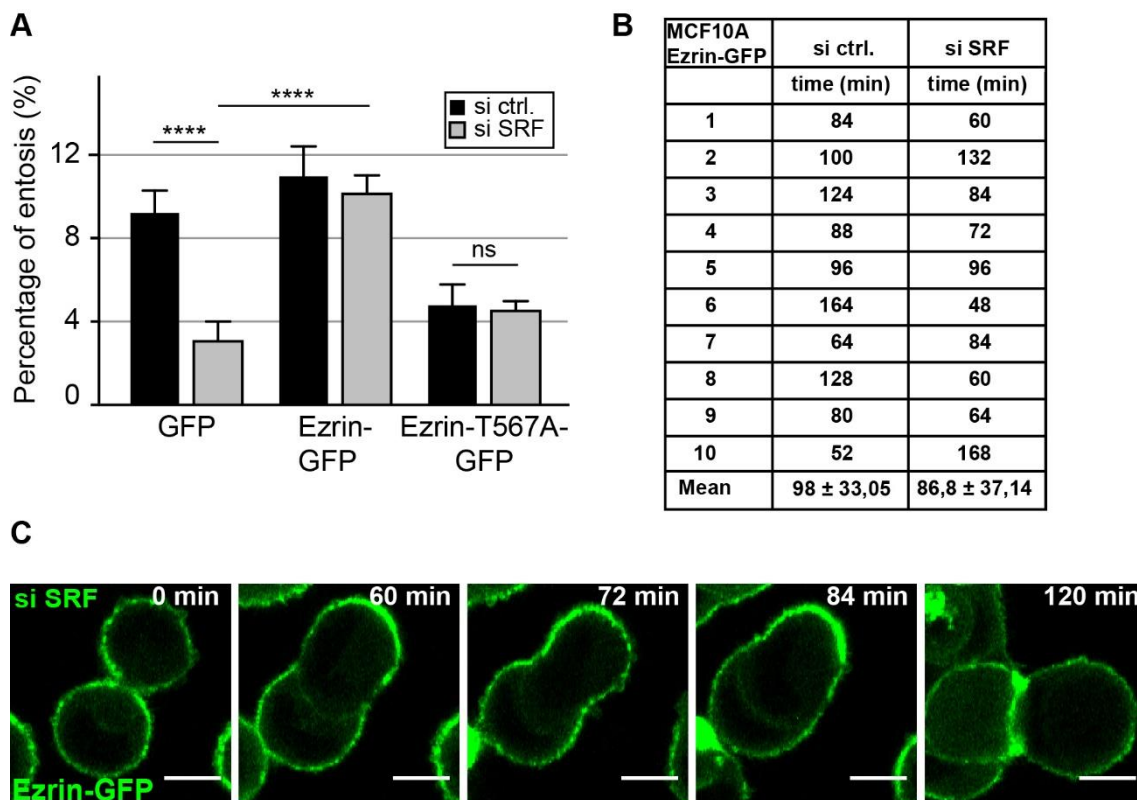
Figure 38: Ezrin expression restores entotic invasion in the absence of SRF. (A) Quantification of entosis in MCF10A cells stably expressing GFP, *wild type* Ezrin-GFP or the non-phosphorylatable mutant Ezrin-T567A-GFP were treated with control or SRF siRNA for 72h and entotic cell-in-cell invasion events were quantified as percentage of total cells. Entotic events were counted from three independent experiments. Error bars indicate SD. Asterisks indicate statistical significance (****, P < 0.0001). ns indicates no significance (P ≥ 0.05). **(B)** Quantification of entotic invasion time in MCF10A cells stably expressing Ezrin-GFP transfected with siRNA directed against control or SRF were monitored over time using live cell imaging. Ten independent entosis events were counted. **(C)** Live MCF10A stably expressing Ezrin-GFP transfected with siRNA against SRF for 72h were plated on poly-HEMA to follow the process of entotic invasion. Scale bars, 10 μm.

4.3.   Regulation of the MRTF/SRF pathway in amoeboid invasion

Given the association between the MRTF/SRF-actin regulated transcriptional feedback and a bleb-dependent way of invasion, entosis (Soto Hinojosa et al. 2017), we hypothesized that the MRTF/SRF pathway plays a role in bleb-associated amoeboid invasion.

4.3.1. Role of SRF on amoeboid phenotype

To study amoeboid migration, melanoma A375-M2 cells were plated on top of a matrix and cell morphology was monitored over time. Here, we observed two different modes of invasion, the most predominant was amoeboid blebbing motility, even though some of the cells also undergo the elongated mesenchymal type (Figure 39 A). We next tested whether MRTF/SRF plays a role in amoeboid blebbing invasion. Therefore, A375 cells stably co-expressing LifeAct-GFP (green) and H2B-mCherry (red) silenced for SRF (Figure 39 B) were imaged on top of Matrigel for 16 hours, and their phenotype was compared with control siRNA-treated cells to study the effects of SRF depletion on bleb-associated migration. Importantly, we observed a switch from amoeboid rounded blebbing morphology to the elongated mesenchymal morphology in SRF-depleted melanoma A375-M2 cells (Figure 39 A). After seeding melanoma cells for 16h on 2.5 μg/ml Matrigel, elongated morphology was more predominant than the blebbing rounded morphology in SRF-depleted cells (Figure 39 A). In addition, treatment with the ROCK inhibitor Y27632 was reported to trigger mesenchymal morphology (Gadea et al. 2008), and thus, we used it as a control condition to evaluate the phenotypic switch in morphology (Figure 39 A). Our data suggest that SRF might play an important role for amoeboid, blebbing mode of cell invasion.
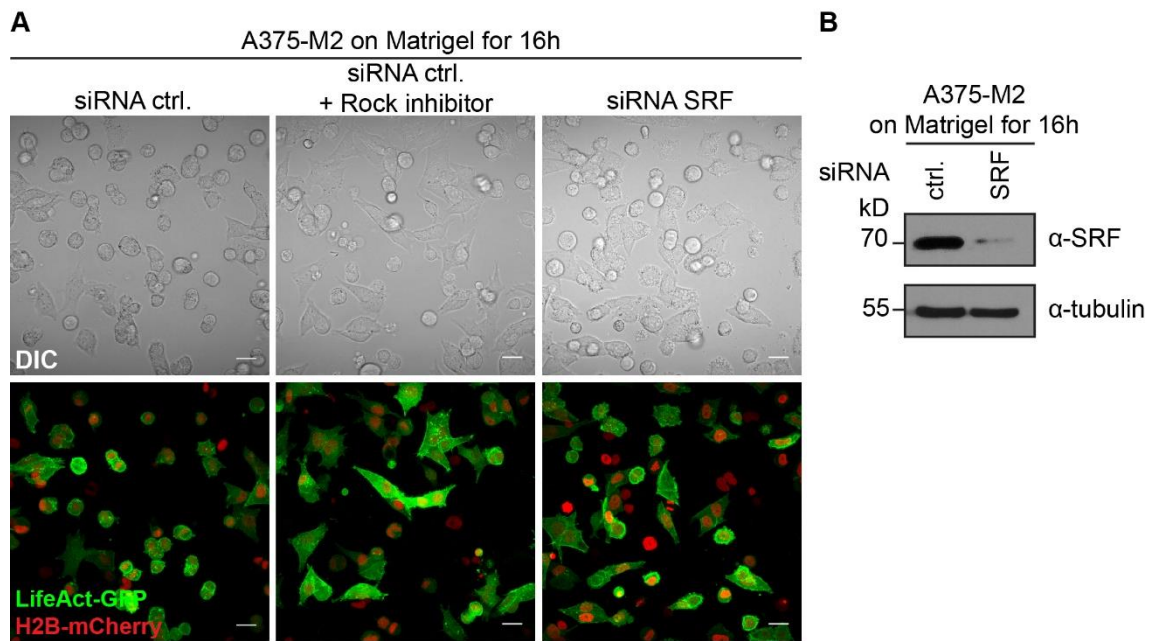
Figure 39: Cell morphology phenotype is affected in SRF-depleted melanoma cells. (A) Live melanoma A375-M2 cells stably co-expressing the nuclear marker H2B-mCherry (red) together with LifeAct-GFP (green) treated with control siRNA or siRNA directed against SRF for 72h were plated on 2.5 µg/ml Matrigel coated dishes to monitor cell motility and the mode of invasion for a time course of 16h. ROCK inhibitor treatment (Y27632, 10 µM), which promotes a mesenchymal elongated morphology, was used as a control. Differential interference contrast (DIC) was added for each frame to visualize cell morphology. Scale bars, 25 µm. **(B)** Western blot confirming SRF knockdown efficiency in melanoma A375-M2 cells. Tubulin served as loading control.

4.3.2. MRTF-SRF transcription and formin mDia1 regulate amoeboid blebbing

We next investigated the effects of the SRF transcriptional coactivator, the actin-binding MRTF-A, on blebbing. Melanoma A375-M2 cells stably expressing LifeAct-GFP (green) were treated with siRNA directed against MRTF-A and B (Figure 40 B) and then cultured on top of 2.5 µg/ml Matrigel to monitor cell morphology and motility over time. Our results showed an increase in elongated mesenchymal morphology in MRTF-A/B-depleted cells and reduced blebbing in the absence of MRTF-A/B (Figure 40 A). Similarly, ROCK inhibitor Y27632 treatment resulted in more cells showing an elongated phenotype (Figure 40 A).

Previous findings revealed the importance of the RhoA-mediated formin mDia1 downstream of LPAR2 in non-apoptotic plasma membrane blebbing for entotic invasion (Purvanov et al. 2014). In this context, recent studies also identified a critical role for another diaphanous-related formin, mDia2, in amoeboid blebbing in tumor cells and in the control of the mesenchymal to amoeboid morphological transition (Wyse et al. 2017). Hence, we aimed to elucidate whether mDia1 affects amoeboid blebbing. For that, mDia1-depleted A375-M2 cells stably expressing

LifeAct-GFP (Figure 40 D) were imaged on top of 2.5 µg/ml Matrigel to track cell morphology and motility over time. Interestingly, melanoma cells in which mDia1 was silenced appear to switch their morphology towards an elongated mesenchymal compared to control cells, which predominantly display a rounded blebbing morphology (Figure 40 C).
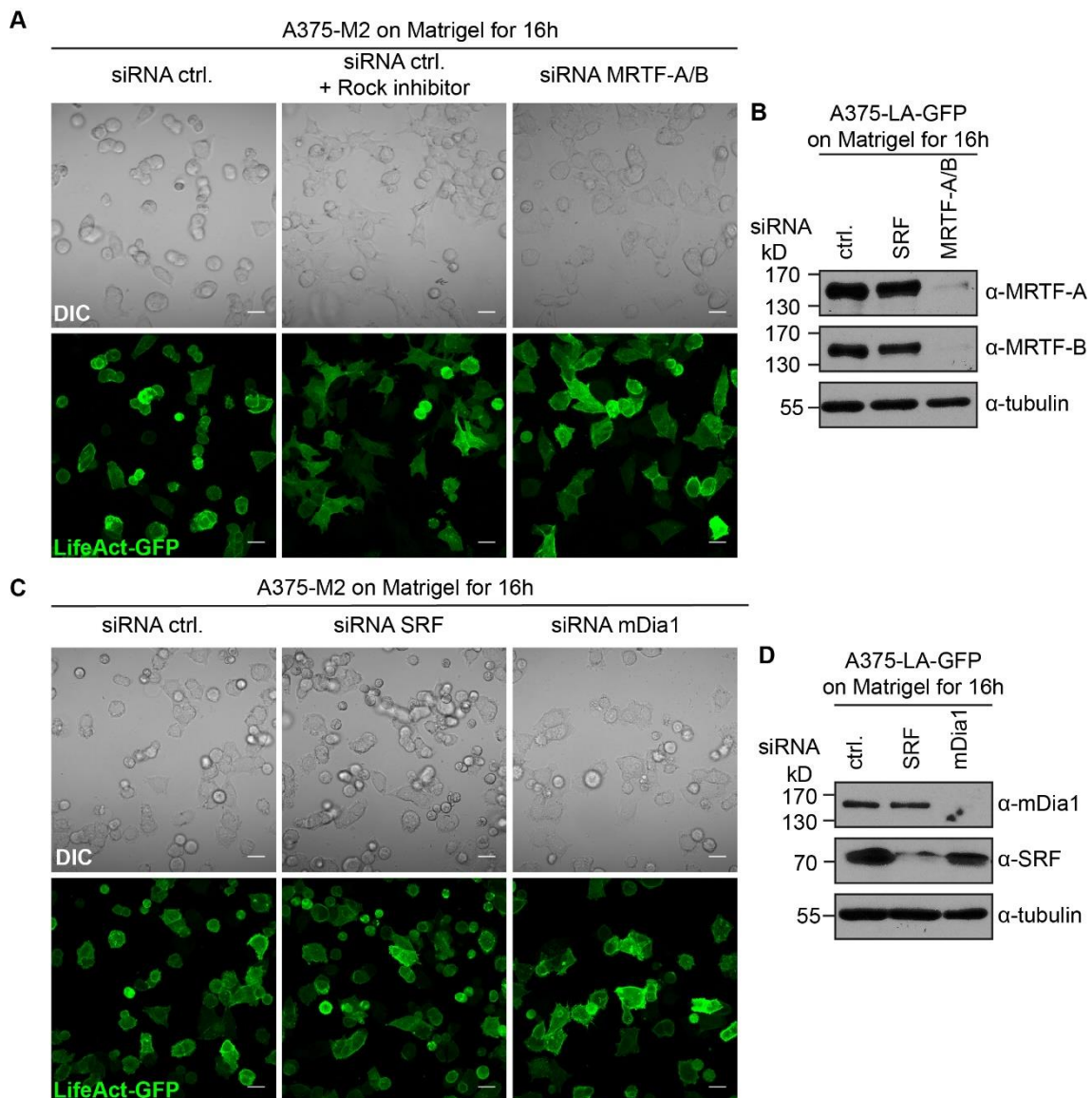
Figure 40: MRTF/SRF and mDia1 play important roles during amoeboid blebbing. (A) Live A375-M2 cells stably expressing LifeAct-GFP to label the actin cytoskeleton transfected with siRNA against control or MRTF-A together with MRTF-B for 72h were seeded on top of 2.5 µg/ml Matrigel coated dishes to monitor amoeboid blebbing invasion over the time course of 16h. ROCK inhibitor treatment (Y27632, 10 µM) was used as control to induce the elongated mesenchymal phenotype. Differential interference contrast (DIC) was added for each frame to visualize cell morphology. Scale bars, 25 µm. **(B)** Western blot demonstrating double siRNA knockdown efficiencies for MRTF-A together with MRTF-B in A375-M2 cells stably expressing LifeAct-GFP (A375-LA-GFP). Tubulin served as loading control. **(C)** Live A375-M2 cells stably expressing LifeAct-GFP treated with siRNA directed against control, SRF or formin mDia1 for 72h. Cells

were plated on Matrigel and analyzed as explained in **A.** Scale bars, 25 µm. **(D)** Western blot showing siRNA-mediated knockdown efficiencies for SRF and formin mDia1. Tubulin served as loading control.

To evaluate the phenotypic switch, we quantified different parameters including the cell roundness using Image J. Quantification of cell roundness was assessed in A375-M2 melanoma cells stably expressing LifeAct-GFP seeded on Matrigel for 16h. Our results showed that cell roundness was significantly reduced upon depletion of either SRF or MRTF-A/B (Figure 41 A-B), suggesting a switch of cell morphology to more elongated cells, which could be explained by the Amoeboid to Mesenchymal Transition (AMT). Additionally, the ROCK inhibitor Y27632 served as a positive control for the amoeboid to mesenchymal cell morphology transition (Figure 41 A-B) (Gadea et al. 2008).

Another approach was considered in order to determine the amoeboid to mesenchymal morphological phenotypic transition by employing a cell impedance assay that allows forces during cell adhesion to be measured (Hamidi, Lilja, and Ivaska 2017). Melanoma A375-M2 cells silenced with siRNA directed against SRF or control siRNA were treated either with or without the ROCK inhibitor Y27632. Subsequently, cells were seeded on top of collagen-coated 96-well E-plates to measure cell impedance over time using the xCELLigence system. Cell impedance measurements showed a significant increase for control-siRNA cells treated with 10 µM Y27632, although cell impedance was not significantly increased for the SRF-depleted cells (Figure 41 C).
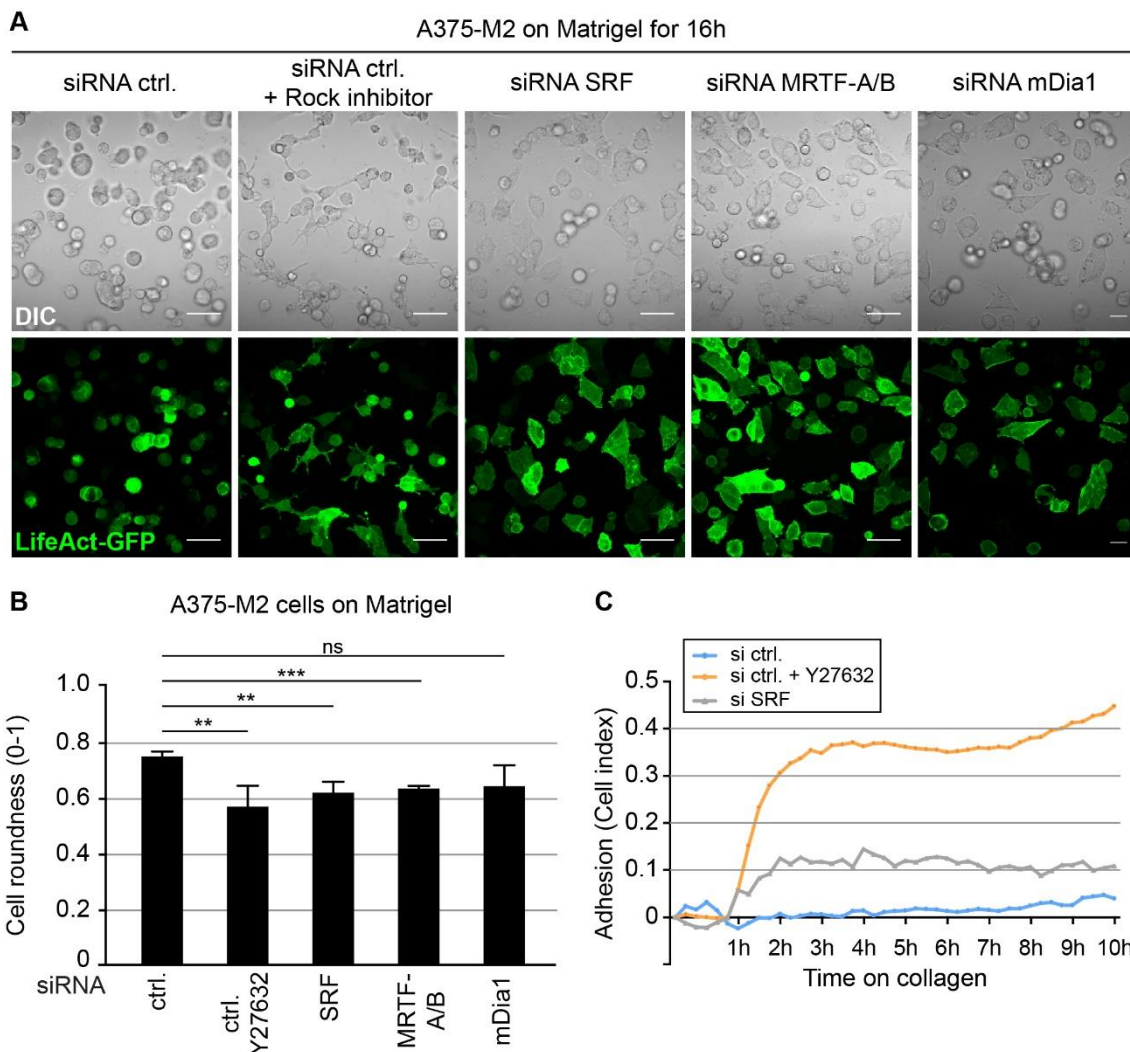
Figure 41: MRTF/SRF is essential for amoeboid blebbing morphology. (A) Live A375-M2 cells stably expressing LifeAct-GFP treated with siRNAs as indicated were seeded on 2.5 µg/ml Matrigel for 16h and imaged for further phenotype quantifications. Differential interference contrast (DIC) was used to visualize cell morphology. The ROCK inhibitor (Y27632, 10 µM) was applied to siRNA control cells. At least six different areas were imaged for each independent experiment and condition. Scale bars, 50 µm. **(B)** Quantification of cell roundness using ImageJ for A375-M2 cells corresponding to **A.** At least six independent experiments were quantified for each condition. Error bars indicate SD. Asterisks indicate statistical significance (**, P < 0.01; *** P < 0.001). ns indicates no significance (P ≥ 0.05). **(C)** Cell impedance measurement in melanoma A375-M2 cells. Control or SRF siRNA was transfected 72h before seeding on top of 1.7 mg/ml collagen coated E-plates. Cell index was normalized to 0h and impedance was recorded over time. 10 µM Y27632 were added to control siRNA-treated cells for the ROCK inhibitor condition.

Given the novel role of MRTF for non-apoptotic sustained plasma membrane blebbing (Soto Hinojosa et al. 2017), as well as our recent results supporting MRTF/SRF for PM blebbing, we aimed to examine the subcellular localization of MRTF-A during amoeboid blebbing invasion. Thus, A375 melanoma cells stably expressing GFP tagged to full length MRTF-A were imaged on a 1.7 mg/ml collagen matrix over time to monitor MRTF-A localization. Our data reveal nuclear MRTF-A accumulation in cells moving in an amoeboid blebbing invasion mode (Figure 42 A), while in cells moving in a non-blebbing dependent way MRTF-A was localized in the cytoplasm (Figure 42 A). These data support the idea that a non-apoptotic blebbing mode of cell motility such as amoeboid blebbing requires nuclear MRTF-A translocation, which in turn is crucial to promote MRTF/SRF activity via SRF-dependent gene expression. Together these results implicate the MRTF/SRF signaling pathway in plasma membrane blebbing.
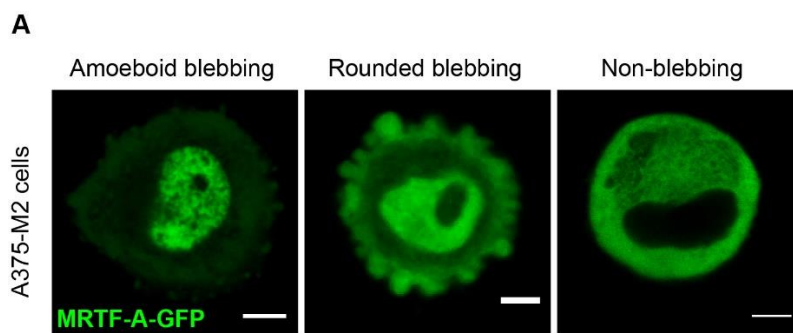
Figure 42: Amoeboid blebbing triggers nuclear MRTF-A localization. (A) Live melanoma A375-M2 cells stably expressing inducible MRTF-A-GFP were induced with doxycycline for 24h and plated on a 1.7 mg/ml collagen matrix to monitor MRTF-A subcellular distribution using live cell imaging during amoeboid blebbing and compared with non-blebbing cells. Scale bars, 5 µm.

4.3.3. Molecular regulators are involved in MRTF/SRF-mediated AMT

Our data until now suggest that the MRTF/SRF signaling pathway is involved during the transition from amoeboid blebbing to the elongated mesenchymal morphological phenotype. In order to verify this hypothesis, we next characterized which molecular regulators play a role for the observed phenotype. Therefore, A375 melanoma cells treated either with control siRNA or siRNA directed against SRF for 72h were seeded on Matrigel for 16h followed by RNA isolation, we then analyzed the mRNA transcript level of different molecular regulators known to be implicated in the amoeboid to mesenchymal transition. In addition, a control condition was included, in which non-siRNA transfected cells were treated with the 10 µM ROCK inhibitor Y27632. Here, we observed SRF knockdown efficiency in A375 cells (Figure 43 A-B) and intriguingly, Integrin β1 expression was slightly increased in SRF-depleted melanoma cells (Figure 43 A), which correlates with the observed increase of an elongated-mesenchymal phenotype. We also examined another elongated-mesenchymal invasion molecular marker, the

Matrix Metalloproteinase-9 (MMP9). MMP9 has been shown to drive mesenchymal invasion modes, while its inhibition leads to a switch from mesenchymal mode of migration to rounded amoeboid type (Wolf et al. 2003). Remarkably, MMP9 was upregulated in SRF-depleted A375 cells, but also upon ROCK inhibitor treatment (Figure 43 A) indicating a correlation with the mesenchymal mode. We also checked the expression levels of different molecular regulators involved in rounded amoeboid migration, for instance Myosin and RhoA. Although RhoA transcript levels were unaffected upon SRF depletion, Myosin mRNA expression was slightly decreased in SRF-depleted cells (Figure 43 A), pointing towards an increase of actomyosin in control cells, in which more amoeboid rounded cells were detected. In contrast, Rac-1 mRNA levels, known to be upregulated for the mesenchymal migration, were not altered in the absence of SRF (Figure 43 A).
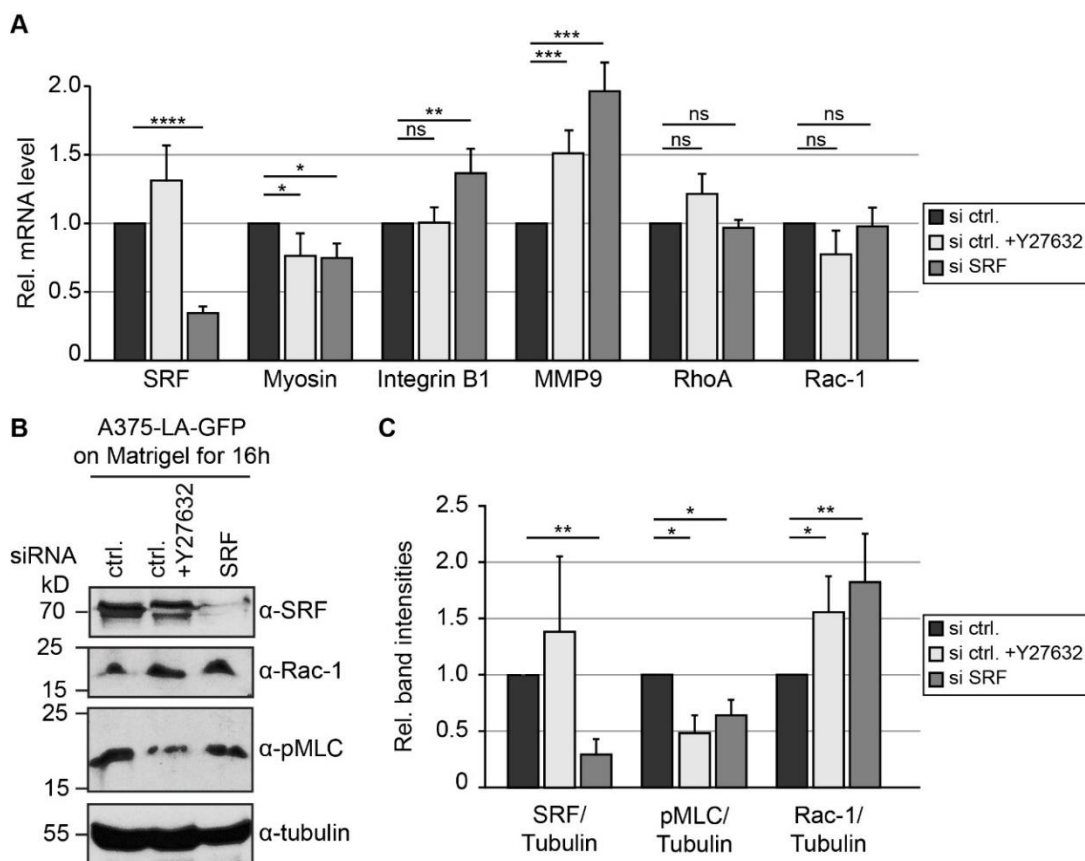
Figure 43: Amoeboid to mesenchymal transition is dependent on MRTF/SRF and actomyosin contractility. (A) Relative mRNA levels of SRF, Myosin, Integrin β1, MMP9, RhoA and Rac-1 were assessed from melanoma A375-M2 cells treated with siRNA directed against SRF or control for 72h. Cells were treated with or without 10 µM Y27632 as indicated and seeded on 2.5 µg/ml Matrigel for 16h followed by RNA extraction. Results are shown as the mean from three independent experiments. Error bars indicate SD. Asterisks indicate statistical significance (*, P < 0.05; **, P < 0.01; ***, P < 0.001; ****, P < 0.0001). ns indicates no significance (P ≥ 0.05). (B) Western blot confirming SRF knockdown efficiency in A375 stably expressing LifeAct (LA)-GFP seeded on a matrix. A375-M2 cells were treated as described in

A. Rac-1 and pMLC proteins were detected by immunoblotting. Tubulin was used as loading control. **(C)** Western blot band intensities corresponding to **B.** were quantified from three independent experiments using ImageJ. Error bars indicate SD. Asterisks indicate statistical significance (*, P < 0.05; **, P < 0.01).

These data indicated that SRF depletion is associated with changes in amoeboid to mesenchymal morphology which correlate with altered molecular regulators at the transcript level. Thus, we further analyzed the impact of regulators at a protein level. These results revealed decreased phospho-Myosin (pMLC2) protein levels in SRF-depleted melanoma cells (Figure 43 B-C), but also upon 10 µM ROCK inhibitor treatment (Figure 43 B-C), indicating reduced pMLC and actomyosin contractility in the absence of SRF, which are associated with less amoeboid rounded cells and an increased mesenchymal elongated mode. Consistent with this, Rac-1 protein levels were upregulated in the absence of SRF and upon ROCK inhibitor treatment (Figure 43 B-C), which correlate with the observed morphological phenotype. In conclusion, these data provide evidence that MRTF/SRF signaling acts as a molecular mechanism controlling the amoeboid to mesenchymal phenotypic transition.

5. Discussion

5.1. Effects of MRTF/SRF on plasma membrane blebbing

Besides the changes in actin cytoskeletal dynamics and gene expression mediated by MRTF/SRF (E. N. Olson and Nordheim 2010), the SRF transcription factor together with its coactivator MRTF-A have also been reported to play a role in cell proliferation, motility and migration (Medjkane et al. 2009). Interestingly, depletion of MRTF-A or SRF in invasive cells leads to downregulation of cytoskeletal target genes required for actomyosin contractility, and also implicated in tumor cell invasion (Medjkane et al. 2009).

Several studies have provided evidence that SRF acts as a key regulator of cytoskeletal target gene expression, which is also controlled by the MRTFs and Rho-actin-signaling (Esnault et al. 2014). The importance of SRF for several cell functions has been identified. For instance, SRF knockdown affects actin cytoskeleton organization and inhibits expression of genes related to actin cytoskeleton homeostasis (Sun et al. 2006). Consistent with this, SRF and MRTF-loss of function phenotypes displayed defects in myogenesis and migration (Pipes, Creemers, and Olson 2006). Similarly, SRF-depleted embryonic stem cells had actin cytoskeleton organization defects that in turn impaired cell spreading, adhesion and migration (Schratt et al. 2002).

Therefore, given the association between the MRTF/SRF signaling pathway and the contractile actin cytoskeleton, we first evaluated the effects of MRTF/SRF on sustained plasma membrane blebbing. Blebs are actin-rich membrane protrusions essential for cell motility processes, and which are highly regulated by actin cytoskeleton dynamics and actomyosin contractility forces (Fackler and Grosse 2008). Notably, our data show that suppression of SRF affects plasma membrane blebbing, specifically bleb retraction (Figure 22). In this context, previous studies have shown that bleb retraction requires the recruitment of ERM proteins and actomyosin contractility (Guillaume T Charras et al. 2006). Thus, our results reveal that dynamic bleb retraction is controlled by the MRTF/SRF transcriptional pathway. In addition, other actin cell cortex proteins may contribute to the plasma membrane tension necessary for efficient bleb expansion and retraction.

Several studies have suggested the importance of different formins for blebbing, such as FHOD1, FMNL2, DIAPH3 and mDia1 (Thomas M Kitzing et al. 2007; Hannemann et al. 2008; T M Kitzing et al. 2010; Stastna et al. 2012; Bovellan et al. 2014). Recent findings reported the critical role of the actin nucleator formin mDia1 in plasma membrane blebbing (Bovellan et al. 2014) and subsequent entotic invasion (Purvanov et al. 2014). Hence, we further analyzed whether formin mDia1 expression is affected in SRF-depleted cells. Even though depletion of mDia1 was shown to reduce bleb activity (Purvanov et al. 2014) and resulted in larger blebs (Bovellan et al. 2014), expression levels of formin mDia1 were not altered in the absence of SRF (Figure 30), in which blebbing activity was also decreased (Figure 22). These data indicate that the MRTF/SRF transcriptional pathway has no effect on formin mDia1 expression during non-apoptotic plasma membrane blebbing.

Although SRF is a target gene of its own transcriptional activity (Esnault et al. 2014), our studies between induced non-apoptotic plasma membrane blebbing and MRTF/SRF transcription revealed a direct association, in which sustained long-term blebbing enhances MRTF/SRF activity (Figure 26). Our findings show that during dynamic plasma membrane blebbing MRTF/SRF transcription is regulated by the contractile actin cortex.

5.2. Cortical blebbing controls subcellular localization and nucleocytoplasmic translocation of MRTF-A

Several triggers such as mechanical stress, serum, LPA or formins can induce MRTF-A nuclear accumulation (Baarlink, Wang, and Grosse 2013). In this study, we hypothesized that dynamic blebbing, known to be regulated by the contractile actin cytoskeleton (Guillaume T Charras et al. 2006), could lead to changes in the G-/F-actin ratio resulting in nuclear shuttling of MRTF-A. Consistent with our findings demonstrating the relevance of the SRF transcription factor for non-apoptotic PM blebbing, we next tested the functional significance of the SRF coactivator MRTF-A during induced blebbing. Surprisingly, we found a striking correlation between induced non-apoptotic blebbing and dynamic nucleocytoplasmic shuttling of the actin-binding protein MRTF-A. Here, in blebbing cells MRTF-A is located in the nucleus, while in non-blebbing cells MRTF-A is located predominantly in the cytoplasm (Figure 24, Figure 44). Thus, our data suggest that cortical contractility is important for nuclear translocation of MRTF-A.

In addition to sustained blebbing activity triggering nuclear MRTF-A accumulation and therefore enhancing MRTF/SRF transcription, we next examined whether there is a direct link between MRTF-A localization and the contractile actin cortex during induced PM blebbing by blocking blebbing activity. Indeed, Blebbistatin treatment resulted in MRTF-A export to the cytoplasm (Figure 25), suggesting that sustained and induced PM blebbing together with the associated contractile actin cortex regulate the subcellular localization and nucleocytoplasmic shuttling of MRTF-A. Although several triggers are known to induce actin polymerization leading to nuclear MRTF-A accumulation (Baarlink, Wang, and Grosse 2013), our work reveals cortical blebbing as a novel trigger that controls the subcellular localization of MRTF-A (Figure 44).
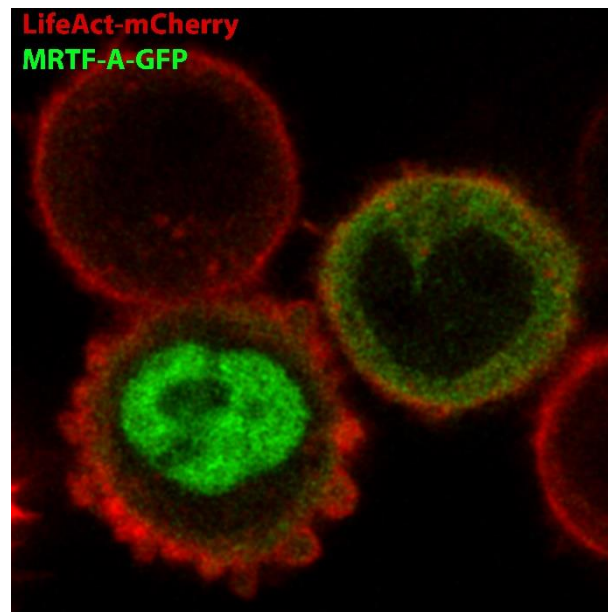
Figure 44: Plasma membrane blebbing is tightly coupled to dynamic actin-driven MRTF-A nucleocytoplasmic shuttling.

5.3. Ezrin as a regulator of MRTF/SRF-dependent transcription

Previous studies have reported the involvement of the Rho-ROCK pathway and the recruitment of ERM proteins, in particular Ezrin, together with actin in the reassembly of the contractile actin cortex during bleb retraction (Guillaume T Charras et al. 2006). In this thesis, ERM proteins and different actin-related proteins were examined as potential target genes. It is noteworthy that our results reveal that Ezrin expression is upregulated upon induced continuous non-apoptotic blebbing on a protein as well as transcript level (Figure 27). Although Ezrin, Radixin and Moesin are highly homologous, they are implicated in different cellular functions. Therefore, we assessed the involvement of other ERMs and myosin in order to understand whether ERMs or myosin, which are known to play important roles during blebbing, are regulated in a similar manner to Ezrin, or whether Ezrin is specifically upregulated in response to induced long-term

blebbing. Interestingly, our data showed that induced PM blebbing leads to upregulation of the specific ERM Ezrin, whereas Radixin, Moesin and Myosin were unaffected (Figure 27), suggesting a specificity for Ezrin induction in response to blebbing activity. This is consistent with recent work that reported the relevance of Ezrin phosphorylation by ROCK for the recruitment of Epidermal growth factor receptor kinase substrate 8 (Eps8) to the plasma membrane. This is required for reassembly of the actin cortex and efficient bleb retraction (Ikenouchi and Aoki 2017; Aoki et al. 2016).

Besides the regulation of target genes related to proliferation, contractility or ECM remodelling by MRTF/SRF (Esnault et al. 2014; Gualdrini et al. 2016), our identification of targets implicated during induced long-term PM blebbing mediated by the MRTF/SRF pathway was crucial to further understand this mechanism driving blebbing and subsequent entotic invasion. Notably, induction of Ezrin was significantly reduced in the absence of either SRF or MRTF-A/B during induced PM blebbing (Figure 27). In contrast, expression levels of other ERMs were unaffected upon suppression of SRF (Figure 27), indicating that these proteins are not controlled by the MRTF/SRF pathway upon induced blebbing activity. Consistent with our results where Ezrin is upregulated in a MRTF/SRF-dependent manner, Ezrin specificity was further confirmed using the prototypic serum stimulation assay known to induce the MRTF/SRF pathway (Figure 28) (Baarlink, Wang, and Grosse 2013; Vartiainen et al. 2007).

Furthermore, several triggers have been identified that induce blebbing for bleb-associated migration, for instance increase of cortical contractility forces, cell physical confinement and low adhesion to the extracellular matrix (Martin Bergert et al. 2015; Ruprecht et al. 2015; Liu et al. 2015). Hence, we confirmed that our model of induced blebbing by matrix deadhesion is sufficient to trigger PM blebbing. As a result of pharmacological interference with blebbing, Ezrin and SRF upregulation were inhibited upon conditions of low adhesion (Figure 29). This validates our model and hypothesis, in which preventing attachment leads to cortical blebbing.

A recent study showed that bleb expansion requires Rnd3 recruitment, whereas bleb retraction is mediated by RhoA and ROCK phosphorylation that leads to Rnd3 inactivation and subsequent Ezrin activation (Aoki et al. 2016). In addition, this study reported that Ezrin and Eps8 are essential regulators of actin reassembly for blebbing dynamics (Aoki et al. 2016). This is consistent with our data, in which Ezrin is recruited to the plasma membrane to reassemble the actin cortex and therefore is upregulated during sustained blebbing activity. Moreover, our results point a critical role for Ezrin as a MRTF/SRF-dependent target gene in the regulation of induced cortical blebbing and suggesting a role in bleb-associated invasion.

5.4. The importance of MRTF/SRF transcription and Ezrin for entotic invasion

Our data demonstrate that Ezrin upregulation via the MRTF/SRF transcriptional pathway controls dynamic PM blebbing. To further explore this process, we tested the impact of MRTF/SRF transcription and Ezrin on bleb-associated entotic invasion. Remarkably, analysis of Ezrin subcellular localization during cell-in-cell invasion revealed that Ezrin is redistributed and polarized in the invading cell (Figure 21 and Figure 31), which in turn requires sustained actin-driven PM blebbing (Purvanov et al. 2014).

Given the fundamental role of Ezrin during entotic invasion, we focused on the phosphorylation of the ERM Ezrin, which is an essential process known to regulate its activation. Herein, we examined the activation state of this actin-membrane linker during the entotic process by analyzing its phosphorylation state. We observed that endogenous phosphorylated-ERM colocalizes with Ezrin and actin during entotic invasion at advanced stages (Figure 31) showing a polarized enrichment of pERM at the rear of the invading cell. These findings reveal the importance of Ezrin phosphorylation during entotic invasion, in which the actin cytoskeleton-plasma membrane linker Ezrin is found polarized and highly enriched during cell-in-cell invasion. These data are consistent with the idea that invading cells display polarized Ezrin and actin enrichment at the rear, which provides actomyosin contractility to generate the force to invade the host cell. Similarly, cell motility in migrating cells is mediated by the formation of actin-rich protrusions dependent on actomyosin contractile forces at the rear end of the invading cell (G. Charras and Paluch 2008). Accordingly, the driving force is generated by the actin-rich bleb structures, while the direction of movement is defined by the Ezrin-rich uropod-like structure (ERULS) at the rear of amoeboid blebbing cells (Lorentzen et al. 2011).

Even though entosis is a long-term process, whether transcriptional activity regulates entotic invasion was unknown. Thus, we aimed to examine the impact of transcriptional activity on entosis by interfering with global transcription. Interestingly, our data showed that entosis ability was strongly reduced by inhibiting transcription (Figure 32), suggesting that global transcription is necessary for entotic invasion. In a similar manner, translation inhibition by blocking protein synthesis led to inhibition of entosis (Figure 32), indicating the crucial role of global transcription and translation for efficient entotic invasion.

Previous studies have reported that the MRTF/SRF transcriptional pathway plays an important role during tumor invasion. For instance, several studies have revealed the relevance of MRTF-A during invasive migration (Brandt et al. 2009; Medjkane et al. 2009). Depletion of SRF or MRTF-A/B reduces cell adhesion, and the spread and invasiveness of tumor cells (Medjkane et al. 2009). In contrast, the expression of constitutively active SRF enhances the formation of liver

nodules, which promotes hepatocellular carcinoma (Ohrnberger et al. 2015). In this work, we examined the importance of MRTF/SRF transcription for bleb-associated entotic invasion. It is noteworthy that suppression of either the ERM Ezrin, SRF or simultaneous depletion of MRTF-A and MRTF-B, significantly reduced entosis ability, although to a much more moderate degree than in the absence of SRF (Figure 33). Similarly, Ezrin knockdown inhibited the invasion of melanoma cells (Lorentzen et al. 2011). Consistent with this, we show that expression of constitutively active MRTF-A promotes entotic invasion (Figure 34). These data provide support that not only global transcription, but also the specific MRTF/SRF transcriptional pathway and our recently identified target gene Ezrin are required for efficient entotic invasion. In addition, given the mutual dependence between the MRTF/SRF and the YAP-TAZ signaling pathways in controlling cell contractility and TGFβ-signaling in cancer-associated fibroblasts (Foster, Gualdrini, and Treisman 2018), it would be interesting to further test whether the YAP-TAZ pathway is involved for blebbing and entotic invasion.

Consistent with the importance of MRTF/SRF transcription for entosis, SRF depletion in the invading cell remarkably reduced entosis, whereas knockdown of SRF in the host cell had no effect (Figure 35). In turn, SRF appears to be specifically necessary in the actively invading cell to promote entotic invasion. Notably, SRF-depleted cells fail to successfully complete entotic invasion (Figure 35), suggesting that the invading cell, which showed extensive blebbing before cell engulfment, fails to produce enough mechanical force to invade into the host cell due to disrupted bleb dynamics in the absence of SRF. In this context, recent studies showed that actomyosin contractility and cell stiffness are essential forces driving entosis (Sun, Luo, et al. 2014). Furthermore, focusing on the SRF transcriptional coactivator MRTF-A subcellular localization during entotic invasion, we identified a nuclear MRTF-A accumulation in the actively invading cells before cell engulfment to initiate entotic invasion (Figure 36). Together, these data indicate that the actin-controlled MRTF/SRF pathway is fundamental in entosis, providing the driving force for blebbing and subsequent entotic invasion at the invading cells. These findings also highlight the role of MRTF/SRF in cell-in-cell invasion involving expression of Ezrin.

Although the physiological consequences of entosis are not yet well known, some evidence supports entosis as a tumor-suppressive mechanism to clear dysfunctional cells after non-apoptotic death of the internalized entotic cell (Florey et al. 2011). Whereas other studies revealed that entosis triggers aneuploidy due to failed cytokinesis in the host cell thus enhancing tumor progression (Matej Krajcovic et al. 2011). In addition to the prevalence of entosis in cancer, LPA and LPAR2, which are key regulators of entosis (Purvanov et al. 2014), are also known to play a role during cancer metastasis (Choi et al. 2010), suggesting a correlation

between entosis and malignancy. Further studies are required to investigate the therapeutic clinical potential of entosis in cancer.

5.5.   Functional significance of Ezrin expression for bleb dynamics and entosis

Several studies have identified Ezrin as a novel regulator of invasion and metastasis (Lorentzen et al. 2011; Y. Yu et al. 2004; Ren et al. 2009). Additionally, Ezrin is involved in amoeboid blebbing driving cell motility (Lorentzen et al. 2011). Consistent with the correlation between blebbing and Ezrin, increased activity of the ERMs is associated with reduced blebbing in different cell types such as melanoma cells, mast cells and zebrafish primordial germ cells (Goudarzi et al. 2012; Yanase et al. 2011; Lorentzen et al. 2011). In contrast to previous studies, which have observed a negative regulation between the ERMs and blebbing activity, we uncovered a positive feedback loop to sustain PM blebbing activity by Ezrin upregulation. Hence, given that induction of Ezrin expression depends on MRTF/SRF and PM blebbing, we further focused on the significance of Ezrin in this phenotype. Therefore, we stably expressed our identified MRTF-SRF target gene, *wild-type* Ezrin, and examined bleb dynamics compared to the control GFP-expressing cells upon suppression of SRF. These data demonstrate that *wild-type* Ezrin expression is sufficient to restore efficient bleb dynamics in the absence of SRF (Figure 37). In contrast, GFP-expressing cells in which SRF was depleted fail to produce dynamic blebbing, indicating the functional relevance of Ezrin re-expression to rescue defective bleb retraction in response to SRF suppression. These findings are consistent with the essential function of Ezrin in the reassembly of the contractile actin cortex during bleb retraction mediated by actomyosin contractility (Guillaume T Charras et al. 2006). As a consequence of the restored plasma membrane blebbing, expression of *wild-type* Ezrin is necessary and sufficient to rescue entotic invasion in the absence of SRF, whereas entosis was impaired in control cells expressing GFP upon SRF depletion (Figure 38). In turn, these data support Ezrin as a MRTF/SRF target gene controlling bleb dynamics and entosis.

Furthermore, we analyzed the impact of the non-phosphorylatable Ezrin mutant form, Ezrin-T567A (TA), on bleb dynamics and subsequent entosis. This inactive mutant fails to link the plasma membrane to the underlying actin cytoskeleton (Gautreau, Louvard, and Arpin 2000). However, expression of the TA mutant, which does not block blebbing activity, has no effect on amoeboid invasion in melanoma cells (Lorentzen et al. 2011). Alternatively, expression of the phosphomimetic Ezrin T567D, which acts as a constitutively active form, robustly inhibits blebbing activity leading to significantly reduced amoeboid invasion (Guillaume T Charras et al. 2006; Lorentzen et al. 2011). Consistently, our data reveal that expression of the non-phosphorylatable Ezrin mutant triggers non-functional bleb dynamics and less blebbing activity

resulting in reduced entotic invasion (Figure 37 and Figure 38). Ezrin T567A fails to link the PM to the actin cytoskeleton (Gautreau, Louvard, and Arpin 2000), which explains the importance of phosphorylation for efficient Ezrin activation and dynamic blebbing. Taken together, our results report that MRTF/SRF-dependent upregulation of Ezrin is critical for sustained PM blebbing to promote entosis.

5.6.   Role of the MRTF/SRF pathway on amoeboid to mesenchymal transition

Given the association between the actin-regulated MRTF/SRF transcriptional feedback and non-apoptotic blebbing for subsequent entotic invasion, we next focused on another bleb-associated motility mode, amoeboid blebbing, to further investigate the impact of the MRTF/SRF transcriptional pathway. Amoeboid blebbing is often observed during cancer invasion, in which cells are characterized by rounded blebbing morphology, fast migration, low adhesion and high cortical actomyosin contractility (Sahai and Marshall 2003; Sanz-Moreno et al. 2008). Interestingly, amoeboid blebbing invasion bears similarities with entotic invasion, both being regulated by the actin cytoskeleton, Rho-ROCK signaling and actomyosin forces. Our results reveal the importance of the MRTF/SRF pathway for amoeboid blebbing, suggesting a cell morphology switch in response to either MRTF-A/B or SRF depletion, triggering the amoeboid to mesenchymal transition (AMT) (Figure 41).

In addition to the relevance of MRTF/SRF transcription for invasive cell migration, this pathway controls expression of target genes involved in cell contractility and extracellular matrix remodelling (Gualdrini et al. 2016). Here, we show that amoeboid blebbing is dependent on the MRTF/SRF transcriptional pathway and actomyosin contractility (Figure 43). In turn, we confirmed that SRF-depleted cells undergo mesenchymal morphology leading to upregulation of previously described target genes related to actomyosin contractility (Figure 4) (Gadea et al. 2008; Wolf et al. 2003). In contrast to amoeboid to mesenchymal transition, recent studies reported that cortical contractility and low adhesion conditions trigger mesenchymal to amoeboid motility transition (MAT) in confined 3D environments (Ruprecht et al. 2015; Liu et al. 2015). Further studies are required to characterize the molecular mechanisms driving AMT and MAT. Therefore, it remains a future challenge to identify the mechanism and target genes, that are responsible for regulating MRTF/SRF transcription in amoeboid blebbing invasion and its transition to the mesenchymal elongated invasion.

5.7. Conclusion

The work presented in this thesis is focused on the transcriptional regulation of the actin-mediated MRTF/SRF pathway and its role in blebbing and bleb-associated invasion. In this study, we demonstrate that bleb dynamics and efficient entosis require MRTF/SRF transcriptional activity mediated by upregulation of the metastasis-associated ERM protein Ezrin (Figure 45). Consistent with the importance of the MRTF/SRF pathway for sustained blebbing, we find that cortical plasma membrane blebbing regulates dynamic MRTF-A nuclear translocation (Figure 44) to enhance SRF transcriptional activity necessary for entotic invasion. Our findings reveal Ezrin as an MRTF/SRF target gene to promote bleb-associated cell-in-cell invasion. Our results highlight the importance of transcriptional feed forward signaling for bleb-associated invasive motility and entosis. Thereby, this study opens new avenues providing a transcriptional regulation feed forward loop controlling bleb-associated motility.
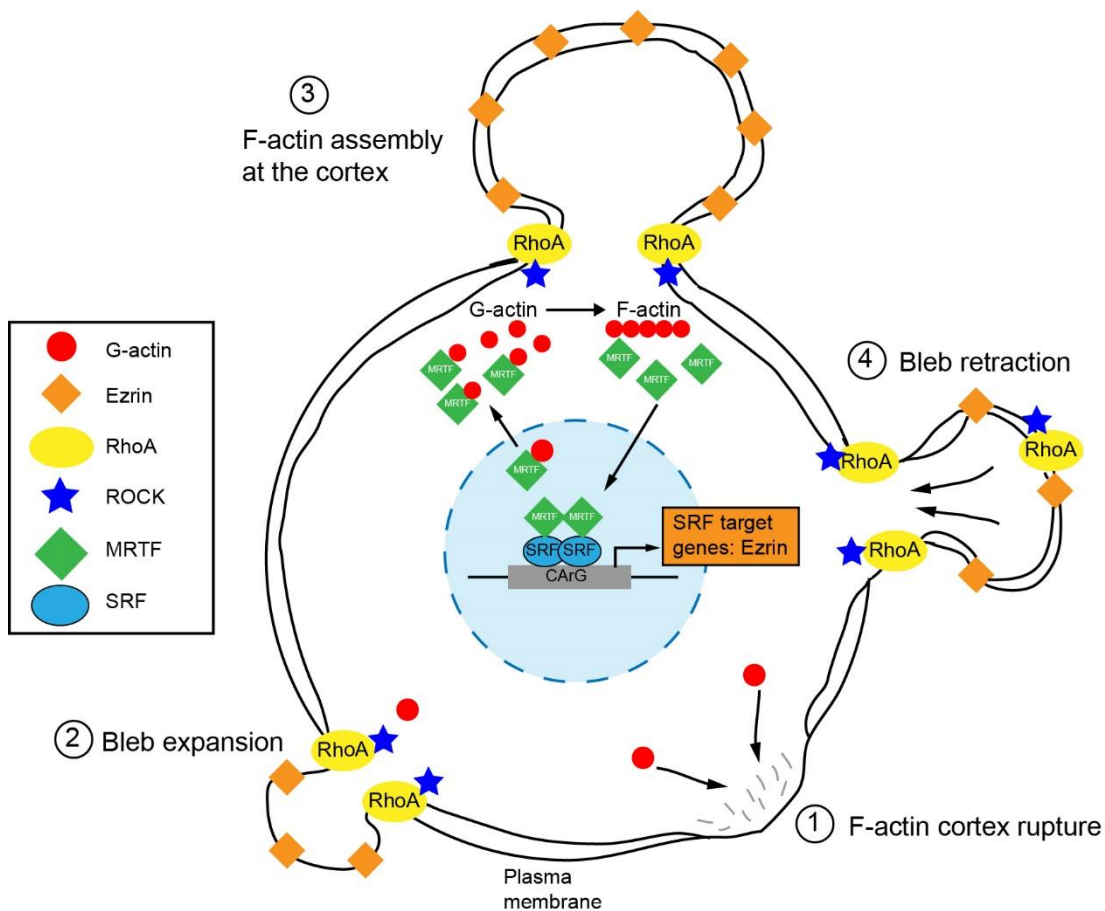

Figure 45: Schematic model of this work. This cartoon shows actin-regulated MRTF/SRF-mediated upregulation of Ezrin and actomyosin contractility, which are critical for sustained bleb dynamics.

References

Adams, Josephine C. 2004. "Roles of Fascin in Cell Adhesion and Motility." *Current Opinion in Cell Biology* 16 (5): 590–96. https://doi.org/10.1016/J.CEB.2004.07.009.

Angus, Annette A, Amanda Ackerman Lee, Danielle K Augustin, Ellen J Lee, David J Evans, and Suzanne M J Fleiszig. 2008. "Pseudomonas Aeruginosa Induces Membrane Blebs in Epithelial Cells, Which Are Utilized as a Niche for Intracellular Replication and Motility." *Infection and Immunity* 76 (5): 1992–2001. https://doi.org/10.1128/IAI.01221-07.

Aoki, Kana, Fumiyo Maeda, Tomoya Nagasako, Yuki Mochizuki, Seiichi Uchida, and Junichi Ikenouchi. 2016. "A RhoA and Rnd3 Cycle Regulates Actin Reassembly during Membrane Blebbing." *Proceedings of the National Academy of Sciences of the United States of America* 113 (13): E1863-71. https://doi.org/10.1073/pnas.1600968113.

Arpin, Monique, Dafne Chirivino, Alexandra Naba, and Ingrid Zwaenepoel. 2011. "Emerging Role for ERM Proteins in Cell Adhesion and Migration." *Cell Adhesion & Migration* 5 (2): 199–206. https://doi.org/10.4161/CAM.5.2.15081.

Baarlink, Christian, Haicui Wang, and Robert Grosse. 2013. "Nuclear Actin Network Assembly by Formins Regulates the SRF Coactivator MAL." *Science* 340 (6134).

Baker, Jessica M, and Frederick M Boyce. 2014. "High-Throughput Functional Screening Using a Homemade Dual-Glow Luciferase Assay." *Journal of Visualized Experiments : JoVE*, no. 88 (June). https://doi.org/10.3791/50282.

Baumgartner, Martin, Amy L Sillman, Elizabeth M Blackwood, Jyoti Srivastava, Nikki Madson, James W Schilling, Jocelyn H Wright, and Diane L Barber. 2006. "The Nck-Interacting Kinase Phosphorylates ERM Proteins for Formation of Lamellipodium by Growth Factors." *Proceedings of the National Academy of Sciences of the United States of America* 103 (36): 13391–96. https://doi.org/10.1073/pnas.0605950103.

Belkina, Natalya V, Yin Liu, Jian-Jiang Hao, Hajime Karasuyama, and Stephen Shaw. 2009. "LOK Is a Major ERM Kinase in Resting Lymphocytes and Regulates Cytoskeletal Rearrangement through ERM Phosphorylation." www.pnas.org/cgi/content/full/.

Bensaude, Olivier. 2011. "Inhibiting Eukaryotic Transcription: Which Compound to Choose? How to Evaluate Its Activity?" *Transcription*. https://doi.org/10.4161/trns.2.3.16172.

Bergert, M., S. D. Chandradoss, R. A. Desai, and E. Paluch. 2012. "Cell Mechanics Control Rapid Transitions between Blebs and Lamellipodia during Migration." *Proceedings of the National Academy of Sciences*. https://doi.org/10.1073/pnas.1207968109.

Bergert, Martin, Anna Erzberger, Ravi A. Desai, Irene M. Aspalter, Andrew C. Oates, Guillaume Charras, Guillaume Salbreux, and Ewa K. Paluch. 2015. "Force Transmission during Adhesion-Independent Migration." *Nature Cell Biology*. https://doi.org/10.1038/ncb3134.

Biro, Maté, Yves Romeo, Sonja Kroschwald, Miia Bovellan, Annett Boden, Joseph Tcherkezian, Philippe P. Roux, Guillaume Charras, and Ewa K. Paluch. 2013. "Cell Cortex Composition and Homeostasis Resolved by Integrating Proteomics and Quantitative Imaging." *Cytoskeleton* 70 (11): 741–54. https://doi.org/10.1002/cm.21142.

Blaser, Heiko, Michal Reichman-Fried, Irinka Castanon, Karin Dumstrei, Florence L Marlow, Koichi Kawakami, Lilianna Solnica-Krezel, Carl-Philipp Heisenberg, and Erez Raz. 2006. "Migration of Zebrafish Primordial Germ Cells: A Role for Myosin Contraction and

Cytoplasmic Flow." *Developmental Cell* 11 (5): 613–27. https://doi.org/10.1016/j.devcel.2006.09.023.

Bovellan, Miia, Yves Romeo, Maté Biro, Annett Boden, Priyamvada Chugh, Amina Yonis, Malti Vaghela, et al. 2014. "Cellular Control of Cortical Actin Nucleation." *Current Biology : CB* 24 (14): 1628–35. https://doi.org/10.1016/j.cub.2014.05.069.

Brandt, Dominique T., Christian Baarlink, Thomas M. Kitzing, Elisabeth Kremmer, Johanna Ivaska, Peter Nollau, and Robert Grosse. 2009. "SCAI Acts as a Suppressor of Cancer Cell Invasion through the Transcriptional Control of B1-Integrin." *Nature Cell Biology*. https://doi.org/10.1038/ncb1862.

Bretscher, A. 1983. "Purification of an 80,000-Dalton Protein That Is a Component of the Isolated Microvillus Cytoskeleton, and Its Localization in Nonmuscle Cells." *The Journal of Cell Biology* 97 (2): 425–32. https://doi.org/10.1083/JCB.97.2.425.

Bretscher, Anthony, Kevin Edwards, and Richard G. Fehon. 2002. "ERM Proteins and Merlin: Integrators at the Cell Cortex." *Nature Reviews Molecular Cell Biology* 3 (8): 586–99. https://doi.org/10.1038/nrm882.

Brown, L, A Waseem, I N Cruz, J Szary, E Gunic, T Mannan, M Unadkat, et al. 2014. "Desmoglein 3 Promotes Cancer Cell Migration and Invasion by Regulating Activator Protein 1 and Protein Kinase C-Dependent-Ezrin Activation." *Oncogene* 33 (18): 2363–74. https://doi.org/10.1038/onc.2013.186.

Bruce, Benjamin, Gaurav Khanna, Ling Ren, Goran Landberg, Karin Jirström, Charles Powell, Alain Borczuk, et al. 2007. "Expression of the Cytoskeleton Linker Protein Ezrin in Human Cancers." *Clinical & Experimental Metastasis* 24 (2): 69–78. https://doi.org/10.1007/s10585-006-9050-x.

Buchwalter, Gilles, Christian Gross, and Bohdan Wasylyk. 2004. "Ets Ternary Complex Transcription Factors." *Gene* 324 (January): 1–14. http://www.ncbi.nlm.nih.gov/pubmed/14693367.

Bugyi, Beáta, and Marie-France Carlier. 2010. "Control of Actin Filament Treadmilling in Cell Motility." *Annual Review of Biophysics* 39 (1): 449–70. https://doi.org/10.1146/annurev-biophys-051309-103849.

Canals, Daniel, Russell W Jenkins, Patrick Roddy, María José Hernández-Corbacho, Lina M Obeid, and Yusuf A Hannun. 2010. "Differential Effects of Ceramide and Sphingosine 1-Phosphate on ERM Phosphorylation: Probing Sphingolipid Signaling at the Outer Plasma Membrane." *The Journal of Biological Chemistry* 285 (42): 32476–85. https://doi.org/10.1074/jbc.M110.141028.

Canel, M., A. Serrels, M. C. Frame, and V. G. Brunton. 2013. "E-Cadherin-Integrin Crosstalk in Cancer Invasion and Metastasis." *Journal of Cell Science* 126 (2): 393–401. https://doi.org/10.1242/jcs.100115.

Cant, Sarah H., and Julie A. Pitcher. 2005. "G Protein-Coupled Receptor Kinase 2–mediated Phosphorylation of Ezrin Is Required for G Protein-Coupled Receptor–dependent Reorganization of the Actin Cytoskeleton." *Molecular Biology of the Cell* 16 (7): 3088. https://doi.org/10.1091/MBC.E04-10-0877.

Carreno, Sébastien, Ilektra Kouranti, Edith Szafer Glusman, Margaret T Fuller, Arnaud Echard, and François Payre. 2008. "Moesin and Its Activating Kinase Slik Are Required for Cortical Stability and Microtubule Organization in Mitotic Cells." *The Journal of Cell Biology* 180 (4): 739–46. https://doi.org/10.1083/jcb.200709161.

Charras, G. T. 2008. "A Short History of Blebbing." In *Journal of Microscopy*. https://doi.org/10.1111/j.1365-2818.2008.02059.x.

Charras, Guillaume, and Ewa Paluch. 2008. "Blebs Lead the Way: How to Migrate without Lamellipodia." *Nature Reviews Molecular Cell Biology* 9 (9): 730–36. https://doi.org/10.1038/nrm2453.

Charras, Guillaume T, Margaret Coughlin, Timothy J Mitchison, and L Mahadevan. 2008. "Life and Times of a Cellular Bleb." *Biophysical Journal* 94 (5): 1836–53. https://doi.org/10.1529/biophysj.107.113605.

Charras, Guillaume T, Chi-Kuo Hu, Margaret Coughlin, and Timothy J Mitchison. 2006. "Reassembly of Contractile Actin Cortex in Cell Blebs." *The Journal of Cell Biology* 175 (3): 477–90. https://doi.org/10.1083/jcb.200602085.

Charras, Guillaume T, Justin C Yarrow, Mike A Horton, L Mahadevan, T J Mitchison, and Guillaume Charras. 2005. "Non-Equilibration of Hydrostatic Pressure in Blebbing Cells." *Nature*. Vol. 435. https://www.ncbi.nlm.nih.gov/pmc/articles/PMC1564437/pdf/nihms4384.pdf.

Chesarone, Melissa A., Amy Grace DuPage, and Bruce L. Goode. 2010. "Unleashing Formins to Remodel the Actin and Microtubule Cytoskeletons." *Nature Reviews Molecular Cell Biology* 11 (1): 62–74. https://doi.org/10.1038/nrm2816.

Cheung, A., J. A. Dantzig, S. Hollingworth, S. M. Baylor, Y.E. Goldman, T. J. Mitchison, and A. F. Straight. 2002. "A Small-Molecule Inhibitor of Skeletal Muscle Myosin II." *Nature Cell Biology* 4 (1): 83–88. https://doi.org/10.1038/ncb734.

Chhabra, Ekta Seth, and Henry N. Higgs. 2007. "The Many Faces of Actin: Matching Assembly Factors with Cellular Structures." *Nature Cell Biology* 9 (10): 1110–21. https://doi.org/10.1038/ncb1007-1110.

Choi, Ji Woong, Deron R. Herr, Kyoko Noguchi, Yun C. Yung, Chang-Wook Lee, Tetsuji Mutoh, Mu-En Lin, et al. 2010. "LPA Receptors: Subtypes and Biological Actions." *Annual Review of Pharmacology and Toxicology*. https://doi.org/10.1146/annurev.pharmtox.010909.105753.

Chuan, Y-C, D Iglesias-Gato, L Fernandez-Perez, A Cedazo-Minguez, S-T Pang, G Norstedt, Å Pousette, and A Flores-Morales. 2010. "Ezrin Mediates C-Myc Actions in Prostate Cancer Cell Invasion." *Oncogene* 29 (10): 1531–42. https://doi.org/10.1038/onc.2009.442.

Chuan, Yin-Choy, See-Tong Pang, Angel Cedazo-Minguez, Gunnar Norstedt, Ake Pousette, and Amilcar Flores-Morales. 2006. "Androgen Induction of Prostate Cancer Cell Invasion Is Mediated by Ezrin." *The Journal of Biological Chemistry* 281 (40): 29938–48. https://doi.org/10.1074/jbc.M602237200.

Chugh, Priyamvada, and Ewa K Paluch. 2018. "The Actin Cortex at a Glance." *Journal of Cell Science* 131 (14): jcs186254. https://doi.org/10.1242/jcs.186254.

Clucas, Jarama, and Ferran Valderrama. 2015. "ERM Proteins in Cancer Progression." *Journal of Cell Science* 127: 267–75. https://doi.org/10.1242/jcs.170027.

Coene, Elisabeth D, Catarina Gadelha, Nicholas White, Ashraf Malhas, Benjamin Thomas, Michael Shaw, and David J Vaux. 2011. "A Novel Role for BRCA1 in Regulating Breast Cancer Cell Spreading and Motility." *The Journal of Cell Biology* 192 (3): 497–512. https://doi.org/10.1083/jcb.201004136.

Copeland, John W., and Richard Treisman. 2002. "The Diaphanous-Related Formin MDia1

Controls Serum Response Factor Activity through Its Effects on Actin Polymerization." Edited by David Drubin. *Molecular Biology of the Cell* 13 (11): 4088–99. https://doi.org/10.1091/mbc.02-06-0092.

Creemers, Esther E, Lillian B Sutherland, John McAnally, James A Richardson, and Eric N Olson. 2006. "Myocardin Is a Direct Transcriptional Target of Mef2, Tead and Foxo Proteins during Cardiovascular Development." *Development (Cambridge, England)* 133 (21): 4245–56. https://doi.org/10.1242/dev.02610.

Crepaldi, T, A Gautreau, P M Comoglio, D Louvard, and M Arpin. 1997. "Ezrin Is an Effector of Hepatocyte Growth Factor-Mediated Migration and Morphogenesis in Epithelial Cells." *The Journal of Cell Biology* 138 (2): 423–34. https://doi.org/10.1083/JCB.138.2.423.

Cunningham, C C, J B Gorlin, D J Kwiatkowski, J H Hartwig, P A Janmey, H R Byers, and T P Stossel. 1992. "Actin-Binding Protein Requirement for Cortical Stability and Efficient Locomotion." *Science (New York, N.Y.)* 255 (5042): 325–27. https://doi.org/10.1126/SCIENCE.1549777.

Curran, T, G Peters, C Van Beveren, N M Teich, and I M Verma. 1982. "FBJ Murine Osteosarcoma Virus: Identification and Molecular Cloning of Biologically Active Proviral DNA." *Journal of Virology* 44 (2): 674–82. http://www.ncbi.nlm.nih.gov/pubmed/6292525.

Debnath, Jayanta, and Joan S. Brugge. 2005. "Modelling Glandular Epithelial Cancers in Three-Dimensional Cultures." *Nature Reviews Cancer*. https://doi.org/10.1038/nrc1695.

Debnath, Jayanta, Senthil K Muthuswamy, and Joan S Brugge. 2003. "Morphogenesis and Oncogenesis of MCF-10A Mammary Epithelial Acini Grown in Three-Dimensional Basement Membrane Cultures." *Methods (San Diego, Calif.)* 30 (3): 256–68. http://www.ncbi.nlm.nih.gov/pubmed/12798140.

Deng, Xiyun, Sarah H. Tannehill-Gregg, Murali V. P. Nadella, Guangchun He, Andrea Levine, Ya Cao, and Thomas J. Rosol. 2007. "Parathyroid Hormone-Related Protein and Ezrin Are up-Regulated in Human Lung Cancer Bone Metastases." *Clinical & Experimental Metastasis* 24 (2): 107–19. https://doi.org/10.1007/s10585-007-9059-9.

Diz-Muñoz, Alba, Michael Krieg, Martin Bergert, Itziar Ibarlucea-Benitez, Daniel J. Muller, Ewa Paluch, and Carl-Philipp Heisenberg. 2010. "Control of Directed Cell Migration In Vivo by Membrane-to-Cortex Attachment." Edited by William A. Harris. *PLoS Biology* 8 (11): e1000544. https://doi.org/10.1371/journal.pbio.1000544.

Dominguez, Roberto, and Kenneth C Holmes. 2011. "Actin Structure and Function." *Annual Review of Biophysics* 40: 169–86. https://doi.org/10.1146/annurev-biophys-042910-155359.

Durgan, J., and O. Florey. 2018. "Cancer Cell Cannibalism: Multiple Triggers Emerge for Entosis." *Biochimica et Biophysica Acta - Molecular Cell Research*. https://doi.org/10.1016/j.bbamcr.2018.03.004.

Durgan, Joanne, Yun Yu Tseng, Jens C. Hamann, Marie Charlotte Domart, Lucy Collinson, Alan Hall, Michael Overholtzer, and Oliver Florey. 2017. "Mitosis Can Drive Cell Cannibalism through Entosis." *ELife*. https://doi.org/10.7554/eLife.27134.

Elliott, Bruce E, Jalna A Meens, Sandip K SenGupta, Daniel Louvard, and Monique Arpin. 2005. "The Membrane Cytoskeletal Crosslinker Ezrin Is Required for Metastasis of Breast Carcinoma Cells." *Breast Cancer Research : BCR* 7 (3): R365-73. https://doi.org/10.1186/bcr1006.

Ennomani, Hajer, Gaëlle Letort, Christophe Guérin, Jean-Louis Martiel, Wenxiang Cao, François Nédélec, Enrique M De La Cruz, Manuel Théry, and Laurent Blanchoin. 2016. "Architecture and Connectivity Govern Actin Network Contractility." *Current Biology : CB* 26 (5): 616–26. https://doi.org/10.1016/j.cub.2015.12.069.

Er, Ekrem Emrah, Manuel Valiente, Karuna Ganesh, Yilong Zou, Saloni Agrawal, Jing Hu, Bailey Griscom, et al. 2018. "Pericyte-like Spreading by Disseminated Cancer Cells Activates YAP and MRTF for Metastatic Colonization." *Nature Cell Biology* 20 (8): 966–78. https://doi.org/10.1038/s41556-018-0138-8.

Esnault, Cyril, Aengus Stewart, Francesco Gualdrini, Phil East, Stuart Horswell, Nik Matthews, and Richard Treisman. 2014. "Rho-Actin Signaling to the MRTF Coactivators Dominates the Immediate Transcriptional Response to Serum in Fibroblasts." *Genes and Development*. https://doi.org/10.1101/gad.239327.114.

Fackler, Oliver T, and Robert Grosse. 2008. "Cell Motility through Plasma Membrane Blebbing." *The Journal of Cell Biology* 181 (6): 879–84. https://doi.org/10.1083/jcb.200802081.

Federici, Cristina, Daria Brambilla, Francesco Lozupone, Paola Matarrese, Angelo de Milito, Luana Lugini, Elisabetta Iessi, et al. 2009. "Pleiotropic Function of Ezrin in Human Metastatic Melanomas." *International Journal of Cancer* 124 (12): 2804–12. https://doi.org/10.1002/ijc.24255.

Fehon, Richard G., Andrea I. McClatchey, and Anthony Bretscher. 2010. "Organizing the Cell Cortex: The Role of ERM Proteins." *Nature Reviews Molecular Cell Biology* 11 (4): 276–87. https://doi.org/10.1038/nrm2866.

Fievet, Bruno T, Alexis Gautreau, Christian Roy, Laurence Del Maestro, Paul Mangeat, Daniel Louvard, and Monique Arpin. 2004. "Phosphoinositide Binding and Phosphorylation Act Sequentially in the Activation Mechanism of Ezrin." *The Journal of Cell Biology* 164 (5): 653–59. https://doi.org/10.1083/jcb.200307032.

Fletcher, Daniel A, and R Dyche Mullins. 2010. "Cell Mechanics and the Cytoskeleton." *Nature* 463 (7280): 485–92. https://doi.org/10.1038/nature08908.

Florey, Oliver, Sung Eun Kim, Cynthia P. Sandoval, Cole M. Haynes, and Michael Overholtzer. 2011. "Autophagy Machinery Mediates Macroendocytic Processing and Entotic Cell Death by Targeting Single Membranes." *Nature Cell Biology* 13 (11): 1335–43. https://doi.org/10.1038/ncb2363.Autophagy.

Foster, Charles T., Francesco Gualdrini, and Richard Treisman. 2018. "Mutual Dependence of the MRTF-SRF and YAP-TEAD Pathways in Cancer-Associated Fibroblasts Is Indirect and Mediated by Cytoskeletal Dynamics." *Genes and Development*. https://doi.org/10.1101/gad.304501.117.

Friedl, Peter, and Stephanie Alexander. 2011. "Cancer Invasion and the Microenvironment: Plasticity and Reciprocity." *Cell* 147 (5): 992–1009. https://doi.org/10.1016/j.cell.2011.11.016.

Friedl, Peter, and Katarina Wolf. 2003. "Tumour-Cell Invasion and Migration: Diversity and Escape Mechanisms." *Nature Reviews Cancer* 3 (5): 362–74. https://doi.org/10.1038/nrc1075.

———. 2009. "Proteolytic Interstitial Cell Migration: A Five-Step Process." *Cancer and Metastasis Reviews* 28 (1–2): 129–35. https://doi.org/10.1007/s10555-008-9174-3.

———. 2010. "Plasticity of Cell Migration: A Multiscale Tuning Model." *The Journal of Cell Biology* 188 (1): 11–19. https://doi.org/10.1083/jcb.200909003.

Gadea, Gilles, Victoria Sanz-Moreno, Annette Self, Anna Godi, and Christopher J Marshall. 2008. "DOCK10-Mediated Cdc42 Activation Is Necessary for Amoeboid Invasion of Melanoma Cells." *Current Biology : CB* 18 (19): 1456–65. https://doi.org/10.1016/j.cub.2008.08.053.

Gandalovičová, Aneta, Tomáš Vomastek, Daniel Rosel, and Jan Brábek. 2016. "Cell Polarity Signaling in the Plasticity of Cancer Cell Invasiveness." *Oncotarget* 7 (18). www.impactjournals.com/oncotarget.

Gary, R, and A Bretscher. 1995. "Ezrin Self-Association Involves Binding of an N-Terminal Domain to a Normally Masked C-Terminal Domain That Includes the F-Actin Binding Site." *Molecular Biology of the Cell* 6 (8): 1061–75. http://www.ncbi.nlm.nih.gov/pubmed/7579708.

Gautreau, Alexis, Daniel Louvard, and Monique Arpin. 2000. "Morphogenic Effects of Ezrin Require a Phosphorylation-Induced Transition from Oligomers to Monomers at the Plasma Membrane." *Journal of Cell Biology*. https://doi.org/10.1083/jcb.150.1.193.

Geneste, Olivier, John W. Copeland, and Richard Treisman. 2002. "LIM Kinase and Diaphanous Cooperate to Regulate Serum Response Factor and Actin Dynamics." *Journal of Cell Biology*. https://doi.org/10.1083/jcb.200203126.

Gille, Hendrik, Andrew D. Sharrocks, and Peter E. Shaw. 1992. "Phosphorylation of Transcription Factor P62TCF by MAP Kinase Stimulates Ternary Complex Formation at C-Fos Promoter." *Nature* 358 (6385): 414–17. https://doi.org/10.1038/358414a0.

Gimona, Mario, Roberto Buccione, Sara A Courtneidge, and Stefan Linder. 2008. "Assembly and Biological Role of Podosomes and Invadopodia." *Current Opinion in Cell Biology* 20 (2): 235–41. https://doi.org/10.1016/J.CEB.2008.01.005.

Gineitis, D, and R Treisman. 2001. "Differential Usage of Signal Transduction Pathways Defines Two Types of Serum Response Factor Target Gene." *The Journal of Biological Chemistry* 276 (27): 24531–39. https://doi.org/10.1074/jbc.M102678200.

Glotzer, Michael. 2001. "Animal Cell Cytokinesis." *Annual Review of Cell and Developmental Biology* 17 (1): 351–86. https://doi.org/10.1146/annurev.cellbio.17.1.351.

Goudarzi, Mehdi, Torsten U Banisch, Mehrpouya B Mobin, Nicola Maghelli, Katsiaryna Tarbashevich, Ina Strate, Jana van den Berg, et al. 2012. "Identification and Regulation of a Molecular Module for Bleb-Based Cell Motility." *Developmental Cell* 23 (1): 210–18. https://doi.org/10.1016/j.devcel.2012.05.007.

Graham, F L, J Smileyt, W C Russell, and R Nairn. 1977. "Characteristics of a Human Cell Line Transformed by DNA from Human Adenovirus Type 5." *J. Gen. Virol* 36: 59–66. www.microbiologyresearch.org.

Greenberg, M E, L A Greene, and E B Ziff. 1985. "Nerve Growth Factor and Epidermal Growth Factor Induce Rapid Transient Changes in Proto-Oncogene Transcription in PC12 Cells." *The Journal of Biological Chemistry* 260 (26): 14101–10. http://www.ncbi.nlm.nih.gov/pubmed/3877054.

Greenberg, M E, and E B Ziff. 1984. "Stimulation of 3T3 Cells Induces Transcription of the C-Fos Proto-Oncogene." *Nature* 311 (5985): 433–38. http://www.ncbi.nlm.nih.gov/pubmed/6090941.

Gschwantler-Kaulich, Daphne, Camilla Natter, Stefan Steurer, Ingrid Walter, Almut Thomas, Mohamed Salama, and Christian F Singer. 2013. "Increase in Ezrin Expression from Benign to Malignant Breast Tumours." *Cellular Oncology (Dordrecht)* 36 (6): 485–91.

https://doi.org/10.1007/s13402-013-0153-5.

Gualdrini, Francesco, Cyril Esnault, Stuart Horswell, Aengus Stewart, Nik Matthews, and Richard Treisman. 2016. "SRF Co-Factors Control the Balance between Cell Proliferation and Contractility." *Molecular Cell* 64 (6): 1048–61. https://doi.org/10.1016/j.molcel.2016.10.016.

Guettler, S., M. K. Vartiainen, F. Miralles, B. Larijani, and R. Treisman. 2008. "RPEL Motifs Link the Serum Response Factor Cofactor MAL but Not Myocardin to Rho Signaling via Actin Binding." *Molecular and Cellular Biology*. https://doi.org/10.1128/MCB.01623-07.

Hamann, Jens C., Alexandra Surcel, Ruoyao Chen, Carolyn Teragawa, John G. Albeck, Douglas N. Robinson, and Michael Overholtzer. 2017. "Entosis Is Induced by Glucose Starvation." *Cell Reports*. https://doi.org/10.1016/j.celrep.2017.06.037.

Hamidi, Hellyeh, Johanna Lilja, and Johanna Ivaska. 2017. "Using XCELLigence RTCA Instrument to Measure Cell Adhesion." *BIO-PROTOCOL* 7 (24). https://doi.org/10.21769/BioProtoc.2646.

Hanahan, Douglas, and Robert A Weinberg. 2011. "Hallmarks of Cancer: The next Generation." *Cell* 144 (5): 646–74. https://doi.org/10.1016/j.cell.2011.02.013.

Hannemann, Sebastian, Ricardo Madrid, Jana Stastna, Thomas Kitzing, Judith Gasteier, André Schönichen, Jerome Bouchet, et al. 2008. "The Diaphanous-Related Formin FHOD1 Associates with ROCK1 and Promotes Src-Dependent Plasma Membrane Blebbing." *The Journal of Biological Chemistry* 283 (41): 27891–903. https://doi.org/10.1074/jbc.M801800200.

Hatzoglou, Anastassia, Isabelle Ader, Anne Splingard, James Flanders, Evelyne Saade, Ingrid Leroy, Sabine Traver, Sandra Aresta, and Jean de Gunzburg. 2007. "Gem Associates with Ezrin and Acts via the Rho-GAP Protein Gmip to down-Regulate the Rho Pathway." *Molecular Biology of the Cell* 18 (4): 1242–52. https://doi.org/10.1091/mbc.e06-06-0510.

Heath, J.P., and G.A. Dunn. 1978. "Cell to Substratum Contacts of Chick Fibroblasts and Their Relation to the Microfilament System. A Correlated Interference-Reflexion and High-Voltage Electron-Microscope Study." *Journal of Cell Science* 29 (1). http://jcs.biologists.org/content/29/1/197.long.

Helander, Tuula S., Olli Carpén, Ossi Turunen, Panu E. Kovanen, Antti Vaheri, and Tuomo Timonen. 1996. "ICAM-2 Redistributed by Ezrin as a Target for Killer Cells." *Nature* 382 (6588): 265–68. https://doi.org/10.1038/382265a0.

Hermann, Michaela-Rosemarie, Madis Jakobson, Georgina P. Colo, Emanuel Rognoni, Maili Jakobson, Christian Kupatt, Guido Posern, and Reinhard Fässler. 2016. "Integrins Synergise to Induce Expression of the MRTF-A–SRF Target Gene ISG15 for Promoting Cancer Cell Invasion." *Journal of Cell Science*. https://doi.org/10.1242/jcs.177592.

Hill, C S, and R Treisman. 1995. "Differential Activation of C-Fos Promoter Elements by Serum, Lysophosphatidic Acid, G Proteins and Polypeptide Growth Factors." *The EMBO Journal* 14 (20): 5037–47. http://www.ncbi.nlm.nih.gov/pubmed/7588632.

Hill, Caroline S, Judy Wynne, and Richard Treisman. 1995. "The Rho Family GTPases RhoA, Racl, and CDC42Hs Regulate Transcriptional Activation by SRF." *Cell*. Vol. 81. https://www.cell.com/cell/pdf/S0092-8674(05)80020-0.pdf?_returnURL=https%3A%2F%2Flinkinghub.elsevier.com%2Fretrieve%2Fpii%2FS0092867405800200%3Fshowall%3Dtrue.

Hirao, M, N Sato, T Kondo, S Yonemura, M Monden, T Sasaki, Y Takai, S Tsukita, and S Tsukita.

1996. "Regulation Mechanism of ERM (Ezrin/Radixin/Moesin) Protein/Plasma Membrane Association: Possible Involvement of Phosphatidylinositol Turnover and Rho-Dependent Signaling Pathway." *The Journal of Cell Biology* 135 (1): 37–51. https://doi.org/10.1083/JCB.135.1.37.

Holmes, Kenneth C., David Popp, Werner Gebhard, and Wolfgang Kabsch. 1990. "Atomic Model of the Actin Filament." *Nature* 347 (6288): 44–49. https://doi.org/10.1038/347044a0.

Holtfreter, J. 1943. "A Study of the Mechanisms of Gastrulation." *I. J. Exp. Zool.* 94: 261 – 318.

Ikenouchi, Junichi, and Kana Aoki. 2017. "Membrane Bleb: A Seesaw Game of Two Small GTPases." *Small GTPases* 8 (2): 85–89. https://doi.org/10.1080/21541248.2016.1199266.

Janknecht, R, W H Ernst, V Pingoud, and A Nordheim. 1993. "Activation of Ternary Complex Factor Elk-1 by MAP Kinases." *The EMBO Journal* 12 (13): 5097–5104. http://www.ncbi.nlm.nih.gov/pubmed/8262053.

Kaksonen, Marko, Christopher P. Toret, and David G. Drubin. 2006. "Harnessing Actin Dynamics for Clathrin-Mediated Endocytosis." *Nature Reviews Molecular Cell Biology* 7 (6): 404–14. https://doi.org/10.1038/nrm1940.

Kang, Yun Kyung, Seong Woo Hong, Hyucksang Lee, and Woo Ho Kim. 2010. "Prognostic Implications of Ezrin Expression in Human Hepatocellular Carcinoma." *Molecular Carcinogenesis* 49 (9): n/a-n/a. https://doi.org/10.1002/mc.20653.

Kim, Taekyung, John A Cooper, and David Sept. 2010. "The Interaction of Capping Protein with the Barbed End of the Actin Filament." *Journal of Molecular Biology* 404 (5): 794–802. https://doi.org/10.1016/j.jmb.2010.10.017.

Kitzing, T M, Y Wang, O Pertz, J W Copeland, and R Grosse. 2010. "Formin-like 2 Drives Amoeboid Invasive Cell Motility Downstream of RhoC." *Oncogene* 29 (16): 2441–48. https://doi.org/10.1038/onc.2009.515.

Kitzing, Thomas M, Arul S Sahadevan, Dominique T Brandt, Helga Knieling, Sebastian Hannemann, Oliver T Fackler, Jörg Grosshans, and Robert Grosse. 2007. "Positive Feedback between Dia1, LARG, and RhoA Regulates Cell Morphology and Invasion." *Genes & Development* 21 (12): 1478–83. https://doi.org/10.1101/gad.424807.

Klooster, Jean Paul ten, Marnix Jansen, Jin Yuan, Viola Oorschot, Harry Begthel, Valeria Di Giacomo, Frédéric Colland, et al. 2009. "Mst4 and Ezrin Induce Brush Borders Downstream of the Lkb1/Strad/Mo25 Polarization Complex." *Developmental Cell* 16 (4): 551–62. https://doi.org/10.1016/j.devcel.2009.01.016.

Konstantinovsky, Sophya, Ben Davidson, and Reuven Reich. 2012. "Ezrin and BCAR1/P130Cas Mediate Breast Cancer Growth as 3-D Spheroids." *Clinical & Experimental Metastasis* 29 (6): 527–40. https://doi.org/10.1007/s10585-012-9468-2.

Krajcovic, M., S. Krishna, L. Akkari, J. A. Joyce, and M. Overholtzer. 2013. "MTOR Regulates Phagosome and Entotic Vacuole Fission." *Molecular Biology of the Cell*. https://doi.org/10.1091/mbc.E13-07-0408.

Krajcovic, Matej, Nicole B Johnson, Qiang Sun, Guillaume Normand, Nicholas Hoover, Evelyn Yao, Andrea L Richardson, et al. 2011. "A Non-Genetic Route to Aneuploidy in Human Cancers." *Nature Cell Biology* 13 (3): 324–30. https://doi.org/10.1038/ncb2174.

Krajcovic, Matej, and Michael Overholtzer. 2012. "Mechanisms of Ploidy Increase in Human Cancers: A New Role for Cell Cannibalism." *Cancer Research*.

https://doi.org/10.1158/0008-5472.CAN-11-3127.

Kunda, Patricia, Andrew E Pelling, Tao Liu, and Buzz Baum. 2008. "Moesin Controls Cortical Rigidity, Cell Rounding, and Spindle Morphogenesis during Mitosis." *Current Biology : CB* 18 (2): 91–101. https://doi.org/10.1016/j.cub.2007.12.051.

Lankes, Wolfgang, Andrea Griesmacher, Jorg Grunwaldt, Reinhard Schwartz-Albiez, and Ruprecht Keller. 1988. "A Heparin-Binding Protein Involved in Inhibition of Smooth-Muscle Cell Proliferation." *Biochem. J*. https://www.ncbi.nlm.nih.gov/pmc/articles/PMC1149078/pdf/biochemj00232-0201.pdf.

Laster, S M, and J M Mackenzie. 1996. "Bleb Formation and F-Actin Distribution during Mitosis and Tumor Necrosis Factor-Induced Apoptosis." *Microscopy Research and Technique* 34 (3): 272–80. https://doi.org/10.1002/(SICI)1097-0029(19960615)34:3<272::AID-JEMT10>3.0.CO;2-J.

Le, Christophe, and Marie-France Carlier. 2008. "Regulation of Actin Assembly Associated With Protrusion and Adhesion in Cell Migration." www.prv.org.

Legg, James W., Charlotte A. Lewis, Maddy Parsons, Tony Ng, and Clare M. Isacke. 2002. "A Novel PKC-Regulated Mechanism Controls CD44–ezrin Association and Directional Cell Motility." *Nature Cell Biology* 4 (6): 399–407. https://doi.org/10.1038/ncb797.

Lehtimaki, Jaakko, Markku Hakala, and Pekka Lappalainen. 2017. "Actin Filament Structures in Migrating Cells." *Handbook of Experimental Pharmacology*. https://doi.org/10.1007/164_2016_28.

Leitner, Laura, Dmitry Shaposhnikov, Alexander Mengel, Arnaud Descot, Sylvia Julien, Reinhard Hoffmann, and Guido Posern. 2011. "MAL/MRTF-A Controls Migration of Non-Invasive Cells by Upregulation of Cytoskeleton-Associated Proteins." *Journal of Cell Science*. https://doi.org/10.1242/jcs.092791.

Levayer, Romain, and Thomas Lecuit. 2012. "Biomechanical Regulation of Contractility: Spatial Control and Dynamics." *Trends in Cell Biology* 22 (2): 61–81. https://doi.org/10.1016/j.tcb.2011.10.001.

Li, Qingchang, Hui Gao, Hongtao Xu, Xin Wang, Yongqi Pan, Fengxia Hao, Xueshan Qiu, Maggie Stoecker, Endi Wang, and Enhua Wang. 2012. "Expression of Ezrin Correlates with Malignant Phenotype of Lung Cancer, and in Vitro Knockdown of Ezrin Reverses the Aggressive Biological Behavior of Lung Cancer Cells." *Tumor Biology* 33 (5): 1493–1504. https://doi.org/10.1007/s13277-012-0400-9.

Liang, Jianqing, Jie Fan, Manna Wang, Zubiao Niu, Zhengrong Zhang, Long Yuan, Yanhong Tai, et al. 2018. "CDKN2A Inhibits Formation of Homotypic Cell-in-Cell Structures." *Oncogenesis* 7 (6): 50. https://doi.org/10.1038/s41389-018-0056-4.

Limouze, John, Aaron F Straight, Timothy Mitchison, and James R Sellers. 2004. "Specificity of Blebbistatin, an Inhibitor of Myosin II." *Journal of Muscle Research and Cell Motility* 25 (4–5): 337–41. https://doi.org/10.1007/s10974-004-6060-7.

Liu, Yan Jun, Maël Le Berre, Franziska Lautenschlaeger, Paolo Maiuri, Andrew Callan-Jones, Mélina Heuzé, Tohru Takaki, Raphaël Voituriez, and Matthieu Piel. 2015. "Confinement and Low Adhesion Induce Fast Amoeboid Migration of Slow Mesenchymal Cells." *Cell*. https://doi.org/10.1016/j.cell.2015.01.007.

Loitto, Vesa-Matti, Tony Forslund, Tommy Sundqvist, Karl-Eric Magnusson, and Mikael Gustafsson. 2002. "Neutrophil Leukocyte Motility Requires Directed Water Influx." *Journal of Leukocyte Biology* 71 (2): 212–22.

http://www.ncbi.nlm.nih.gov/pubmed/11818441.

Lorentzen, Anna, Jeffrey Bamber, Amine Sadok, Ilan Elson-Schwab, and Christopher J. Marshall. 2011. "An Ezrin-Rich, Rigid Uropod-like Structure Directs Movement of Amoeboid Blebbing Cells." *Journal of Cell Science* 124 (8).

Lubbe, Wilhelm J, Zengyi Y Zhou, Weili Fu, David Zuzga, Stephanie Schulz, Rafael Fridman, Ruth J Muschel, Scott A Waldman, and Giovanni M Pitari. 2006. "Tumor Epithelial Cell Matrix Metalloproteinase 9 Is a Target for Antimetastatic Therapy in Colorectal Cancer." *Clinical Cancer Research : An Official Journal of the American Association for Cancer Research* 12 (6): 1876–82. https://doi.org/10.1158/1078-0432.CCR-05-2686.

Machicoane, Mickael, Cristina A de Frutos, Jenny Fink, Murielle Rocancourt, Yannis Lombardi, Sonia Garel, Matthieu Piel, and Arnaud Echard. 2014. "SLK-Dependent Activation of ERMs Controls LGN-NuMA Localization and Spindle Orientation." *The Journal of Cell Biology* 205 (6): 791–99. https://doi.org/10.1083/jcb.201401049.

Mackay, D J, F Esch, H Furthmayr, and A Hall. 1997. "Rho- and Rac-Dependent Assembly of Focal Adhesion Complexes and Actin Filaments in Permeabilized Fibroblasts: An Essential Role for Ezrin/Radixin/Moesin Proteins." *The Journal of Cell Biology* 138 (4): 927–38. https://doi.org/10.1083/JCB.138.4.927.

Madsen, Chris D., Steven Hooper, Melda Tozluoglu, Andreas Bruckbauer, Georgina Fletcher, Janine T. Erler, Paul A. Bates, Barry Thompson, and Erik Sahai. 2015. "STRIPAK Components Determine Mode of Cancer Cell Migration and Metastasis." *Nature Cell Biology*. https://doi.org/10.1038/ncb3083.

Mak, Hannah, Alexandra Naba, Sonal Varma, Colleen Schick, Andrew Day, Sandip K SenGupta, Monique Arpin, and Bruce E Elliott. 2012. "Ezrin Phosphorylation on Tyrosine 477 Regulates Invasion and Metastasis of Breast Cancer Cells." *BMC Cancer* 12 (March): 82. https://doi.org/10.1186/1471-2407-12-82.

Martin, Tracey A, Gregory Harrison, Robert E Mansel, and Wen G Jiang. 2003. "The Role of the CD44/Ezrin Complex in Cancer Metastasis." *Critical Reviews in Oncology/Hematology* 46 (2): 165–86. https://doi.org/10.1016/S1040-8428(02)00172-5.

Matsui, T, M Maeda, Y Doi, S Yonemura, M Amano, K Kaibuchi, S Tsukita, and S Tsukita. 1998. "Rho-Kinase Phosphorylates COOH-Terminal Threonines of Ezrin/Radixin/Moesin (ERM) Proteins and Regulates Their Head-to-Tail Association." *The Journal of Cell Biology* 140 (3): 647–57. https://doi.org/10.1083/JCB.140.3.647.

McClatchey, Andrea I. 2014. "ERM Proteins at a Glance." *Journal of Cell Science* 127: 3199–3204. https://doi.org/10.1242/jcs.098343.

Medjkane, Souhila, Cristina Perez-Sanchez, Cedric Gaggioli, Erik Sahai, and Richard Treisman. 2009. "Myocardin-Related Transcription Factors and SRF Are Required for Cytoskeletal Dynamics and Experimental Metastasis." *Nature Cell Biology*. https://doi.org/10.1038/ncb1833.

Meerbrey, Kristen L, Guang Hu, Jessica D Kessler, Kevin Roarty, Mamie Z Li, Justin E Fang, Jason I Herschkowitz, et al. 2011. "The PINDUCER Lentiviral Toolkit for Inducible RNA Interference in Vitro and in Vivo." *Proceedings of the National Academy of Sciences of the United States of America* 108 (9): 3665–70. https://doi.org/10.1073/pnas.1019736108.

Meng, Yunxiao, Zhaohui Lu, Shuangni Yu, Qiang Zhang, Yihui Ma, and Jie Chen. 2010. "Ezrin Promotes Invasion and Metastasis of Pancreatic Cancer Cells." https://doi.org/10.1186/1479-5876-8-61.

Miralles, Francesc, Guido Posern, Alexia Ileana Zaromytidou, and Richard Treisman. 2003. "Actin Dynamics Control SRF Activity by Regulation of Its Coactivator MAL." *Cell*. https://doi.org/10.1016/S0092-8674(03)00278-2.

Mohun, T, N Garrett, and R Treisman. 1987. "Xenopus Cytoskeletal Actin and Human C-Fos Gene Promoters Share a Conserved Protein-Binding Site." *The EMBO Journal* 6 (3): 667–73. http://www.ncbi.nlm.nih.gov/pubmed/3582369.

Mouilleron, Stéphane, Carola A. Langer, Sebastian Guettler, Neil Q. McDonald, and Richard Treisman. 2011. "Structure of a Pentavalent G-Actin•MRTF-A Complex Reveals How G-Actin Controls Nucleocytoplasmic Shuttling of a Transcriptional Coactivator." *Science Signaling* 4 (177).

Müller, R, R Bravo, J Burckhardt, and T Curran. 1984. "Induction of C-Fos Gene and Protein by Growth Factors Precedes Activation of c-Myc." *Nature* 312 (5996): 716–20. http://www.ncbi.nlm.nih.gov/pubmed/6334806.

Nakamura, F, M R Amieva, and H Furthmayr. 1995. "Phosphorylation of Threonine 558 in the Carboxyl-Terminal Actin-Binding Domain of Moesin by Thrombin Activation of Human Platelets." *The Journal of Biological Chemistry* 270 (52): 31377–85. https://doi.org/10.1074/JBC.270.52.31377.

Ng, T, M Parsons, W E Hughes, J Monypenny, D Zicha, A Gautreau, M Arpin, et al. 2001. "Ezrin Is a Downstream Effector of Trafficking PKC-Integrin Complexes Involved in the Control of Cell Motility." *The EMBO Journal* 20 (11): 2723–41. https://doi.org/10.1093/emboj/20.11.2723.

Niggli, Verena, Christophe Andréoli, Christian Roy, and Paul Mangeat. 1995. "Identification of a Phosphatidylinositol-4,5-Bisphosphate-Binding Domain in the N-Terminal Region of Ezrin." *FEBS Letters* 376 (3): 172–76. https://doi.org/10.1016/0014-5793(95)01270-1.

Norman, Leann, Kheya Sengupta, and Helim Aranda-Espinoza. 2011. "Blebbing Dynamics during Endothelial Cell Spreading." *European Journal of Cell Biology* 90 (1): 37–48. https://doi.org/10.1016/j.ejcb.2010.09.013.

Nürnberg, Alexander, Thomas Kitzing, and Robert Grosse. 2011. "Nucleating Actin for Invasion." *Nature Reviews Cancer*. https://doi.org/10.1038/nrc3003.

O'Brien, T P, G P Yang, L Sanders, and L F Lau. 1990. "Expression of Cyr61, a Growth Factor-Inducible Immediate-Early Gene." *Molecular and Cellular Biology* 10 (7): 3569–77. http://www.ncbi.nlm.nih.gov/pubmed/2355916.

Ohrnberger, Stefan, Abhishek Thavamani, Albert Braeuning, Daniel B. Lipka, Milen Kirilov, Robert Geffers, Stella E. Authenrieth, et al. 2015. "Dysregulated Serum Response Factor Triggers Formation of Hepatocellular Carcinoma." *Hepatology* 61 (3): 979–89. https://doi.org/10.1002/hep.27539.

Olson, Eric N., and Alfred Nordheim. 2010. "Linking Actin Dynamics and Gene Transcription to Drive Cellular Motile Functions." *Nature Reviews Molecular Cell Biology*. https://doi.org/10.1038/nrm2890.

Olson, Michael F., and Erik Sahai. 2009. "The Actin Cytoskeleton in Cancer Cell Motility." *Clinical & Experimental Metastasis* 26 (4): 273–87. https://doi.org/10.1007/s10585-008-9174-2.

Orgaz, Jose L., Pahini Pandya, Rimple Dalmeida, Panagiotis Karagiannis, Berta Sanchez-Laorden, Amaya Viros, Jean Albrengues, et al. 2014. "Diverse Matrix Metalloproteinase Functions Regulate Cancer Amoeboid Migration." *Nature Communications*.

https://doi.org/10.1038/ncomms5255.

Overholtzer, Michael, and Joan S. Brugge. 2008. "The Cell Biology of Cell-in-Cell Structures." *Nature Reviews Molecular Cell Biology* 9 (10): 796–809. https://doi.org/10.1038/nrm2504.

Overholtzer, Michael, Arnaud A Mailleux, Ghassan Mouneimne, Guillaume Normand, Stuart J Schnitt, Randall W King, Edmund S Cibas, and Joan S Brugge. 2007. "A Nonapoptotic Cell Death Process, Entosis, That Occurs by Cell-in-Cell Invasion." *Cell* 131 (5): 966–79. https://doi.org/10.1016/j.cell.2007.10.040.

Paluch, Ewa K., and Erez Raz. 2013. "The Role and Regulation of Blebs in Cell Migration." *Current Opinion in Cell Biology*. https://doi.org/10.1016/j.ceb.2013.05.005.

Panayiotou, Richard, Francesc Miralles, Rafal Pawlowski, Jessica Diring, Helen R Flynn, Mark Skehel, and Richard Treisman. 2016. "Phosphorylation Acts Positively and Negatively to Regulate MRTF-A Subcellular Localisation and Activity." *ELife* 5. https://doi.org/10.7554/eLife.15460.

Pandya, Pahini, Jose L Orgaz, and Victoria Sanz-Moreno. 2017. "Modes of Invasion during Tumour Dissemination." *Molecular Oncology* 11 (1): 5–27. https://doi.org/10.1002/1878-0261.12019.

Paňková, K., D. Rösel, M. Novotný, and Jan Brábek. 2010. "The Molecular Mechanisms of Transition between Mesenchymal and Amoeboid Invasiveness in Tumor Cells." *Cellular and Molecular Life Sciences*. https://doi.org/10.1007/s00018-009-0132-1.

Patara, Marcelo, Erika Maria Monteiro Santos, Renata de Almeida Coudry, Fernando Augusto Soares, Fábio Oliveira Ferreira, and Benedito Mauro Rossi. 2011. "Ezrin Expression as a Prognostic Marker in Colorectal Adenocarcinoma." *Pathology & Oncology Research* 17 (4): 827–33. https://doi.org/10.1007/s12253-011-9389-4.

Pawłowski, Rafał, Eeva Kaisa Rajakylä, Maria K. Vartiainen, and Richard Treisman. 2010. "An Actin-Regulated Importin α/β-Dependent Extended Bipartite NLS Directs Nuclear Import of MRTF-A." *EMBO Journal*. https://doi.org/10.1038/emboj.2010.216.

Pellegrini, Luca, Song Tan, and Timothy J. Richmond. 1995. "Structure of Serum Response Factor Core Bound to DNA." *Nature* 376 (6540): 490–98. https://doi.org/10.1038/376490a0.

Pietromonaco, S F, P C Simons, A Altman, and L Elias. 1998. "Protein Kinase C-Theta Phosphorylation of Moesin in the Actin-Binding Sequence." *The Journal of Biological Chemistry* 273 (13): 7594–7603. https://doi.org/10.1074/JBC.273.13.7594.

Pipes, G C Teg, Esther E Creemers, and Eric N Olson. 2006. "The Myocardin Family of Transcriptional Coactivators: Versatile Regulators of Cell Growth, Migration, and Myogenesis." *Genes & Development* 20 (12): 1545–56. https://doi.org/10.1101/gad.1428006.

Plessner, Matthias, Michael Melak, Pilar Chinchilla, Christian Baarlink, and Robert Grosse. 2015. "Nuclear F-Actin Formation and Reorganization upon Cell Spreading." *The Journal of Biological Chemistry* 290 (18): 11209–16. https://doi.org/10.1074/jbc.M114.627166.

Pollard, Thomas D, and Gary G Borisy. 2003. "Cellular Motility Driven by Assembly and Disassembly of Actin Filaments." *Cell* 112 (4): 453–65. http://www.ncbi.nlm.nih.gov/pubmed/12600310.

Pollard, Thomas D, and John A Cooper. 2009. "Actin, a Central Player in Cell Shape and

Movement." *Science (New York, N.Y.)* 326 (5957): 1208–12. https://doi.org/10.1126/science.1175862.

Poola, Indira, Robert L DeWitty, Josephine J Marshalleck, Rakesh Bhatnagar, Jessy Abraham, and LaSalle D Leffall. 2005. "Identification of MMP-1 as a Putative Breast Cancer Predictive Marker by Global Gene Expression Analysis." *Nature Medicine* 11 (5): 481–83. https://doi.org/10.1038/nm1243.

Pore, Debasis, and Neetu Gupta. 2015. "The Ezrin-Radixin-Moesin Family of Proteins in the Regulation of B-Cell Immune Response." *Critical Reviews in Immunology* 35 (1): 15–31. http://www.ncbi.nlm.nih.gov/pubmed/25746045.

Posern, Guido, Athanassia Sotiropoulos, and Richard Treisman. 2002. "Mutant Actins Demonstrate a Role for Unpolymerized Actin in Control of Transcription by Serum Response Factor." Edited by Keith R. Yamamoto. *Molecular Biology of the Cell* 13 (12): 4167–78. https://doi.org/10.1091/mbc.02-05-0068.

Pring, M, A Weber, and M R Bubb. 1992. "Profilin-Actin Complexes Directly Elongate Actin Filaments at the Barbed End." *Biochemistry* 31 (6): 1827–36. http://www.ncbi.nlm.nih.gov/pubmed/1737036.

Pujuguet, Philippe, Laurence Del Maestro, Alexis Gautreau, Daniel Louvard, and Monique Arpin. 2003. "Ezrin Regulates E-Cadherin-Dependent Adherens Junction Assembly through Rac1 Activation." *Molecular Biology of the Cell* 14 (5): 2181–91. https://doi.org/10.1091/mbc.e02-07-0410.

Purvanov, Vladimir, Manuel Holst, Jameel Khan, Christian Baarlink, and Robert Grosse. 2014. "G-Protein-Coupled Receptor Signaling and Polarized Actin Dynamics Drive Cell-in-Cell Invasion." *ELife* 3 (June). https://doi.org/10.7554/eLife.02786.

Reczek, D, M Berryman, and A Bretscher. 1997. "Identification of EBP50: A PDZ-Containing Phosphoprotein That Associates with Members of the Ezrin-Radixin-Moesin Family." *The Journal of Cell Biology* 139 (1): 169–79. https://doi.org/10.1083/JCB.139.1.169.

Rees, Martin D, and Shane R Thomas. 2015. "Using Cell-Substrate Impedance and Live Cell Imaging to Measure Real-Time Changes in Cellular Adhesion and de-Adhesion Induced by Matrix Modification." *Journal of Visualized Experiments : JoVE*, no. 96 (February). https://doi.org/10.3791/52423.

Ren, L, S H Hong, J Cassavaugh, T Osborne, A J Chou, S Y Kim, R Gorlick, S M Hewitt, and C Khanna. 2009. "The Actin-Cytoskeleton Linker Protein Ezrin Is Regulated during Osteosarcoma Metastasis by PKC." *Oncogene* 28 (6): 792–802. https://doi.org/10.1038/onc.2008.437.

Ridley, A. J. 2003. "Cell Migration: Integrating Signals from Front to Back." *Science* 302 (5651): 1704–9. https://doi.org/10.1126/science.1092053.

Ridley, Anne J. 2011. "Life at the Leading Edge." *Cell*. https://doi.org/10.1016/j.cell.2011.06.010.

Ruprecht, Verena, Stefan Wieser, Andrew Callan-Jones, Michael Smutny, Hitoshi Morita, Keisuke Sako, Vanessa Barone, et al. 2015. "Cortical Contractility Triggers a Stochastic Switch to Fast Amoeboid Cell Motility." *Cell*. https://doi.org/10.1016/j.cell.2015.01.008.

Sahai, Erik. 2005. "Mechanisms of Cancer Cell Invasion." *Current Opinion in Genetics & Development* 15 (1): 87–96. https://doi.org/10.1016/j.gde.2004.12.002.

———. 2007. "Illuminating the Metastatic Process." *Nature Reviews Cancer* 7 (10): 737–49.

https://doi.org/10.1038/nrc2229.

Sahai, Erik, and Christopher J. Marshall. 2003. "Differing Modes of Tumour Cell Invasion Have Distinct Requirements for Rho/ROCK Signalling and Extracellular Proteolysis." *Nature Cell Biology* 5 (8): 711–19. https://doi.org/10.1038/ncb1019.

Sanz-Moreno, Victoria, Gilles Gadea, Jessica Ahn, Hugh Paterson, Pierfrancesco Marra, Sophie Pinner, Erik Sahai, and Christopher J. Marshall. 2008. "Rac Activation and Inactivation Control Plasticity of Tumor Cell Movement." *Cell*. https://doi.org/10.1016/j.cell.2008.09.043.

Sanz-Moreno, Victoria, and Christopher J Marshall. 2010. "The Plasticity of Cytoskeletal Dynamics Underlying Neoplastic Cell Migration." *Current Opinion in Cell Biology* 22 (5): 690–96. https://doi.org/10.1016/j.ceb.2010.08.020.

Sarrió, David, Socorro María Rodríguez-Pinilla, Ana Dotor, Francisco Calero, David Hardisson, and José Palacios. 2006. "Abnormal Ezrin Localization Is Associated with Clinicopathological Features in Invasive Breast Carcinomas." *Breast Cancer Research and Treatment* 98 (1): 71–79. https://doi.org/10.1007/s10549-005-9133-4.

Sato, Naruki, Noriko Funayama, Akira Nagafuchi, Shigenobu Yonemura, Sachiko Tsukita, and Shoichiro Tsukita. 1992. "A Gene Family Consisting of Ezrin, Radixin and Moesin Its Specific Localization at Act in Filameni/Plasma Membrane Association Sites." *Journal of Cell Science*. Vol. 103. http://jcs.biologists.org/content/joces/103/1/131.full.pdf.

SCHERER, W F, J T SYVERTON, and G O GEY. 1953. "Studies on the Propagation in Vitro of Poliomyelitis Viruses. IV. Viral Multiplication in a Stable Strain of Human Malignant Epithelial Cells (Strain HeLa) Derived from an Epidermoid Carcinoma of the Cervix." *The Journal of Experimental Medicine* 97 (5): 695–710. http://www.ncbi.nlm.nih.gov/pubmed/13052828.

Schratt, Gerhard, Ulrike Philippar, Jürgen Berger, Heinz Schwarz, Olaf Heidenreich, and Alfred Nordheim. 2002. "Serum Response Factor Is Crucial for Actin Cytoskeletal Organization and Focal Adhesion Assembly in Embryonic Stem Cells." *The Journal of Cell Biology* 156 (4): 737–50. https://doi.org/10.1083/jcb.200106008.

Sedzinski, Jakub, Maté Biro, Annelie Oswald, Jean-Yves Tinevez, Guillaume Salbreux, and Ewa Paluch. 2011. "Polar Actomyosin Contractility Destabilizes the Position of the Cytokinetic Furrow." *Nature* 476 (7361): 462–66. https://doi.org/10.1038/nature10286.

Shaposhnikov, Dmitry, Christian Kuffer, Zuzana Storchova, and Guido Posern. 2013. "Myocardin Related Transcription Factors Are Required for Coordinated Cell Cycle Progression." *Cell Cycle* 12 (11): 1762–72. https://doi.org/10.4161/cc.24839.

Small, J.Victor. 1995. "Getting the Actin Filaments Straight: Nucleation-Release or Treadmilling?" *Trends in Cell Biology* 5 (2): 52–55. https://doi.org/10.1016/S0962-8924(00)88939-4.

Soto Hinojosa, Laura, Manuel Holst, Christian Baarlink, and Robert Grosse. 2017. "MRTF Transcription and Ezrin-Dependent Plasma Membrane Blebbing Are Required for Entotic Invasion." *The Journal of Cell Biology* 216 (10): 3087–95. https://doi.org/10.1083/jcb.201702010.

Srivastava, J., B. E. Elliott, D. Louvard, and M. Arpin. 2005. "Src-Dependent Ezrin Phosphorylation in Adhesion-Mediated Signaling." *Molecular Biology of the Cell* 16 (3): 1481–90. https://doi.org/10.1091/mbc.e04-08-0721.

Stastna, Jana, Xiaoyu Pan, Haicui Wang, Alina Kollmannsperger, Stefan Kutscheidt, Volker

Lohmann, Robert Grosse, and Oliver T Fackler. 2012. "Differing and Isoform-Specific Roles for the Formin DIAPH3 in Plasma Membrane Blebbing and Filopodia Formation." *Cell Research* | 22 (4): 728–45. https://doi.org/10.1038/cr.2011.202.

Stewart, Martin P., Jonne Helenius, Yusuke Toyoda, Subramanian P. Ramanathan, Daniel J. Muller, and Anthony A. Hyman. 2011. "Hydrostatic Pressure and the Actomyosin Cortex Drive Mitotic Cell Rounding." *Nature* 469 (7329): 226–30. https://doi.org/10.1038/nature09642.

Straight, A. F., Amy Cheung, John Limouze, Irene Chen, Nick J Westwood, James R Sellers, and Timothy J Mitchison. 2003. "Dissecting Temporal and Spatial Control of Cytokinesis with a Myosin II Inhibitor." *Science* 299 (5613): 1743–47. https://doi.org/10.1126/science.1081412.

Sullivan, Amy L, Christopher Benner, Sven Heinz, Wendy Huang, Lan Xie, Joseph M Miano, and Christopher K Glass. 2011. "Serum Response Factor Utilizes Distinct Promoter- and Enhancer-Based Mechanisms to Regulate Cytoskeletal Gene Expression in Macrophages." *Molecular and Cellular Biology* 31 (4): 861–75. https://doi.org/10.1128/MCB.00836-10.

Sun, Qiang, Guang Chen, Jeffrey W Streb, Xiaochun Long, Yumei Yang, Christian J Stoeckert, and Joseph M Miano. 2006. "Defining the Mammalian CArGome." *Genome Research* 16 (2): 197–207. https://doi.org/10.1101/gr.4108706.

Sun, Qiang, Edmund S. Cibas, Hongyan Huang, Louis Hodgson, and Michael Overholtzer. 2014. "Induction of Entosis by Epithelial Cadherin Expression." *Cell Research*. https://doi.org/10.1038/cr.2014.137.

Sun, Qiang, Tianzhi Luo, Yixin Ren, Oliver Florey, Senji Shirasawa, Takehiko Sasazuki, Douglas N. Robinson, and Michael Overholtzer. 2014. "Competition between Human Cells by Entosis." *Cell Research*. https://doi.org/10.1038/cr.2014.138.

Tait, Larry, Herbert D Soule, and Jose Russo2. 1990. "Ultrastructural and Immunocytochemical Characterization of an Immortalized Human Breast Epithelial Cell Line, MCF-101." *CANCER RESEARCH* 50: 6087–94.

Takeuchi, K, N Sato, H Kasahara, N Funayama, A Nagafuchi, S Yonemura, S Tsukita, and S Tsukita. 1994. "Perturbation of Cell Adhesion and Microvilli Formation by Antisense Oligonucleotides to ERM Family Members." *The Journal of Cell Biology* 125 (6): 1371–84. https://doi.org/10.1083/JCB.125.6.1371.

Tournaviti, Stella, Sebastian Hannemann, Stefan Terjung, Thomas M Kitzing, Carolin Stegmayer, Julia Ritzerfeld, Paul Walther, Robert Grosse, Walter Nickel, and Oliver T Fackler. 2007. "SH4-Domain-Induced Plasma Membrane Dynamization Promotes Bleb-Associated Cell Motility." *Journal of Cell Science* 120 (Pt 21): 3820–29. https://doi.org/10.1242/jcs.011130.

Tran Quang, C, A Gautreau, M Arpin, and R Treisman. 2000. "Ezrin Function Is Required for ROCK-Mediated Fibroblast Transformation by the Net and Dbl Oncogenes." *The EMBO Journal* 19 (17): 4565–76. https://doi.org/10.1093/emboj/19.17.4565.

Treisman, R. 1985. "Transient Accumulation of C-Fos RNA Following Serum Stimulation Requires a Conserved 5' Element and c-Fos 3' Sequences." *Cell* 42 (3): 889–902. http://www.ncbi.nlm.nih.gov/pubmed/2414012.

———. 1986. "Identification of a Protein-Binding Site That Mediates Transcriptional Response of the c-Fos Gene to Serum Factors." *Cell* 46 (4): 567–74. http://www.ncbi.nlm.nih.gov/pubmed/3524858.

Tseng, Yiider, Thomas P. Kole, Jerry S.H. Lee, Elena Fedorov, Steven C. Almo, Benjamin W. Schafer, and Denis Wirtz. 2005. "How Actin Crosslinking and Bundling Proteins Cooperate to Generate an Enhanced Cell Mechanical Response." *Biochemical and Biophysical Research Communications* 334 (1): 183–92. https://doi.org/10.1016/J.BBRC.2005.05.205.

Tsukita, S, Y Hieda, and S Tsukita. 1989. "A New 82-KD Barbed End-Capping Protein (Radixin) Localized in the Cell-to-Cell Adherens Junction: Purification and Characterization." *The Journal of Cell Biology* 108 (6): 2369–82. https://doi.org/10.1083/JCB.108.6.2369.

Turunen, O, T Wahlström, and A Vaheri. 1994. "Ezrin Has a COOH-Terminal Actin-Binding Site That Is Conserved in the Ezrin Protein Family." *The Journal of Cell Biology* 126 (6): 1445–53. https://doi.org/10.1083/JCB.126.6.1445.

Valderrama, F., S. Thevapala, and A. J. Ridley. 2012. "Radixin Regulates Cell Migration and Cell-Cell Adhesion through Rac1." *Journal of Cell Science*. https://doi.org/10.1242/jcs.094383.

Vartiainen, Maria K., Sebastian Guettler, Banafshe Larijani, and Richard Treisman. 2007. "Nuclear Actin Regulates Dynamic Subcellular Localization and Activity of the SRF Cofactor MAL." *Science*. https://doi.org/10.1126/science.1141084.

Wang, D.-Z., S. Li, D. Hockemeyer, L. Sutherland, Z. Wang, G. Schratt, J. A. Richardson, A. Nordheim, and E. N. Olson. 2002. "Potentiation of Serum Response Factor Activity by a Family of Myocardin-Related Transcription Factors." *Proceedings of the National Academy of Sciences* 99 (23): 14855–60. https://doi.org/10.1073/pnas.222561499.

Wang, D, P S Chang, Z Wang, L Sutherland, J A Richardson, E Small, P A Krieg, and E N Olson. 2001. "Activation of Cardiac Gene Expression by Myocardin, a Transcriptional Cofactor for Serum Response Factor." *Cell* 105 (7): 851–62. https://doi.org/10.1016/S0092-8674(01)00404-4.

Wang, Zhigao, Da-Zhi Wang, Dirk Hockemeyer, John McAnally, Alfred Nordheim, and Eric N. Olson. 2004. "Myocardin and Ternary Complex Factors Compete for SRF to Control Smooth Muscle Gene Expression." *Nature* 428 (6979): 185–89. https://doi.org/10.1038/nature02382.

Wang, Zhigao, Da-Zhi Wang, G C Teg Pipes, and Eric N Olson. 2003. "Myocardin Is a Master Regulator of Smooth Muscle Gene Expression." *Proceedings of the National Academy of Sciences of the United States of America* 100 (12): 7129–34. https://doi.org/10.1073/pnas.1232341100.

Wegner, Albrecht. 1976. "Head to Tail Polymerization of Actin." *Journal of Molecular Biology* 108 (1): 139–50. https://doi.org/10.1016/S0022-2836(76)80100-3.

Wolf, Katarina, Irina Mazo, Harry Leung, Katharina Engelke, Ulrich H. Von Andrian, Elena I. Deryugina, Alex Y. Strongin, Eva B. Bröcker, and Peter Friedl. 2003. "Compensation Mechanism in Tumor Cell Migration: Mesenchymal-Amoeboid Transition after Blocking of Pericellular Proteolysis." *Journal of Cell Biology*. https://doi.org/10.1083/jcb.200209006.

Wolf, Katarina, Yi I. Wu, Yueying Liu, Jörg Geiger, Eric Tam, Christopher Overall, M. Sharon Stack, and Peter Friedl. 2007. "Multi-Step Pericellular Proteolysis Controls the Transition from Individual to Collective Cancer Cell Invasion." *Nature Cell Biology* 9 (8): 893–904. https://doi.org/10.1038/ncb1616.

Wu, Yongqing, Raja Dey, Aidong Han, Nimanthi Jayathilaka, Michael Philips, Jun Ye, and Lin Chen. 2010. "Structure of the MADS-Box/MEF2 Domain of MEF2A Bound to DNA and Its Implication for Myocardin Recruitment." *Journal of Molecular Biology* 397 (2): 520–33. https://doi.org/10.1016/j.jmb.2010.01.067.

Wyse, Meghan M., Silvia Goicoechea, Rafael Garcia-Mata, Andrea L. Nestor-Kalinoski, and Kathryn M. Eisenmann. 2017. "MDia2 and CXCL12/CXCR4 Chemokine Signaling Intersect to Drive Tumor Cell Amoeboid Morphological Transitions." *Biochemical and Biophysical Research Communications*. https://doi.org/10.1016/j.bbrc.2017.01.087.

Yamashiro, Sawako, David S Gokhin, Sumiko Kimura, Roberta B Nowak, and Velia M Fowler. 2012. "Tropomodulins: Pointed-End Capping Proteins That Regulate Actin Filament Architecture in Diverse Cell Types." *Cytoskeleton (Hoboken, N.J.)* 69 (6): 337–70. https://doi.org/10.1002/cm.21031.

Yanase, Yuhki, Izumi Hide, Shoji Mihara, Yasuhito Shirai, Naoaki Saito, Yoshihiro Nakata, Michihiro Hide, and Norio Sakai. 2011. "A Critical Role of Conventional Protein Kinase C in Morphological Changes of Rodent Mast Cells." *Immunology and Cell Biology* 89 (1): 149–59. https://doi.org/10.1038/icb.2010.67.

Yonemura S, Matsui T, Tsukita S and Tsukita S. 2002. "Rho-Dependent and -Independent Activation Mechanisms of Ezrin/Radixin/Moesin Proteins: An Essential Role for Polyphosphoinositides in Vivo." *Journal of Cell Science* 112 (Pt 8 (8): 1149–58. http://www.ncbi.nlm.nih.gov/pubmed/10085250.

Yu, Olivia M., Jorge A. Benitez, Steven W. Plouffe, Daniel Ryback, Andrea Klein, Jeff Smith, Jason Greenbaum, et al. 2018. "YAP and MRTF-A, Transcriptional Co-Activators of RhoA-Mediated Gene Expression, Are Critical for Glioblastoma Tumorigenicity." *Oncogene*, 1–16. https://doi.org/10.1038/s41388-018-0301-5.

Yu, Yanlin, Javed Khan, Chand Khanna, Lee Helman, Paul S Meltzer, and Glenn Merlino. 2004. "Expression Profiling Identifies the Cytoskeletal Organizer Ezrin and the Developmental Homeoprotein Six-1 as Key Metastatic Regulators." *Nature Medicine* 10 (2): 175–81. https://doi.org/10.1038/nm966.

Zaromytidou, Alexia-Ileana, Francesc Miralles, and Richard Treisman. 2006. "MAL and Ternary Complex Factor Use Different Mechanisms to Contact a Common Surface on the Serum Response Factor DNA-Binding Domain." *Molecular and Cellular Biology* 26 (11): 4134–48. https://doi.org/10.1128/MCB.01902-05.

Appendix

List of academic teachers

My academic teachers from the University of Barcelona were Dr. Aguade Porres, Dr. Aguado Tomás, Dr. Albalat, Dr. Arcas Pons, Dr. Auladell, Dr. Azcón Bieto, Dr. Blasco, Dr. Bonada Caparrós, Dr. Bueno, Dr. Butturini, Dr. Cambra Sánchez, Dr. Casado Merediz, Dr. Cebrià Sánchez, Dr. Civit Vives, Dr. Cotrufo, Dr. Felip Benach, Dr. Fernández Novell, Dr. Llorente Cabrera, Dr. López Soriano, Dr. Lucena Gutiérrez, Dr. Marfany Nadal, Dr. Martínez Garcia, Dr. Mestres, Dr. Muñoa, Dr. Nogués Mestres, Dr. Oliva Cuyas, Dr. Palacín, Dr. Pastor Blanco, Dr. Pérez-Pérez, Dr. Pretus Real, Dr. Rubio Sanz, Dr. Sagristà, Dr. Segarra Robert, Dr. Ureña, Dr. Valledor Fernández and Dr.Viñas.

My academic teachers from the University of Helsinki were Dr. Gahmberg and Dr. Grönholm. Finally, my academic teachers from the University Pompeu Fabra were Dr. Ayte del Olmo, Dr. Aramburu Beltran, Dr. Baños Diez, Dr. Fernández-Fernández, Dr. Garcia de Herreros, Dr. Hidalgo Hernando, Dr. López Rodriguez, Dr. Maldonado López, Dr. Muñoz Canoves, Dr. Muñoz López, Dr. Nadal Clanchet, Dr. Ozaita Mintegui, Dr. Pujades Corbí and Dr. Real Arribas.

Acknowledgments

Reprint of original publication